UNIVERSIDADE ESTADUAL DE CAMPINAS
Faculdade De Engenharia Mecânica

JOSE MARIA HERRERA SARAVIA

INJECTIVITY OF BIOPOLYMERS SOLUTIONS THROUGH POROUS MEDIA

INJETIVIDADE DE SOLUÇÕES DE BIOPOLÍMEROS ATRAVÉS DE MEIOS POROSOS

CAMPINAS
2023

JOSE MARIA HERRERA SARAVIA

INJECTIVITY OF BIOPOLYMERS SOLUTIONS THROUGH POROUS MEDIA

INJETIVIDADE DE SOLUÇÕES DE BIOPOLÍMEROS ATRAVÉS DE MEIOS POROSOS

Dissertation presented to the School of Mechanical Engineering of the University of Campinas in partial fulfillment of the requirements for the degree of Master in Sciences and Petroleum Engineering in the area of Reservoirs and Management.

Dissertação apresentada à Faculdade de Engenharia Mecânica da Universidade Estadual de Campinas como parte dos requisitos exigidos para a obtenção do título de Mestre em Ciências e Engenharia de Petróleo na área de Reservatórios e Gestão.

Orientadora: Profa. Dra. Rosangela Barros Zanoni Lopes Moreno

ESTE TRABALHO CORRESPONDE À VERSÃO FINAL DA DISSERTAÇÃO DEFENDIDA PELO ALUNO JOSE MARIA HERRERA SARAVIA E ORIENTADO PELA PROFA. DRA. ROSANGELA BARROS ZANONI LOPES MORENO.

CAMPINAS

2023

Ficha catalográfica
Universidade Estadual de Campinas
Biblioteca da Área de Engenharia e Arquitetura
Rose Meire da Silva - CRB 8/5974

H433i

Herrera Saravia, Jose Maria, 1994-
Injectivity of biopolymers solutions through porous media / Jose Maria Herrera Saravia. – Campinas, SP : [s.n.], 2023.

Orientador: Rosangela Barros Zanoni Lopes Moreno.
Dissertação (mestrado) – Universidade Estadual de Campinas, Faculdade de Engenharia Mecânica.

1. Engenharia de petróleo. 2. Recuperação avançada de petróleo. 3. Injeção de polímeros. 4. Biopolímeros. I. Moreno, Rosangela Barros Zanoni Lopes, 1966-. II. Universidade Estadual de Campinas. Faculdade de Engenharia Mecânica. III. Título.

Informações Complementares

Título em outro idioma: Injetividade de soluções de biopolímeros através de meios porosos
Palavras-chave em inglês:
Oil petroleum
Enhanced oil recovery
Polymer flooding
Biopolymers
Área de concentração: Reservatórios e Gestão
Titulação: Mestre em Ciências e Engenharia de Petróleo
Banca examinadora:
Rosangela Barros Zanoni Lopes Moreno [Orientador]
Denis José Schiozer
Paulo de Tarso Vieira e Rosa
Data de defesa: 10-07-2023
Programa de Pós-Graduação: Ciências e Engenharia de Petróleo

Identificação e informações acadêmicas do(a) aluno(a)
- ORCID do autor: https://orcid.org/0009-0002-9508-1300
- Currículo Lattes do autor: https://lattes.cnpq.br/4821103435279515

UNIVERSIDADE ESTADUAL DE CAMPINAS
FACULDADE DE ENGENHARIA MECÂNICA
DISSERTAÇÃO DE MESTRADO ACADÊMICO

Injectivity of biopolymers solutions through porous media

Injetividade de soluções de biopolímeros através de meios porosos

Autor: Jose Maria Herrera Saravia

Orientadora: Profa. Dra. Rosangela Barros Zanoni Lopes Moreno

A Banca Examinadora composta pelos membros abaixo aprovou esta Tese:

Profa. Dra. Rosangela Barros Zanoni Lopes Moreno
Departamento de Energia / Faculdade de Engenharia Mecânica / Universidade Estadual de Campinas

Prof. Dr. Denis José Schiozer
Departamento de Energia / Faculdade de Engenharia Mecânica / Universidade Estadual de Campinas

Prof. Dr. Paulo de Tarso Vieira e Rosa
Departamento de Físico-Química / Instituto de Química / Universidade Estadual de Campinas

A Ata de Defesa com as respectivas assinaturas dos membros encontra-se no SIGA/Sistema de Fluxo de Dissertação/Tese e na Secretaria do Programa da Unidade.

Campinas, 10 de julho de 2023

DEDICATION

I dedicate this master's thesis to my beloved parents, Jose Maria and Maria Angelica, for their unwavering emotional and financial support throughout my academic journey. I would like to express my deepest gratitude to my mother, who has been my constant companion in all of my decisions and has been a pillar of strength, teaching me to never give up. To my brother Marco, I owe a debt of gratitude for his invaluable guidance and advice, which have been a source of motivation at every step of the way.

ACKNOWLEDGEMENTS

I would like to express my deepest gratitude to my parents, whose unwavering love and support have been instrumental in helping me achieve both my personal and academic goals. Their encouragement has given me the strength and determination to persevere in the face of adversity and never give up on my dreams. I am truly blessed to have such amazing parents, and I will always be grateful for their unwavering support.

I extend my heartfelt thanks to the van Loon Family for their unconditional support and encouragement during my academic pursuits. Their support has been a crucial factor in the successful completion of this work.

I am deeply grateful to Prof. Dr. Rosângela B. Z. L. Moreno for giving me the chance to conduct this research under her guidance and expertise in the field of polymer injection. Her invaluable support and mentorship will stay with me as I pursue my career goals.

I am grateful to my friends from LABORE, FEM, and CEPETRO for their contributions and suggestions.

I am grateful to my colleagues from the SPE UNICAMP Chapter, particularly Marx M. and Miguel V., for their invaluable assistance, unwavering support, and enduring friendship, which were instrumental in bringing this work to fruition.

I would like to express my appreciation to the Laboratory of Oil Reservoirs (LABORE) and the Center for Petroleum Studies (CEPETRO) at UNICAMP for providing the physical space and necessary facilities for this research project.

This study was financed by the ongoing R&D project registered as ANP 20359-6, “Injeção de Biopolímeros para a Recuperação Avançada de Petróleo de Reservatórios do Pré-Sal Brasileiro” (Universidade de Campinas (Unicamp) / Shell Brasil / ANP) – Biopolymer Injection for Enhanced Oil Recovery in Brazilian Pre-Salt Reservoirs, sponsored by Shell Brasil under the ANP R&D levy as “Compromisso de Investimentos com Pesquisa e Desenvolvimento”.

“Never give up without trying.
Do what you can, no matter how small the effect might be.”
Ōnoki of Both Scales
In the novel Naruto Shippuden
By Masashi Kishimoto

RESUMO

A injeção de polímeros está ganhando cada vez mais interesse como solução para deslocar óleos de alta viscosidade, devido às suas semelhanças com a injeção de água. Os biopolímeros são particularmente atrativos para essa aplicação, dada a sua natureza ambientalmente amigável e propriedades favoráveis em comparação aos polímeros sintéticos. Consequentemente, tem havido um foco crescente na avaliação de soluções de injeção baseadas em biopolímeros para a Recuperação Avançada de Petróleo.

A injetividade é uma variável crucial para qualquer projeto de injeção de polímeros, pois afeta diretamente os custos e o desempenho do processo de injeção. Mudanças nas vazões de injeção ou na concentração de polímeros na solução podem afetar a injetividade, tornando importante entender a influência dessas variáveis em detalhes. A compreensão da injetividade ainda não é madura, e mais estudos são necessárias para entender seu papel no desempenho do processo de recuperação, especialmente em áreas próximas ao poço onde velocidades de fluxo altas estão presentes. Os polímeros, sendo fluidos não-newtonianos, dependem de sua taxa de cisalhamento, o que torna a compreensão da injetividade complexa.

A injetividade é analisada juntamente com outras propriedades-chave, incluindo fator de resistência, fator de resistência residual e viscosidade in-situ, como função da concentração e da vazão de injeção. Essas variáveis são altamente relevantes para os resultados obtidos, e sua avaliação é relativamente fácil. Para investigar essas propriedades, foram selecionados três biopolímeros: goma xantana, goma guar e escleroglucano. Os experimentos foram realizados sob a temperatura do reservatório alvo de 60°C e salinidade de água de injeção é 30905 TDS. Os resultados obtidos neste estudo podem fornecer informações valiosas sobre o desempenho de biopolímeros em projetos de injeção e podem orientar futuras pesquisas nesta área.

Os resultados dos experimentos realizados em rochas calcárias de Indiana revelaram que a injetividade de soluções de biopolímeros depende de vários fatores, incluindo a concentração e o tipo de biopolímero usado, e a permeabilidade da rocha. O aumento da concentração de biopolímeros resultou em diminuição da injetividade, enquanto o aumento da permeabilidade pode levar a valores mais altos de injetividade. O perfil de pressão ao longo da amostra de rocha demonstrou que a primeira seção do núcleo tinha a menor permeabilidade, o que afetou a injetividade das soluções de biopolímeros. Medidas de viscosidade in-situ indicaram uma correlação entre a concentração de biopolímeros e a viscosidade, mas a diferença na viscosidade entre diferentes concentrações não foi significativa.

Palavras Chave: Engenharia de petróleo, Recuperação avançada de petróleo, Injeção de Polímeros, Biopolímero

ABSTRACT

Polymer injection is gaining increasing interest as a solution for displacing high-viscosity oils due to its similarities with Waterflooding. Biopolymers are particularly attractive for this application, given their environmentally friendly nature and favorable properties compared to synthetic polymers. Consequently, a growing focus has been on researching biopolymer-based solutions for Enhanced Oil Recovery.

Injectivity is crucial for any polymer injection project, directly impacting profitability and injection performance. Changes in injection flow rates or concentration can affect the injectivity, making it essential to understand this variable in detail. However, the understanding of injectivity still needs to be mature, and more research is required to know how it affects injection performance, particularly in areas close to the well where high flow velocities are present. Polymers, being non-Newtonian fluids, depend significantly on their shear rate, which further complicates the understanding of injectivity.

In this study, injectivity is analyzed along with other fundamental properties, including resistance factor, residual resistance factor, and in-situ viscosity, as a function of injection concentration and flow rate. These variables are highly relevant to the results obtained, and their manipulation is relatively easy. To investigate these properties, three biopolymers were selected: Xanthan Gum, Guar Gum, and Scleroglucan. The experiments were conducted under reservoir conditions, with a salinity of 30905 TDS and a temperature of 60°T. The results obtained from this study can provide valuable insights into the performance of biopolymers in injection projects and inform future research in this area.

The experiments conducted on Indiana Limestones revealed that the injectivity of biopolymer solutions depends on several factors, including the concentration and type of biopolymer used and the permeability of the rock. Increasing biopolymer concentration resulted in decreased injectivity while increasing permeability can lead to higher injectivity values. The pressure profile along the core demonstrated that the first section of the core had the most negligible permeability, which impacted the injectivity of biopolymer solutions. Viscosity in-situ measurements indicated a correlation between biopolymer concentration and viscosity, but the difference in viscosity between different concentrations was insignificant.

Key Words: Oil Petroleum, Enhanced Oil Recovery, Polymer Flooding, Biopolymers

LIST OF FIGURES

LIST OF TABLES

LIST OF NOMENCLATURES

Latin characters and expressions

A - Area - $L^{2}M^{0}T^{0}\Theta^{0}N^{0}$
c - Concentration - $L^{-3}M^{1}T^{0}\Theta^{0}N^{0\dagger}$
$c*$ - Critical overlap concentration characteristic of the transition between dilute and semi dilute concentration regimes - $L^{-3}M^{1}T^{0}\Theta^{0}N^{0\dagger}$
d_H - Degree of hydrolysis - $L^{0}M^{0}T^{0}\Theta^{0}N^{0}$
$IAPV$ - Inaccessible pore volume - $L^{0}M^{0}T^{0}\Theta^{0}N^{0}$
v - Flow velocity, or apparent velocity, or Darcy velocity - $L^{1}M^{0}T^{-1}\Theta^{0}N^{0}$
k_f - Absolute permeability - $L^{2}M^{0}T^{0}\Theta^{0}N^{0}$
K - Ostwald-de Waele fluid consistency index - $L^{-1}M^{1}T^{n-2}\Theta^{0}N^{0}$ *
L - Length - $L^{1}M^{0}T^{0}\Theta^{0}N^{0}$
m - Mass - $L^{0}M^{1}T^{0}\Theta^{0}N^{0}$
M - Mobility ratio - $L^{0}M^{0}T^{0}\Theta^{0}N^{0}$
N - Injection number - -
P - Pressure - $L^{-1}M^{1}T^{-2}\Theta^{0}N^{0}$
PV - Pore volume - $L^{3}M^{0}T^{0}\Theta^{0}N^{0}$
Q - Volumetric flow rate - $L^{3}M^{0}T^{-1}\Theta^{0}N^{0}$
R^2 - Coefficient of determination - -
RF - Resistance factor - $L^{0}M^{0}T^{0}\Theta^{0}N^{0}$
RRF - Residual resistance factor - $L^{0}M^{0}T^{0}\Theta^{0}N^{0}$
s - Saturation - $L^{0}M^{0}T^{0}\Theta^{0}N^{0}$
t - Time - $L^{0}M^{0}T^{-1}\Theta^{0}N^{0}$
T - Temperature - $L^{0}M^{0}T^{0}\Theta^{1}N^{0}$
V - Volume - $L^{3}M^{0}T^{0}\Theta^{0}N^{0}$
V_R - Viscosity ratio - $L^{0}M^{0}T^{0}\Theta^{0}N^{0}$
VPI - Injected pore volume - $L^{0}M^{0}T^{0}\Theta^{0}N^{0}$
x - Space - $L^{1}M^{0}T^{0}\Theta^{0}N^{0}$

Greek characters

$\dot{\gamma}$ - Shear rate - $L^{0}M^{0}T^{-1}\Theta^{0}N^{0}$
$\dot{\gamma}_0$ - Maximum shear rate for the low shear rate Newtonian plateau - $L^{0}M^{0}T^{-1}\Theta^{0}N^{0}$
$\dot{\gamma}_\infty$ - Minimum shear rate for the high shear rate Newtonian plateau - $L^{0}M^{0}T^{-1}\Theta^{0}N^{0}$
η - Apparent viscosity - $L^{-1}M^{1}T^{-1}\Theta^{0}N^{0}$
η_0 - Viscosity characteristic of the low shear rate Newtonian plateau - $L^{-1}M^{1}T^{-1}\Theta^{0}N^{0}$
η_∞ - Viscosity characteristic of the high shear rate Newtonian plateau - $L^{-1}M^{1}T^{-1}\Theta^{0}N^{0}$
λ - Mobility - $L^{0}M^{0}T^{0}\Theta^{0}N^{0}$
μ - Viscosity - $L^{-1}M^{1}T^{-1}\Theta^{0}N^{0}$
τ - Shear stress - $L^{-1}M^{1}T^{-2}\Theta^{0}N^{0}$
τ_0 - Shear stress above which there is flow - $L^{-1}M^{1}T^{-2}\Theta^{0}N^{0}$
$\tau_{1/2}$ - Shear stress in which the apparent viscosity is half of that characteristic of the Newtonian plateau - $L^{-1}M^{1}T^{-2}\Theta^{0}N^{0}$
ϕ - Effective porosity - $L^{0}M^{0}T^{0}\Theta^{0}N^{0}$

Subscripts

w - Water phase
o - Oil phase
p - Polymer component or polymeric solution
oi - Initial oil
or - Residual Oil
wf - Water flooding
g - gas
pf - Polymer Flooding
i - component
rel - Relative
D - Dimensionless

Acronyms

AA - Acrylic acid
ASP - Alkali-Surfactant-Polymer
API - American petroleum institute
CEOR - Chemical Enhanced Oil Recovery
CMC - Carboxymethylcellulose
DOH - Degree of Hydrolysis
DI - Deionized
EOR - Enhanced oil recovery
HPAM - Partially hydrolyzed polyacrylamide
IOIP - Initial Oil in Place
IFT - Interfacial Tension
IPV - Inaccessible Pore Volume
PAM - Polyacrylamide
PV - Pore volume
RF - Resistance factor
RRF - Residual resistance factor
SP - Surfactant-Polymer
TDS - Total dissolved solids
VPI - Injected pore volume

SUMMARY

1 INTRODUCTION

Enhanced Oil Recovery (EOR) by polymer injection is increasingly common due to the long history of scientific advances. Additionally, significant advancements have been demonstrated in various onshore fields, yielding favorable outcomes with an additional 3% recovery beyond the maximum attainable through waterflooding, further enhancing the overall performance (Pu et al., 2018). Polymer flooding began in the 1950s, with the first pilot field application in the United States in 1964 (Z. Liu et al., 2020). Currently, nanoparticles are being used to improve polymer injection performance further. Many new patents have been registered in the last decade, most related to Chemical Enhanced Oil Recovery (Ostermann, 2016).

Many of these discoveries are attributed to the Daqing Field in China, where various improved oil recovery methods and different types of polymers have been successfully used (Ostermann, 2016). The Daqing Field reservoirs have favorable conditions that ensure the improvement of fluid mobility, including low reservoir temperature, low salinity, low coefficient of heterogeneity (with a variation between 0.4 and 0.7 of the Dykstra-Parsons coefficient), and low content of high valence ions (Dong et al., 2008).

Polymer Flooding involves many steps or stages to perform (V. H. de S. Ferreira & Moreno, 2018); they proposed a workflow consisting of four parts: screening, laboratory testing, simulation, and field implementation. Firstly, parameters must be evaluated and compared with other cases to determine if the reservoir is suitable for applying the Mobility Control Method (Polymer Flooding). Secondly, the polymer solution must be characterized to design the appropriate solution for the reservoir and polymer flooding project. The laboratory results are then used for numerical simulation to prepare an optimal field development model. Finally, the pilot test is a critical step for applying polymer flooding in the target reservoir in the selected field. Given the positive results obtained, there is a promising opportunity to extend this approach across the entire field, maximizing its potential impact and benefits on a broader scale.

Laboratory work is essential for the development of any industry, as it helps to determine solutions to different problems that arise. Injectivity loss in polymer injection projects can play a determining role in demonstrating their profitability. This parameter is related to the polymer viscosity, injection rate, and well-spacing, as well as the mechanisms that can affect it from its preparation to the moment when solutions interact within porous media, as noted by (Glasbergen et al., 2015; Thomas et al., 2019).

Polymers are soluble chemicals composed of repeating chains of monomers. They are mixed with water and injected into the reservoir to improve the water/oil mobility ratio and reduce residual oil saturation by increasing the viscosity of the injected fluid. There are two types of polymers: synthetic and biopolymers. HPAM is the most widely used among synthetic polymers due to its lower cost than other EOR processes. However, HPAM is sensitive to factors such as salinity, temperature, and polymer adsorption, which can impact its viscosity, a critical physical property. In contrast, biopolymers have greater thermal stability and salinity resistance than HPAM. However, the application of biopolymers has been limited due to their high production costs, making them less viable for commercial field projects (Al-Shakry, Skauge, et al., 2019; Muhammed et al., 2020).

Lithology is another factor that affects polymer performance. Carbonate rocks have more heterogeneous characteristics than sandstones due to their diagenetic processes, often resulting in many natural fractures. However, this type of system presents challenges for EOR processes due to the uncertainty of fluid flow caused by high fracture density and areas of high permeability, which complicate the application of EOR solutions. While such systems are beneficial for primary recovery and early production, the problem arises when expensive EOR solutions are injected and easily channeled and diverted by conduits or channels. This reduces the effectiveness of EOR, resulting in excessive water production (Han et al., 2014).

1.1 Motivation

Worldwide energy consumption has been growing at an average annual rate of 2% over the past seven years, with oil and gas accounting for 27% and 22% of the consumption, respectively (Bchini et al., 2022). Despite efforts to reduce CO2 emissions, three projections until 2050 made by BP with current technologies show a relatively high consumption of fossil fuels, indicating that they will continue to dominate the global energy mix (BP, 2022). In 2022, the world's oil reserves were estimated to be 1732.36 billion barrels, with Brazil holding 0.69% of these reserves, or 11.925 million barrels (ANP, 2022).

As global energy consumption rises, maintaining or increasing hydrocarbon reserves becomes essential. Four categories have been established to add new reserves, including discovering new fields and reservoirs, extending reservoirs in known fields, and redefining reserves due to changes in extraction technology economics The importance of EOR lies in the last category, as the average oil recovery worldwide is only around 30 to 35% of Initial Oil in Place (IOIP) (Aadnøy & Looyeh, 2019), and EOR projects could increase the oil recovery. EOR methods can be divided into four main groups: chemical, thermal, miscible, and microbial.

Chemical Enhanced Oil Recovery (CEOR) represents approximately 11% of all EOR projects worldwide, with 77% of those projects using polymer flooding and the remaining 23% combining polymers with surfactants (Surfactant Polymer) or alkalis (Alkali Surfactant Polymer flooding). Polymer flooding is an effective technique for increasing oil recovery, similar to water flooding, but injecting a more viscous slug to displace the oil by increasing the water's viscosity (Mohsenatabar Firozjaii & Saghafi, 2020).

Injectivity is critical parameter for the success of polymer flooding projects (Al-Shakry, Skauge, et al., 2019). However, forecasting reservoir conditions can present a significant challenge due to the complexity of non-Newtonian fluids and their interactions in porous media. This complexity is affected by the rheology of the polymeric solution, as well as the heterogeneous characteristics of the rock (Thomas et al., 2019).

One important factor affecting the performance of polymer injectivity is the behavior of non-Newtonian fluids at different flow rates (Abbasi et al., 2017). These fluids exhibit shear-thinning behavior at high shear rates, which means that the apparent viscosity decreases with increasing shear rate. However, the fluids become dilatant at higher shear rates, and the polymer injectivity decreases due to increased apparent viscosity. Therefore, it is essential to consider the rheological behavior of the polymeric solution at different flow rates to optimize polymer injectivity in oil recovery operations (Al-Shakry, Skauge, et al., 2018).

1.2 Objectives

Evaluate the Injectivity of the Biopolymers Solutions through porous media by considering its concentration, injection flow rate, and rheological characteristics.

The results of this project are expected to reach the following specific objectives:

- Carry out previously proposed procedures to conduct single-phase core flooding experiments
- Analyze the performance of polymer injectivity in single-phase core flooding tests.
- Enhance the understanding of polymer injectivity loss in porous media.

1.3 Dissertation Structure

The present work is divided into 4 chapters:

Chapter 1 shows the introduction, motivation and objectives that involve in this research.

Chapter 2 provides a concise overview of chemical methods for oil recovery, with particular emphasis on polymer flooding. Additionally, it outlines the crucial parameters for polymer flooding design, drawing on insights from previous research, and discusses the rheological properties of polymers, which are critical for their assessment. The chapter concludes by examining the mechanisms that influence polymer injection.

Chapter 3 details the methodology applied to conduct single-phase core-flooding experiments. The chapter is divided into two parts. The first part provides an overview of the materials used at each experiment stage, including the rock cores, the injection fluid, and the instruments used for data acquisition. The second part outlines the experimental procedures that were followed, including preparing the rock cores and the injection fluid, determining the injection parameters, and collecting data during the core-flooding process. The ultimate goal of these experiments was to obtain data that could be used to evaluate the performance of polymer flooding in porous media and better understand the mechanisms that affect polymer injectivity.

Chapter 4 shows the results of single-phase core flooding experiments on carbonate rocks using three different polymers: Xanthan Gum, Guar Gum, and Scleroglucan. The methodology outlined in Chapter 3 was used to investigate injectivity, resistance factor, residual resistance factor, and in-situ viscosity as a function of injection concentration and flow rate. The results were described in detail, with a critical analysis of the selected variables for the study. Emphasis was placed on injectivity, and comparisons were made with data from other sources to provide additional context.

Chapter 5 summarizes the main conclusion and defines recommendations for futures studies.

2 Literature Review and Fundamental Concepts

This chapter shows the literature supporting research on Injectivity Loss, a critical key to polymer injection projects. Initially, the Chemical Enhanced Oil Recovery mechanisms are described. Then, a screening of the different applications is carried out throughout this time. Later, the rheological behavior of the biopolymers is detailed. Finally, the injectivity and the consequences that occur when having low values are described in detail.

2.1 Chemical EOR

The growing global demand for energy leads to the use of techniques that maximize oil recovery. The most common technique is waterflooding, which involves injecting water to maintain pressure and help displace the oil for better recovery. Waterflooding is considered a straightforward and cheap method, but it depends on the performance of the injection wells (Civan, 2000). However, it also has limitations, such as high channeling resulting in an abrupt breakthrough due to the configuration of the porous medium (Ahmed, 2010). For this reason, EOR projects have gained importance in dealing with oil trapping caused by capillary forces in pore structures.

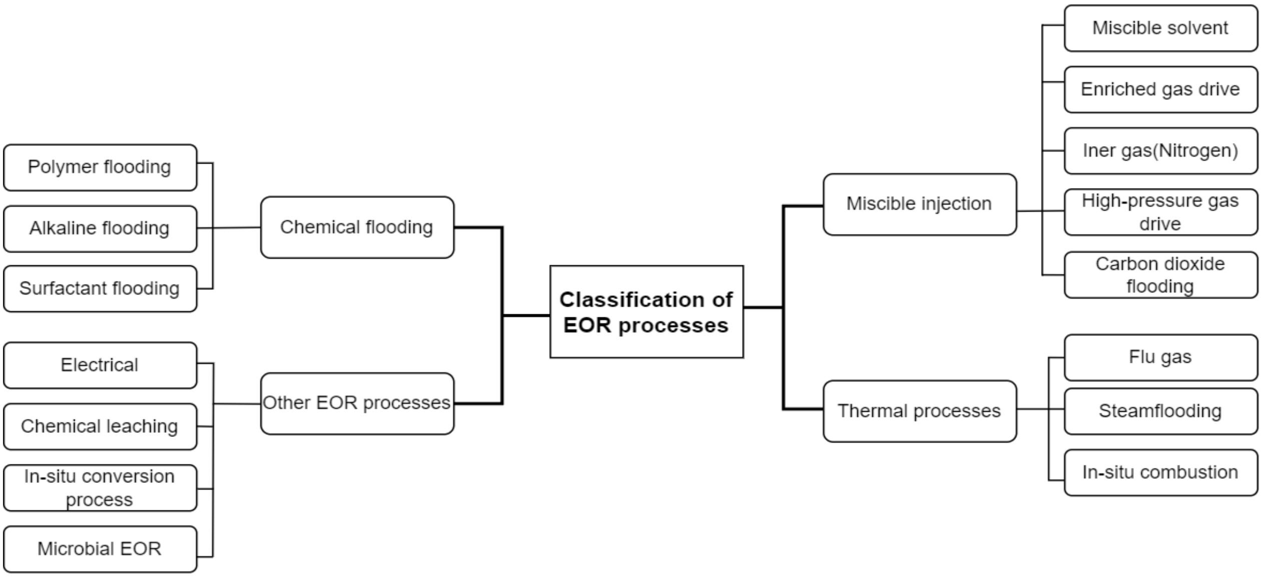

Figure 2-1: Classification of Enhanced Oil Recovery Processes adapted from (Romero-Zeron, 2012)

Figure 2-1 shows the categories of thermal recovery, miscible gas injection, and chemical methods are shown. CEOR methods are considered the most practical after waterflooding due to their impact on the sweep efficiency (Abbasi et al., 2017; Tackie-Otoo et al., 2020).

EOR projects aim to recover the remaining oil through fluid injection and energy that are not present in the reservoir and increase the value of Displacement Efficiency (E_D), which is the relationship between the recovered oil and the initial oil present in the swept volume, as shown in Equation (2.1) The EOR projects should accomplish several objectives, such as boosting the natural energy in the reservoir, creating favorable conditions for residual oil recovery by interacting with the reservoir rock and oil system, reducing interfacial tension between the displacing fluid and oil, increasing the capillary number, reducing capillary forces, increasing the drive water viscosity, providing mobility control, oil swelling, oil viscosity reduction, and altering the reservoir rock wettability (Romero-Zeron, 2012)

$$E_D = \frac{S_{oi} - S_{or}}{S_{oi}} \tag{2.1}$$

where E_D and S are the Displacement Efficiency, Saturation, respectively. The subscripts “oi”, “or” denotes initial oil and residual oil, respectively.

The E_D depends on two types of displacement: microscopic and macroscopic. The first type is related to the oil displacement in the porous medium and measures the performance of the displacement fluid to sweep the oil that has been in contact with the pore. It can be increased by reducing the interfacial tension between fluids and oil viscosity. The second type is associated with the reservoir scale, considering the fluid displacement efficacy from the injector well toward the producer well. As shown in Figure 2-2 compares a waterflooding with polymer injection. In the upper scheme, fingering due to the porous medium configuration or fractured reservoirs is established, resulting in lower sweep performance, and the scheme below shows a bank of polymer, which increases the sweep efficiency. Moreover, this represents an ideal application of polymer flooding, which, in many cases, closely mimics the desired behavior. Additionally, it offers the advantage of reduced water consumption compared to traditional waterflooding methods. (Akbari et al., 2019; Machale et al., 2020; Romero-Zeron, 2012).

The injection rate is determined by using waterflooding as a reference, and the viscosity can be gradually increased by adding polymer banks until the desired viscosity is achieved (Thomas, 2016). On the other hand, it proposes a different approach, suggesting the use of multiple polymer banks. The first bank is utilized to control the pressure, the second acts as the primary bank responsible for displacing the oil, and the final bank, with the lowest injected pore volume, aims to reduce the viscosity contrast between the main bank and the trailing water (Romero-Zeron, 2012).

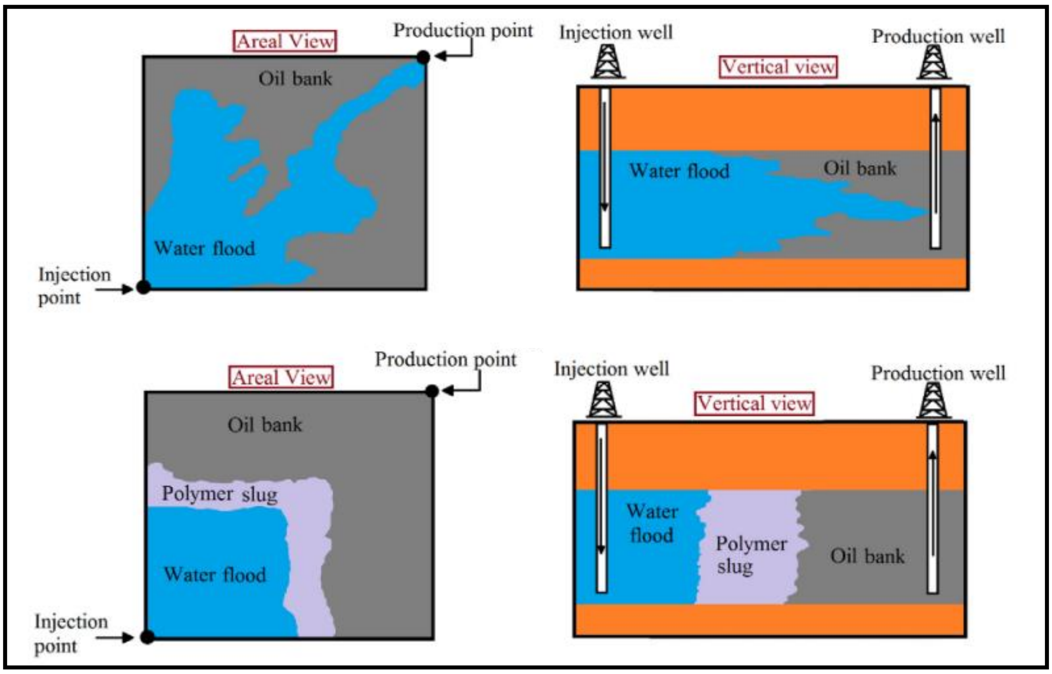

Figure 2-2: Comparison of water flooding and polymer flooding (Akbari et al., 2019)

2.1.1 Polymer Flooding

One effective method in reservoir development is polymer flooding, a type of Chemical Enhanced Oil Recovery (CEOR). This technique has been studied for many years in sandstone reservoirs and has shown good performance by improving sweep efficiency, mitigating viscous fingering, and preventing early breakthroughs. This is achieved by reducing the water-oil mobility ratio (M) to 1, as shown in Equation (2.2). When the mobility ratio exceeds 1, it is considered an "undesired number," meaning oil becomes less mobile than water. By reducing the mobility ratio, the volumetric sweep can be increased (Alfazazi et al., 2020; Li et al., 2020; Machale et al., 2020)

$$M = \frac{\lambda_w}{\lambda_o} = \frac{k_w/\mu_w}{k_o/\mu_o} \tag{2.2}$$

where λ, k, and μ are phase mobility, effective permeability, and viscosity, respectively. The subscripts “w” and “o” denotes water and oil phases, respectively.

This technique improves mobility control by increasing the viscosity of the injected water by adding long-chain polymer molecules and reducing the relative permeability. The retention of polymer inside the reservoir pores gives rise to three phenomena. Absorption of the polymer is predominantly observed in regions farther away from the wellbore, while areas closer to the wellbore experience a more significant impact from mechanical entrapment and hydrodynamic retention. This is attributed to the higher flow velocities near the wellbore. Therefore, the injected fluid would not quickly overtake the oil displaced. Due to the complexity of changing the properties of the rock/fluid reservoir system, the injected fluid is designed to modify its properties according to the features of the reservoir. The polymer injection method can easily displace the oil bank ahead through the reservoir to the producing wells, but this increase could affect an essential indicator of polymer projects, which is its injectivity (Akbari et al., 2019; Glasbergen et al., 2015; Li et al., 2020; Machale et al., 2020; Tackie-Otoo et al., 2020).

Table 2-1 Polymer Flooding Summary

Mechanisms	Limitations	Problems	Source
Viscosity increase	Polymer retention, high injection pressures and high polymer concentration.	Reduced injectivity and operational cost increased.	**(Alfazazi et al., 2020; Romero-Zeron, 2012)**
Mobility control	Polymer retention, high polymer concentration and water quality.	Formation damage, operational cost increased.	**(Delamaide, 2014; Sofia & Djamel, 2016)**
Heterogeneity control	Formation damage, high polymer concentration and permeability effects.	Operational cost increased, reduction in reservoir permeability.	**(Romero-Zeron, 2012)**
Contact improvement	Polymer adsorption, reservoir heterogeneity and high polymer concentration.	Formation damage, operational cost increased.	**(Skauge et al., 2018; Thomas et al., 2019)**
Sweep improvement	Reservoir heterogeneity, fractures and high injection rates.	Reduced injectivity and operational cost increased.	**(Thomas et al., 2019)**

2.1.1.1 Polymers

Chemicals called polymers are added to improve sweep efficiency; many of these polymers are used for well drilling and rock fracturing, improve the injectivity profile, and act as viscosifying agents. EOR projects use two types of polymers: synthetic polymers and biopolymers. The most common synthetic polymer used is partially Hydrolyzed Polyacrylamide (HPAM), while Xanthan Gum is the most common biopolymer used (Al-Shakry, Skauge, et al., 2018; Rosa et al., 2006).

When the polymer solution is injected, as shown in Figure 2-3, it pushes the oil from the reservoir towards the producing well and improves the oil sweep by increasing viscosity. It is essential to verify that the polymer properties are suitable for the geological characteristics of the reservoir to avoid pore plugging. Another factor to consider is the stability of the polymer, as some materials tend to degrade under harsh conditions, especially acrylamide-based polymers (Scott et al., 2020).

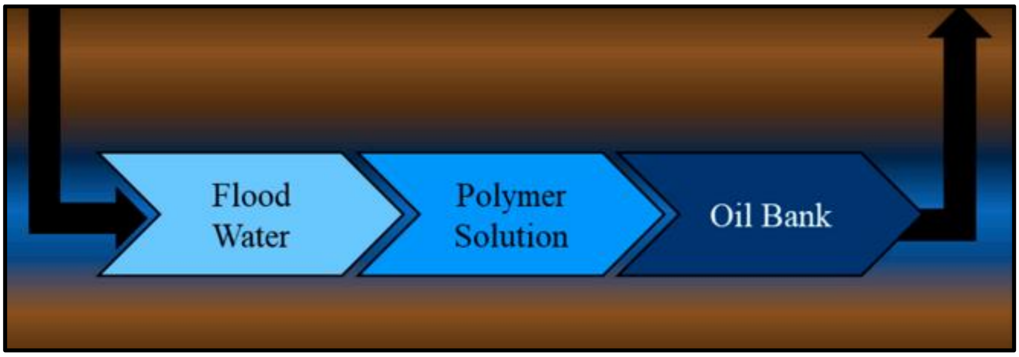

Figure 2-3: Simplified schematic of the polymer flooding process (Scott et al., 2020)

Several factors can affect polymer viscosity, such as salt concentration, solution temperature, degree of hydrolysis, molecular structure, molecular weight, polymer concentration, pH, flow model, and type of forces that dominate the flow. Additionally, pressure can also influence polymer viscosity. It's important to note that the polymer solution's viscosity needs to be suitable for the geological characteristics of the reservoir to avoid pore plugging. Polymer stability is also a critical factor to consider, especially for acrylamide-based polymers, which can degrade under harsh conditions (Al-Shakry, Skauge, et al., 2019; D. A. Z. Wever et al., 2011).

2.1.1.1.1 HPAM

Partially hydrolyzed polyacrylamide (HPAM) is a copolymer of Polyacrylamide (PAM) and a polyacrylic acid. It is the most commonly used polymer in polymer flooding projects due to its low manufacturing cost and availability in large quantities. HPAM is easily modified to suit the specific geological characteristics of the reservoir and can be applied in large-scale projects. Its structure is shown in Figure 2-4 (Alzaabi et al., 2020; Machale et al., 2020; Pu et al., 2018).

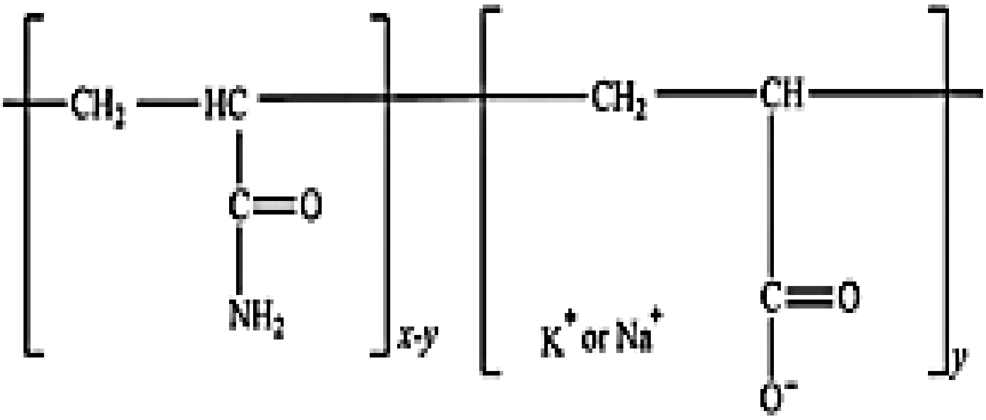

Figure 2-4: HPAM structure (Machale et al., 2020)

It is important to note that the hydrolysis degree of HPAM is a crucial factor that determines its performance. The typical range of hydrolysis degree is between 25-33%, as this range allows the polymeric material to change chemical composition, giving rise to carboxylic acid groups from amide groups. These carboxylic acid groups are responsible for the polymeric structure's electrostatic charges, which are crucial for its stretching and viscosity enhancement. Maintaining a minimum limit of 25% is essential to ensure the optimum performance of HPAM. However, maintaining a high hydrolysis degree can be disadvantageous, as it can make the solution more sensitive to the salinity and hardness of the brine. Hence, the hydrolysis degree must be chosen carefully, keeping in mind the salinity and hardness of the reservoir brine (Alzaabi et al., 2020; Scott et al., 2020; D. A. Z. Wever et al., 2011).

HPAM exhibits pseudoplastic or shear-thinning behavior under rheometer conditions, making it ideal for polymer injectivity. This behavior is described by the power law equation, where the velocity increases in a laminar flow, and the polymer coils unravel and rearrange. However, HPAM exhibits apparent shear thickening above the critical shear rate in porous media or in-situ flow. As a result, the apparent viscosity peaks in regions close to the wellbore, a phenomenon known as extensional viscosity. This behavior is a characteristic of the polymer's extensional flow regime(Al-Shakry, Skauge, et al., 2019; Alzaabi et al., 2020).

Figure 2-5 illustrates the relationship between the apparent viscosity of HPAM and the shear rate. The polymer behaves almost like a Newtonian fluid at low shear rates, with its viscosity remaining constant. As the shear rate increases, the viscosity decreases, indicating shear-thinning behavior. During this period, the polymer molecules unravel and stretch out as the shear rate increases, eventually reaching a highly stretched state where the viscosity levels off at a Newtonian plateau. After this plateau, when the shear rate $\dot{\gamma}c$ is greater than $\dot{\gamma}c2$, the polymer chains do not have enough time to align, resulting in a gradual increase in the apparent viscosity with the shear rate until reaching a maximum point. If the shear rate is increased further, the polymer chains fragment due to mechanical degradation, causing the viscosity to decrease at high shear rates (Al-Shakry, Skauge, et al., 2019).

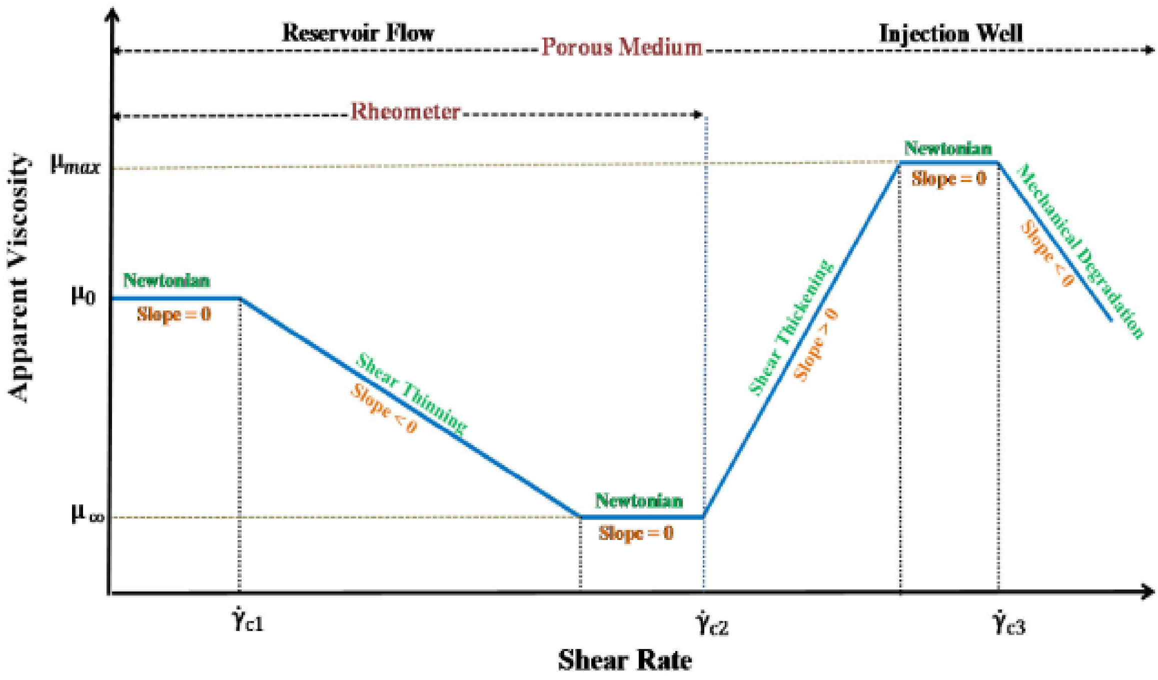

Figure 2-5: HPAM apparent viscosity versus shear rate scheme (Al-Shakry, Skauge, et al., 2019)

2.1.1.1.2 Biopolymers

Recently, there has been a growing interest in using biopolymers for polymer flooding due to their eco-friendliness and higher mechanical stability than synthetic polymers. This is because biopolymers have a unique helical structure that can be double or triple, with stiff and charge-free chains. Table 2-2 Advantages of biopolymers over synthetic polymers

Property	Biopolymer in Comparison with HPAM	Source
Rheological	Biopolymers show stronger shear-thinning because the conformational status exhibited by polysaccharide molecules makes them more rigid ideal for better injectivity.	(Clinckspoor et al., 2021; Pu et al., 2018)
Shear Rate	Biopolymers show better stability against shear rate for polymer viscosity versus shear rate behavior.	(Jang et al., 2015; Pu et al., 2018)
Salinity	The effect of salinity it is insignificant compare with HPAM.	(Clinckspoor et al., 2021; Muhammed et al., 2020)
Temperature	Biopolymer have better thermal stability, could resist temperatures over 80°C and maintain constant the solution about 2 years, there are some exceptions as Guar Gum.	(Fournier et al., 2018; Freire Filho & Moreno, 2022; Jensen et al., 2018)
Adsorption	Biopolymer retention is generally between (38 to 78 Lbm/acre-ft), whereas for HPAM it is between (35 to 1000 Lbm/acre-ft).	(Muhammed et al., 2020)
Polymer Mobility	Based on properties analyzed above, Biopolymers have further performance about effect of viscous fingering and polymer mobility than HPAM.	(Jensen et al., 2018; Tackie-Otoo et al., 2020)

compares the characteristics of the most commonly used biopolymers, showing they have similar advantages. Unlike HPAM, they have good compatibility with salt and harsh conditions. However, their main disadvantage is the high cost and the risk of plugging due to cell debris and chemical degradation(Pu et al., 2018; Scott et al., 2020; Tackie-Otoo et al., 2020).

Table 2-2 Advantages of biopolymers over synthetic polymers

Property	Biopolymer in Comparison with HPAM	Source
Rheological	Biopolymers show stronger shear-thinning because the conformational status exhibited by polysaccharide molecules makes them more rigid ideal for better injectivity.	(Clinckspoor et al., 2021; Pu et al., 2018)
Shear Rate	Biopolymers show better stability against shear rate for polymer viscosity versus shear rate behavior.	(Jang et al., 2015; Pu et al., 2018)
Salinity	The effect of salinity it is insignificant compare with HPAM.	(Clinckspoor et al., 2021; Muhammed et al., 2020)
Temperature	Biopolymer have better thermal stability, could resist temperatures over 80°C and maintain constant the solution about 2 years, there are some exceptions as Guar Gum.	(Fournier et al., 2018; Freire Filho & Moreno, 2022; Jensen et al., 2018)
Adsorption	Biopolymer retention is generally between (38 to 78 Lbm/acre-ft), whereas for HPAM it is between (35 to 1000 Lbm/acre-ft).	(Muhammed et al., 2020)
Polymer Mobility	Based on properties analyzed above, Biopolymers have further performance about effect of viscous fingering and polymer mobility than HPAM.	(Jensen et al., 2018; Tackie-Otoo et al., 2020)

Xanthan gum is a polysaccharide or polycarbohydrate that finds wide usage across several industries such as cosmetics, paint, textiles, food, pharmaceuticals and petroleum. It is produced through the fermentation of glucose by different bacteria, with Xanthomonas campestris considered the most efficient producer. The chemical structure of Xanthan Gum, show in Figure 2-6, reveals the presence of several carbohydrates including glucose, mannose and glucuronic units (Gbadamosi et al., 2019; Machale et al., 2020).

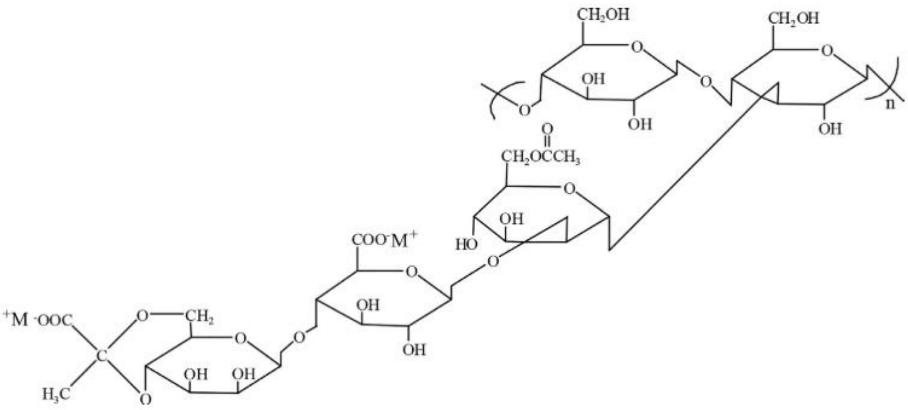

Figure 2-6: Xanthan Gum Structure (Tackie-Otoo et al., 2020)

Compared to HPAM, xanthan gum has a more rigid structure, making it more resistant to mechanical shear and high salinity and divalent ion concentrations. It exhibits shear-thinning behavior at high shear rates, which is appropriate for field operations. This behavior is due to a phenomenon where the hydrogen bonds and polymer entanglements integrate, resulting in high viscosity at low shear rates. However, these aggregations break up in fast shear fields, leading to a rapid decrease in viscosity at high shear rates. To model its non-Newtonian behavior, the Herschel-Bulkley and Ostwald models are used to analyze its rheological properties (Gbadamosi et al., 2019; Pu et al., 2018; Tackie-Otoo et al., 2020).

Xanthan Gum has great viscoelastic behavior that improves the sweep efficiency value due to its behavior being more influenced by its elastic nature than by its viscous nature. As the concentration of Xanthan gum solution is increased, it becomes more elastic and has a slower relaxation mechanism (Machale et al., 2020; Tackie-Otoo et al., 2020).

The use of xanthan gum as a polymeric solution has shown resistance to high temperatures and high ionic strength conditions, with viscosity loss only occurring at temperatures above 100°C. This improved stability is attributed to a transition from a disorderly conformation to a more orderly and rigid structure after the integration of salt. Xanthan gum has also been used in combination with surfactants, resulting in promising outcomes. For instance, the use of a polymer solution with alkyl propoxy ethoxysulfate as a surfactant has led to a residual oil recovery of over 50% when applied after a water injection results obtained by core floodings experiments (Gbadamosi et al., 2019; D. A. Z. Wever et al., 2011).

While Xanthan gum solutions have impressive characteristics, they are susceptible to bacterial degradation by salinity-tolerant aerobic and anaerobic microorganisms. This degradation can result in a loss of viscosity and ultimately reduce the effectiveness of the polymer solution. To combat this issue, biocides can be used to inhibit the growth of these microorganisms. However, the most widely used biocide, formaldehyde, can cancel out the environmental benefits of using the polymer and increase the cost of polymer flooding (Gbadamosi et al., 2019; D. A. Z. Wever et al., 2011).

Scleroglucan is produced through the fermentation of the sclerotium glucanicum fungus. Generally, the 3-chain Scleroglucan is assembled into a triple-stranded helix that is stabilized by hydrogen bonds, as shown in Figure 2-7. Compared to HPAM, the triple helix configuration and rigidity of the polymeric chain improve its resistance to mechanical degradation, making it tolerant to high temperatures and resistant to shear stress. Its thermal stability is due to its lack of easily hydrolysable groups such as acrylamide (Fournier et al., 2018; Muhammed et al., 2020).

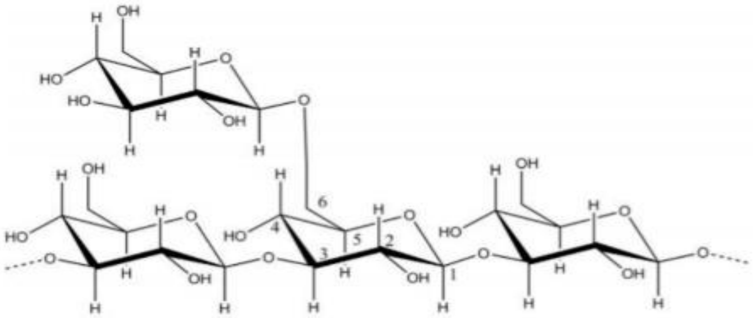

Figure 2-7 Scleroglucan Molecular Structure (Jensen et al., 2018)

Scleroglucan is a non-ionic polymer that exhibits good stability under harsh conditions and high salinity, making it a promising candidate for various applications. Its resistance to mechanical degradation and high temperatures can be attributed to its triple helix configuration and rigid polymeric chain structure. Furthermore, Scleroglucan shows remarkable durability under a range of pH and mineral conditions. However, a major drawback of Scleroglucan is its poor filterability, which limits its field application due to the ineffectiveness of conventional filtering methods. Efforts are underway to overcome this limitation through innovative filtration strategies (Jensen et al., 2018; Pu et al., 2018).

Scleroglucan exhibits similar viscosity behavior to xanthan gum at high flow rates, but it performs better under low flow conditions, displaying higher *in-situ* viscosity. It shows a pseudoplastic behavior with an exponential relationship between its apparent viscosity and the polymer concentration(Jensen et al., 2018; Muhammed et al., 2020).

Guar gum is a polysaccharide obtained from the seeds of the Cyamopsis tetragonolobus plant, and it is widely used in various industrial applications due to its thickening, stabilizing, and binding properties. In the petroleum Industry they have required as drilling fluids formulations, green corrosion inhibitors, dispersants, and other applications. (Freire Filho & Moreno, 2022; Hasan & Abdel-Raouf, 2018; Pu et al., 2018).

The structure of guar gum molecules is composed of a backbone of (1→4)-β-D-mannopyranosyl groups, with side chains of D-galactose randomly attached by α-1,6 linkages, as shown in Figure 2-8 (Clinckspoor et al., 2021; Freire Filho & Moreno, 2022)

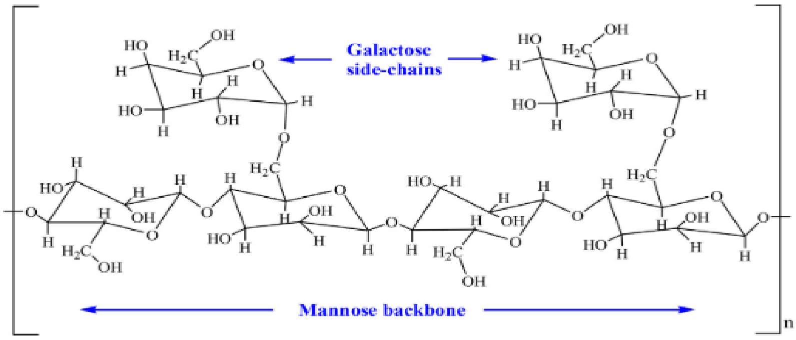

Figure 2-8 Guar Gum Molecular Structure (Pu et al., 2018)

Guar gum solutions exhibit a temperature-dependent viscosity behavior where the viscosity increases with temperature due to the insolubility of some molecules at low temperatures, but rapidly decreases at higher temperatures, indicating poor thermal stability. In terms of rheological properties, the viscosity of guar gum solutions is more sensitive to temperature changes compared to xanthan gum solutions. Additionally, guar solution viscosity is less affected by salinity than xanthan solution viscosity (Freire Filho & Moreno, 2022; Hasan & Abdel-Raouf, 2018).

2.1.2 Surfactant Polymer (SP)

The term "surfactant" is short for "surface active agent". Surfactants reduce interfacial tension (IFT) and can alter the wettability of the reservoir between oil and water due to their hydrophobic and hydrophilic components. In ultra-low IFT reservoirs, surfactants have two main functions. Firstly, they increase the mobility of residual oil and create an oil bank, where a continuous phase of water and oil is formed. Secondly, they prevent the displaced oil from being trapped by capillary forces. However, an adverse effect of water salinity is the potential degradation of synthetic polymer solutions. To alleviate this problem, a pre-wash can be done to displace the seawater, though it can be challenging to remove all the water from the reservoir. Therefore, both smart water flooding and polymer flooding with surfactants exhibit comparable characteristics as they both aim to modify the wettability of the reservoir rock, ultimately leading to improved oil recovery (Kakati et al., 2020; Machale et al., 2020; Rosa et al., 2006).

The order of injection of the chemical agents in an EOR process depends on the specific objective. If the aim is to prevent the fingering of water into the surfactant zone, injecting the polymer charge after the surfactant is recommended. Conversely, when the goal is to achieve a uniform oil sweep, polymers are commonly employed as sacrificial agents to facilitate this process. It is important to note that despite the injection sequence, diffusion and scattering in the pore space could lead to the mixing of the chemicals. The surfactant loading typically ranges from 3% to 30% concerning the pore volume (PV), depending on the design of the EOR process (Gbadamosi et al., 2019).

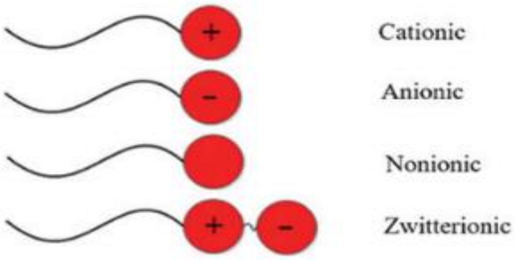

Figure 2-9: Surfactants Classification (Machale et al., 2020)

Figure 2-9 show the amphiphilic structure of surfactants, which consists of two parts: the head, which is the hydrophilic part, and the tail, which is the hydrophobic part. Four types of surfactants are based on the charge presented by their hydrophilic portion: anionic, cationic, non-ionic, and zwitterionic. Anionic surfactants have a negatively charged head and are widely used for their low adsorption capacity in sandstones and clays, stability, and low price compared to other groups. Cationic surfactants have a positive charge and can improve the rate of water imbibition in oil-wet carbonate rocks, but their main disadvantage is the high adsorption that occurs when they are in contact with negatively charged surfaces. Non-ionic surfactants, without a charge, are used as co-surfactants that can improve the physical properties of surfactant solutions. Lastly, there is a group of surfactants known as zwitterionic surfactants, which are distinguished by their unique structure that includes both positive and negative charges within the head group (Gbadamosi et al., 2019; Machale et al., 2020).

2.1.3 Alkali Surfactant Polymer (ASP)

The ASP method combines miscible methods to improve sweep efficiency. This method utilizes alkaline solutions and surfactants with polymers. The alkaline component emulsifies crude oil, reduces IFT, and reduces surfactant adsorption for improved mixture behavior. An essential mechanism of this method is the generation of foam in the porous medium due to the reaction between the alkaline component and organic acids in the oil (Ezekwe, 2010; Machale et al., 2020).

Typically, the first slug is a mixture of alkaline and surfactant, which works synergistically to reduce the IFT between the injected and displaced fluid and reduce residual oil saturation. Next comes the polymer slug, which improves the sweep efficiency by reducing the mobility ratio. Finally, water injection is used to improve oil recovery (Gbadamosi et al., 2019; Rosa et al., 2006).

The application of ASP flooding has some limitations, such as the potential for surfactant precipitation and scale problems, as well as the treatment of produced emulsions and water. These issues can lead to high costs for implementation, making it essential to conduct detailed studies on the geology and engineering of the reservoir before applying the ASP method. By addressing these limitations, ASP flooding can become a more effective method for enhancing oil recovery in reservoirs (Machale et al., 2020; Rosa et al., 2006).

The abovementioned limitations are significant challenges that need to be addressed in applying ASP flooding. For instance, surfactant precipitation can occur due to the interaction between the alkaline solution and the divalent metal cations present in the brine of the formations. Therefore, applying ASP flooding is not recommended for carbonate formations due to the deposition of precipitated materials that can cause wellbore plugging. Also, emulsification is a common issue due to the strong interaction between the solutions and the oil/water interface. The resulting emulsions are difficult to separate and process in the separators, leading to significant operational challenges. Moreover, the chemicals involved in ASP flooding have a great environmental impact due to the high content of oily solids in suspension. Addressing these limitations requires detailed studies on the geology and engineering of the deposit to optimize the design and minimize the environmental impact of the process (Machale et al., 2020).

2.2 Polymer Flooding Screening

The selection process involves evaluating the studied process through a "go/no go" decision-making process. This process consists of collecting and analyzing data from field cases to compare with summary tables of successful applications made previously. It is the starting point of the design of the polymer flood and aims to improve collaboration between researchers to enhance project decision-making based on others' experiences. The process follows a logical sequence from data to information, knowledge, and ultimately wisdom (Alvarado & Manrique, 2010; Carolina et al., 2019).

Screening evaluation includes laboratory and geological work, reservoir modeling, economic analysis, and pilot tests conducted in the field. Procedures for polymer project design should consist of detailed characterization of parameters such as lithology, pressure, temperature, API viscosity, porosity, permeability, net thickness, fractures and heterogeneity, clay content, and salinity. Table 2-3 and Table 2-4 show the range of operating parameters for polymer flooding (Sheng et al., 2015).

Table 2-3 Literature review on screening criteria for polymer flooding section 1

Source	Field Name	Polymer Type	Concentration (ppm)	Lithology	Temperature (°C)	Salinity (ppm)	Oil Viscosity (cP)	Recovery Method	Injection Rate (BPD)	Injected PV
(Sandiford, 1964)	West Cat Canyon	HPAM	370	Sandstones	63	NM	110	Tertiary	500	<0.5
(Pye, 1964)	NIAGARA	PAM	NM	Sandstones	NM	NM	16	Tertiary	NM	NM
(Jones, 1966)	Vernon/Upper Squirrel	HPAM	500	Sandstones	24	NM	75	Tertiary	NM	0.3
(Ustick, 1967)	Huntington Beach/Garfield	HPAM	346	Sandstones	51	11803	76	Tertiary	NM	0.3
(Littmann et al., 1992)	Eddesse-Nord	Xanthan	800	Sandstones	22	120000	7	Tertiary	NM	0.7
(Corlay et al., 1992)	Daqing / Putuahoa form, PO	HPAM	915	Sandstones	45	2000-6000	9.5	Tertiary	455.4	0.75
(Putz et al., 1994)	Chateaurenard / Courtnay	HPAM	900	Sandstones	30	400	40	Tertiary	660.45	1
(Shahin & Thigpen, 1996)	White Castle	HPAM (NaCl 3857)	500	Sandstones	NM	NM	4	NM	513	NM
(De Melo et al., 2005)	Carmopolis	HPAM (Flopam SNF)	1000	Sandstones	50	30000	50	NM	1037	0.1
	Buracica	HPAM	500	Sandstones	60	33000	10.5	Secondary	1258	1.1
	Canto de Amaro	HPAM	800	Sandstones	55	500	20	Tertiary	754.8	
(Tiwari et al., 2008)	Sanand / KS-III	HPAM	600 to 800	Sandstones	85	NM	20	Tertiary	3347.72	0.15
(Moe Soe Let et al., 2012)	Tambaredjo	HPAM	NM	Sandstones	38	5000	500	Tertiary	175	0.16
(Pérez et al., 2017)	Palogrande-cebu	Surfactant + Polymer	1000	Sandstones	98	150	0.64	Tertiary	NM	NM
(Puskas et al., 2017)	Algyo	NM	1500	Sandstones	50	20000	19	Tertiary	NM	NM
(Martino et al., 2017)	Grimbeek	HPAM	NM	limestone	83	230000	0.58	Tertiary	211.34	NM
(Batonyi et al., 2016)	ABK	Flopaam 3330	NM	Sandstones	NM	1000	NM	Secondary/ Tertiary	6300	NM
(Wu et al., 2016)	Medicine Hat	crosslinked polymer and Soft microgel	NM	sand-conglomerate	20	4212	80	Tertiary	NM	NM

Table 2-4 Literature review on screening criteria for polymer flooding section 2

Source	Field Name	Polymer Type	Concentration (ppm)	K (mD)	Ø (%)	Depth (ft)	Thickness (ft)	Water Cut Before PF (%)	Scale
(Sandiford, 1964)	West Cat Canyon	HPAM	370	260	21	3100	48	90	Pilot
(Pye, 1964)	NIAGARA	PAM	NM	20	NM	750	10	75	Pilot
(Jones, 1966)	Vernon/Upper Squirrel	HPAM	500	1-120	20.6	975-1050	17	90	Pilot
(Ustick, 1967)	Huntington Beach/Garfield	HPAM	346	2300	34	2500	53	95	Pilot
(Littmann et al., 1992)	Eddesse-Nord	Xanthan	800	1013	26	1150	16.4	80-97	Pilot
(Corlay et al., 1992)	Daqing / Putuahoa form, PO	HPAM	915	100-3000	31	3051	67.3	85	Pilot
(Putz et al., 1994)	Chateaurenard / Courtnay	HPAM	900	2000	30	1969	10.5	89	Commercial
(Shahin & Thigpen, 1996)	White Castle	HPAM (NaCl 3857)	500	2	32	5756	10	NM	Pilot
(De Melo et al., 2005)	Carmopolis	HPAM (Flopam SNF)	1000	100	NM	NM	NM	NM	Pilot
	Buracica	HPAM	500	300	NM	NM	NM	NM	Pilot
	Canto de Amaro	HPAM	800	204	NM	NM	NM	NM	Pilot
(Tiwari et al., 2008)	Sanand / KS-III	HPAM	600 to 800	1500	24-32	4350	23	50-60	Pilot to Commercial
(Moe Soe Let et al., 2012)	Tambaredjo	HPAM	NM	4000-12000	28.6	1000	40	80	Pilot
(Pérez et al., 2017)	Palogrande-cebu	Surfactant + Polymer	1000	70	23.7	5905-6233	16.4-98.42	NM	NM
(Puskas et al., 2017)	Algyo	NM	1500	500	20-30	3772	65.61	NM	NM
(Martino et al., 2017)	Grimbeek	HPAM	NM	5	20-25	NM	50-60	NM	NM
(Batonyi et al., 2016)	ABK	Flopaam 3330	NM	650	23	2790	23	NM	NM
(Wu et al., 2016)	Medicine Hat	crosslinked polymer and Soft microgel	NM	649	19.9	1141-1410	25.4	NM	NM

Extensive laboratory research has been conducted on biopolymers; however, their practical applications in the field still need to be improved, with Xanthan Gum Solutions being the most widely used (Tackie-Otoo et al., 2020). On the other hand, a pilot test using Scleroglucan had shown promising results, suggesting potential future applications (Kozlowicz et al., 2019). Both works concur that further tests and research are necessary to fully explore the practical applications of these biopolymer solutions in the field.

2.2.1 Lithology

The screening of variables can have two categories: quantitative and qualitative. In the case of lithology, it is a qualitative variable since it shows us the nature of the formation or rock that a number cannot represent. It also has a determining value for the design of a polymer flood since it is related to parameters that can vary too much depending on the type of formation that the reservoir has (e.g., porosity, permeability, clay content, and oil viscosity)(Aldhaheri et al., 2016; Wang, 2013).

Polymer flooding projects are mainly applied in sandstone formations because of their higher permeability than carbonate reservoirs. Furthermore, carbonate formations are more complex due to their mineral composition, matrix pore structures, and fracture density. This is supported by the fact that 1507 projects conducted worldwide show a similar trend, as shown in Figure 2-10 (Alvarado & Manrique, 2010; Han et al., 2014).

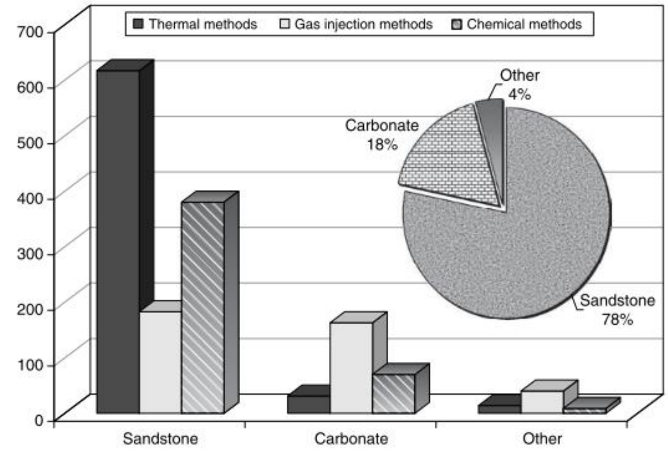

Figure 2-10: EOR methods by lithology(Alvarado & Manrique, 2010)

The existence of different minerals can affect the performance of the polymer injected into the reservoir. For example, the presence of clays is detrimental because when they come into contact with water, they swell, which affects the polymer mobility during injection. Minerals like calcium increase polymer adsorption. (Rellegadla et al., 2017).

2.2.2 Pressure and Depth

The polymer injection is typically carried out below the formation partition pressure to avoid fractures. Depth and Pressure are relevant since the more profound the formation, the higher the injection pressure. In addition, Depth affects the polymer injectivity and the injected volume due to the gelation time of the polymer, and the pressure affects the polymer viscosity (Aldhaheri et al., 2016; D. A. Z. Wever et al., 2011).

2.2.3 Temperature and Salinity

The rheology of the polymer is affected by temperature because it can delay the onset of expansion behavior and affect the critical shear rate of the polymer. In the case of HPAM, high temperatures and salinity can negatively affect its viscosity and cause rapid mechanical degradation. Biopolymers such as Xanthan Gum have greater resistance to harsh conditions, but they are more susceptible to microbial attack, which can lead to Biological degradation (Muhammed et al., 2020; Skauge et al., 2018; Zhu et al., 2017).

Studies have reported that polymer flooding can withstand a reservoir temperature close to 100°C, with an average temperature of 46.1°C. Xanthan gum has been shown to have good thermal stability at 70°C and has a resistance up to a temperature of 100°C; from this temperature, the viscosity of the solution begins to decrease. Its thermal stability depends on the salinity present in the system (Kamal et al., 2015; Muhammed et al., 2020).

Hydrolysis of synthetic polymers can begin at 60°C. When the polymer dissolves in water, its molecules easily expand, and the zone of shear thinning decreases due to the electrostatic repulsion they experience as the degree of hydrolysis increases. Harsh conditions and oxygen contamination can cause hydrolysis at any temperature (Skauge et al., 2018).

The degree of hydrolysis (DOH) is mainly affected by temperature and pH. It has different temperature ranges, with a faster reaction occurring at 90 °C than a negligible reaction at 50°C. In low salinity conditions, HPAM experiences a slight increase in apparent viscosity. Conversely, high concentrations of monovalent ions (e.g., Na^+) show high salinity conditions reduce in viscosity; this impact is higher in the presence of divalent ions. For Xanthan Gum, the presence of electrolytes make the chain more rigid and stable (de Moura & Moreno, 2019; Kamal et al., 2015; Muhammed et al., 2020).

2.2.4 Oil viscosity

The reservoir oil viscosity is a limiting factor for the applicability of polymers because the higher the oil viscosity, the higher the polymer concentration needed, which may not be economically viable. Additionally, increasing the viscosity of the polymer solution can create injection difficulties, as highly viscous fluids may not be able to enter low-permeability areas in the formation (Kamal et al., 2015; Rellegadla et al., 2017).

The reservoir oil viscosity is strongly related to the mobility ratio between the water and oil phases, as high oil viscosity values cause the water to flow through the oil by Fingering effects. It is important to optimize these characteristics to work with the minimum concentration and obtain reasonable performance. Figure 2-11 shows that the recovery factor tends to decrease as the oil viscosity in the reservoir increases, so it is recommended to apply polymer flooding in cases where the oil viscosity is less than 150cP. Therefore, a higher concentration is needed to reduce the mobility ratio (Ghahremani et al., 2018; Wang, 2013).

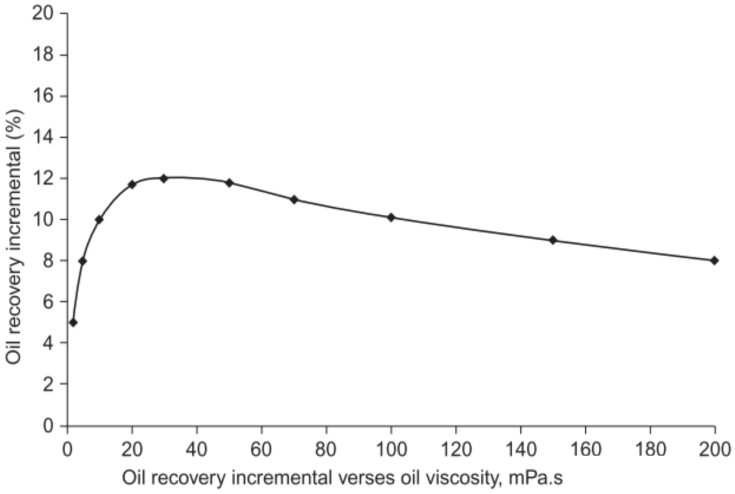

Figure 2-11 Oil viscosity versus oil recovery (Wang, 2013)

2.2.5 Permeability

Reservoir permeability is a critical parameter to consider when screening for polymer flooding. It directly affects the propagation of the polymer within the formation, causing it to be retained in areas of low permeability. As a result, the efficiency of polymer flooding can be reduced if the permeability is too low. Therefore, it is important to carefully evaluate the permeability of the reservoir before deciding on the polymer injection strategy (Wang, 2013; Zhou & Kamal, 2019).

The presence of areas with low permeability in the reservoir can cause a low injection rate, leading to longer polymer flooding times without significant economic improvement. Additionally, a high rate of shear near the wellbore can lead to polymer degradation and reduced polymer injection, affecting the pressure conditions. Therefore, it is important to consider the permeability of the reservoir during the screening process to ensure optimal performance of polymer flooding (Rellegadla et al., 2017).

Reservoir permeability is the parameter that has been studied the most since the limits of application ranges have changed in polymer flooding during the last decades. It has an application range between 10-3000 mD; polymer propagation with high molecular weight will be challenging for a reservoir permeability of less than ten millidarcy. As Figure 2-12 shows, there may be zones of different permeabilities throughout a formation, that is, areal or vertical (Aldhaheri et al., 2016; Z. Liu et al., 2020).

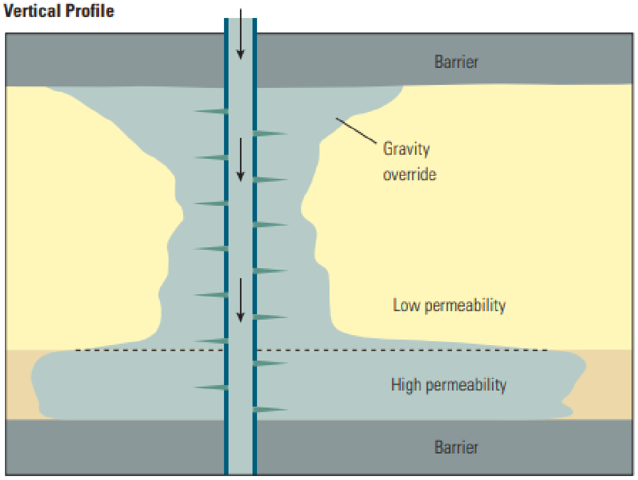

Figure 2-12: Low and **High permeability zones (Al-Mjeni et al., 2010)**

2.2.6 Fractures and Heterogeneity

Formation heterogeneity is a crucial factor to consider in polymer flood projects. Open fractures, channels, and areas of high permeability can create shear zones within the formation, making it difficult to determine its rheology *in-situ* when there is high heterogeneity. Another significant factor is the skin effect, caused by the polymer's adsorption and mechanical entrapment. These factors should be carefully evaluated to ensure the success of the polymer flood project (Alzaabi et al., 2020; Z. Liu et al., 2020).

The permeability variation can be measured by dispersion analysis of values, with a value close to 0 for a homogeneous reservoir and a value close to 1 for a reservoir with considerable heterogeneity (Wang, 2013), Equation (2.3)

$$V_k = \frac{k_{50} - k_{\sigma}}{k_{50}} \tag{2.3}$$

where V_k is the permeability variation, k_{50} is the value permeability at the 50th percentile and k_{σ} is the 84th percentile.

For the design of polymer flood projects, the size of the fracture and its direction must also be considered. Therefore, one way to improve the recovery factor for homogeneous and heterogeneous reservoirs is to inject the fluids under fracturing conditions, i.e., inject above the formation partition pressure (FPP). The generation of fractures is beneficial because they help increase the injection of the polymer solution and can also reduce the degree of mechanical degradation the polymer can undergo. On the other hand, applying this method to reservoirs with high vertical heterogeneity and low oil viscosity may be ineffective (Abbasi et al., 2017; Scott et al., 2020).

Depending on how the fractures have altered the porosity and permeability of the matrix, it can be classified into four types of naturally fractured reservoirs; these can be positive or negative for fluid flow and will depend on how it is structured, i.e., if the fractures are open or sealed by the mineralization that it has had (Tiab & Donaldson, 2016):

1. Fractures provide storage capacity and permeability.
2. The fractures provide the permeability and the matrix provides the porosity.
3. The matrix has good permeability and fractures increase the permeability of the reservoir, which helps to have high flow rates.

4. Fractures have a considerable amount of minerals and impair the permeability and porosity of the reservoir. Normally this type of reservoir is not profitable to produce so it has a high degree of anisotropy and tends to create barriers that prevent fluids from flowing through the rock.

2.3 Polymer Flow Properties

To ensure the success of polymer flooding, it is crucial to thoroughly understand the rheological characteristics and behavior of polymer solutions, whether they are intended for core flooding or well-injection. The viscoelastic properties of the polymer solution play a vital role in the design of polymer flooding, as they determine its ability to modify the viscosity and permeability of the porous medium. We will outline some key aspects in the following section to enhance your understanding of this topic.

2.3.1 Polymer mobility and Permeability reduction

The main objective of polymer flooding is to improve the mobility behavior of the injected fluid concerning the reservoir fluid. The polymer concentration is usually increased to achieve better control, although having a high concentration can generate specific problems, such as injectivity issues and high application costs. Polymer mobility can be measured using the resistance factor (RF). This parameter indicates the change in permeability that has occurred before and after injection under the same conditions (i.e., it is the mobility ratio between the brine and the polymer). The equation for calculating RF is given by Equation (2.4) (Green & Willhite, 2018; Muhammed et al., 2020)

$$RF = \frac{\lambda_{wf}}{\lambda_{pf}} = \frac{\left(\frac{k}{\mu}\right)_{wf}}{\left(\frac{k}{\mu}\right)_{pf}} = \frac{\Delta P_{pf}}{\Delta P_{wf}} \tag{2.4}$$

where λ, k, and μ represent the phase mobility, effective permeability, and viscosity, respectively. RF refers to the resistance factor, and ΔP refers to the differential pressure. The subscripts “wf” and “pf” denote the water and polymer flooding, respectively.

The RF coefficient is an important measure to evaluate the effectiveness of polymer injection in core flooding. For instance, an RF value of 2 suggests that twice the pressure is needed to inject the polymer than water/brine. This coefficient depends on various factors such as the polymer's viscosity, adsorption, and retention (Kakati et al., 2020; Muhammed et al., 2020; Yin et al., 2020).

The reduction in permeability can be evaluated in core flooding by the residual resistance factor (RRF), which indicates the ability of the rock to allow the polymer to flow in front of the water. It is calculated as the ratio of the effective permeability after the polymer injection to the effective permeability before the injection. This parameter provides insight into the degree of adsorption and retention of the polymer in the rock and helps to understand the efficiency of the polymer flooding process. The RRF is expressed by the following Equation (2.5) (Muhammed et al., 2020; Yin et al., 2020)

$$RRF = \frac{\left(\frac{k}{\mu}\right)_{before-pf}}{\left(\frac{k}{\mu}\right)_{after-\,pf}} = \frac{\Delta P_{water\ after-pf}}{\Delta P_{water\ before-pf}} \tag{2.5}$$

where k, and μ represent the effective permeability and viscosity, respectively. RRF refers to the residual resistance factor, and ΔP refers to the differential pressure. The subscripts "pf" denote polymer flooding.

Obtaining a high RRF indicates low injectivity. In addition, a value equal to 1 would be counterproductive since it would mean that there is no reduction in permeability, and fingering could occur due to the adsorption of the polymers and their mechanical entrapment in the porous medium, which is caused by the size of its pores. Therefore, injecting a large polymer bank should be considered to reduce the mobility of the polymer. The RRF is a function of the type and concentration of the polymer, the amount retained in the process, and its size and distribution throughout the core or rock. Retention by polymer adsorption is practically an irreversible process because it needs considerable water to desorb the polymer. This impact can be lessened if the polymer is pre-sheared (Al-Shakry, Skauge, et al., 2018; Green & Willhite, 2018; Sheng, 2013; Sheng et al., 2015).

Low brine salinity has been observed to decrease permeability reduction during polymer flooding, as the brine composition can affect injectivity. The degree of permeability reduction has also been found to remain constant at low shear rates. However, as the shear rate increases, the degree of permeability reduction also increases (Kakati et al., 2020; Veerabhadrappa et al., 2013).

In reservoirs with high heterogeneity, disproportionate permeability reduction can occur. This phenomenon happens due to a poor distribution of permeability, which means having different permeability zones in the rock. When a polymer solution is injected into a heterogeneous reservoir, it can preferentially enter zones with higher permeability, leaving behind zones with lower permeability. As a result, the polymer solution can cause a more significant in permeability in high-permeability zones compared to low-permeability zones, leading to disproportionate permeability reduction. This can lead to the flow of the polymer solution to poor swept zones and increase the oil recovery factor (Gbadamosi et al., 2019).

One way to measure the *in-situ* viscosity of the polymer in the porous medium is to calculate the ratio of the resistance factor to the residual resistance factor. As seen in Equation (2.6), the apparent viscosity describes the macroscopic rheology of the polymer solution in the porous medium. In comparison, the in-situ viscosity it is depends on the configuration of the porous media of the rock, and Bulk viscosity is mainly affected by its molecular structure (Skauge et al., 2018; Sorbie, 1991)

$$\mu_{in\ situ} = \frac{RF}{RRF} * \ \mu_w \tag{2.6}$$

where μ represent the viscosity. RF and RRF refers to the resistance factor and residual resistance factor, respectively. The subscripts “w” refers to water phase.

An alternative method for determining the apparent viscosity of a polymer solution in a porous medium is to use Darcy's law, which requires measuring the permeability and porosity of the rock. These properties are commonly measured in rocks, making this approach convenient. The apparent viscosity can be calculated by combining the measured permeability and porosity values with the flow rate of the injected polymer solution. This method can provide valuable insights into the flow behavior of the polymer in the reservoir, allowing for better design and optimization of polymer flooding operations

$$\mu_{app} = \frac{k * Q * L}{A * \ \Delta P} \tag{2.7}$$

where k, μ, Q, L, A, ΔP refer to Permeability, Viscosity, Flow Rate, Length, Cross sectional Area and Differential Pressure, respectively. The subscript "app" refers to apparent.

Equation (2.7) demonstrates that the Darcy velocity can be calculated by applying Darcy's law, which establishes a relationship between the flow rate, permeability, and pressure gradient of the fluid in the porous medium. It represents the volumetric flow rate per unit cross-sectional area of the core. On the other hand, the superficial velocity is the volumetric flow rate per unit cross-sectional area of the injection pipe. For bulk measurements, the relationship between superficial and average pore velocities can be utilized, as shown in Equation (2.8)

$$\nu = \frac{Q}{A} \tag{2.8}$$

where ν, Q, A refer to Darcy Velocity, Flow Rate and Cross-sectional Area, respectively.

2.3.2 Polymer Retention

A common problem that occurs during polymer flooding is polymer retention, which is a parameter that indicates the amount of polymer that is retained or absorbed within the porous medium. This parameter depends on the polymer concentration, temperature, flow rate, size of the polymer slug, salinity, reservoir rock composition, rock permeability, and wettability. The units of polymer retention are typically expressed in µg/g (Beteta et al., 2020; Kamal et al., 2015; Muhammed et al., 2020).

It is a critical parameter for the polymer flooding design because the slug size must be determined so that the solution can spread inside the reservoir and displace the oil effectively. A high retention value of the polymer could delay the displacement of the oil. Figure 2-13 shows three retention mechanisms: mechanical entrapment, polymer adsorption, and hydrodynamic retention (Carolina et al., 2019; Gbadamosi et al., 2019; Seright, 2017).

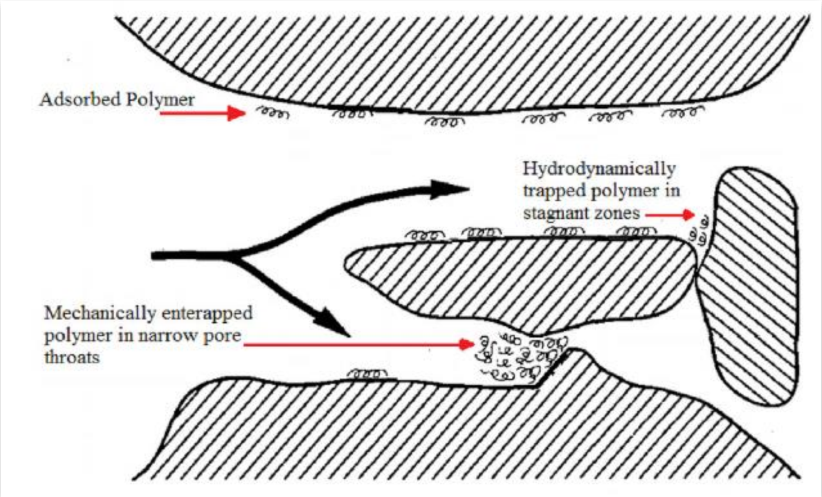

Figure 2-13 Schematic diagram of Polymer retention mechanism in porous medium (Akbari et al., 2019)

Hydrodynamic retention occurs when polymers are temporarily trapped in dead ends or pockets in the porous medium. This retention mechanism has a minor effect and can be disregarded in low flow velocities, as it is only temporary and dependent on the flow rate. Polymer adsorption, on the other hand, has a significant instantaneous and irreversible effect due to the strong interaction between the polymer and the surface of the porous medium. When polymer molecules come into contact with the surface, they can be absorbed by electrostatic interaction due to van der Waal's forces and Hydrogen bonding, leading to retention. This mechanism is mainly dependent on the mineralogy of the rock, especially in the presence of clay and iron content (Akbari et al., 2019; Al-Shakry, 2021; Alfazazi et al., 2020; Scott et al., 2020; Seright, 2017; Sheng, 2013).

Polymer adsorption has been shown not to affect oil relative permeabilities; on the other hand, mechanical entrapment reduces the permeability of the rock as the mechanism increases. It typically occurs when large polymer chains flow through tiny porous throats or narrow pathways that prevent their propagation within the pore space. Generally, the molecules from the polymer solution should be ten times smaller than the pore throat size (Akbari et al., 2019; Scott et al., 2020; Sheng, 2013).

2.3.3 Viscous fingering

Viscous fingering is a phenomenon that occurs due to the instability between the reservoir fluid and the fluid injected into the porous medium. When the oil's viscosity in the reservoir is much higher than the viscosity of the injected solution, it can lead to poor oil displacement performance in polymer flooding. As can be seen in Figure 2-14, fluid B (either the polymer or the displacing fluid) can channel through fluid A (the displaced fluid) because the viscosity of the polymer is lower than that of the displacing fluid (Green & Willhite, 2018; Muhammed et al., 2020).

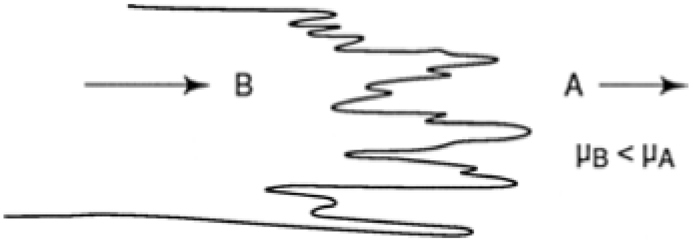

Figure 2-14 Viscous Fingering (Green & Willhite, 2018)

Several factors are related to viscous fingering, including polymer concentration, viscosity, permeability, and temperature. Among these, temperature plays a critical role, as increasing temperature decreases the viscosity and thus lowers the performance. Xanthan Gum is known to have better resistance to viscous fingering than HPAM due to its unique properties (Muhammed et al., 2020).

High salinity can affect HPAM, as it is sensitive to divalent cations. When the polymeric solution comes into contact with a high-salinity environment, the viscosity of the polymer decreases, leading to fingering. This can be attributed to the reduction in the interaction between the polymer chains and the high-salinity environment, resulting in a decrease in the apparent viscosity of the solution (Rellegadla et al., 2017).

2.3.4 Polymer rheology

The rheology of a fluid is analyzed to understand its flow behavior under different conditions and is essential for the design and evaluation of polymer flooding projects. The rheology of a polymer solution depends on factors such as polymer type, polymer concentration, brine composition, and temperature. Under reservoir flow conditions, polymer solutions typically exhibit thinning stress behavior, which is a type of pseudoplastic fluid behavior (Kaminsky et al., 2007; Mohsenatabar Firozjaii & Saghafi, 2020; Muhammed et al., 2020).

The viscosity of the polymer solution is a crucial property for the characterization of fluid rheology, represented by the symbol (η). Two types of flow are relevant for measuring viscosity: shear flow and extensional flow. Shear flow can be measured in the laboratory using a rotational rheometer or viscometer. This flow type is characterized by fluid layers sliding over each other, with the upper layer having the maximum speed and the bottom layer being stationary. To displace the layers, an external force called shear stress (τ) is defined as the force that acts on a specific area. A response to (τ) is needed. Shear stress is defined as the force acting on a particular area. When shear stress is applied, the upper layers are displaced by a distance X concerning the stationary layer, with a vertical distance Y. The resulting relationship between shear stress and shear rate is called the flow curve or viscosity curve. As shown in Figure 2-15, the term shear rate ($\dot{\gamma}$) appears, which is the displacement gradient of the upper layer to the lower layer (Chandran et al., 2019; Sorbie, 1991).

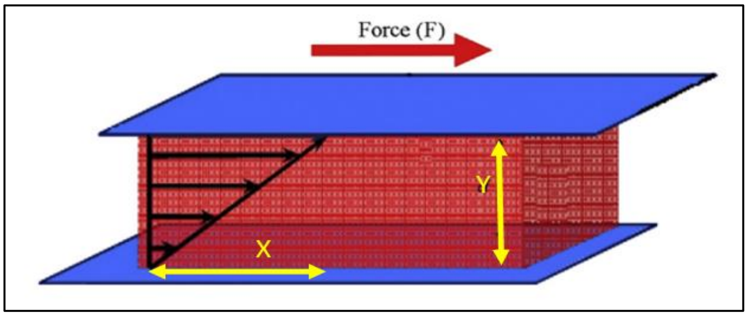

Figure 2-15 Schematic representation of force applied on a fluid placed between two parallel plates (Chandran et al., 2019)

Shear flow has different groups of fluids: Newtonian and Non-Newtonian. The Newtonian flow types are fluids whose viscosity is constant and show a linear behavior between shear stress and shear rate, as shown in Figure 2-16. Polymers have a non-Newtonian fluid behavior (e.g., their behavior is not linear). Dilatant fluids increase viscosity with increasing shear rate (n>1). The most common is pseudoplastic flow, whose apparent viscosity decreases with increasing shear rate (n <1). Pseudoplastic fluids present a rheological profile of 3 regions, as shown in Figure 2-5. The first a low viscosity plateau at high shear rates obtaining infinite viscosity (η_∞). Then, the shear thinning region occurs as the viscosity increases and the shear rate decreases. The third region is found with a low shear rate where the shear viscosity is 0 (η_0). . There are occasions in which the fluid viscosity significantly increases below critical stress, increasing its viscosity to values close to solids. This type of flow is called plastic flow (Chandran et al., 2019; Sorbie, 1991).

Several empirical models have been proposed to describe the behavior of fluid apparent viscosity (η), which is found in Table 2-5. The most common model is the power law model, which describes the behavior of the fluid shear thinning region well and is based on two parameters: the flow consistency index (k) and the flow behavior index (n). Carreou's model represents a fluid that, at low shear rates, follows Newton's law of viscosity, and at high shear rates, it obeys the power law.

Table 2-5 Analytical expressions for η vs γ in simple shear flow (Sorbie, 1991)

Model	Polymer Solution Viscosity	Comments
Power law	$\eta = k * \dot{\gamma}^{n-1}$ k = constant (cps^{n-1}), which is equivalent to Newtonian viscosity as n = 1 n = dimensionless constant, typically in range 0.4 $\leq n \leq$ 1 for pseudoplastic fluids.	• This is mathematically the simplest form of $\eta(\dot{\gamma})$ available • Unsatisfactory behavior of this model at very low and high $\dot{\gamma}$ • n <1 describes pseudoplastic fluid; n >1 describres dilatant fluid
Eyring	$\eta = t_0\tau_0\left(\frac{sinh^{-1} * t_0 * \dot{\gamma}}{t_0 * \dot{\gamma}}\right)$ t_0 = a characteristic time τ_0 = a characteristic stress	• Originally derived from the theory of rate processes. • Empirical extension to the Powell-Eyring model.
Ellis	$\frac{\eta_0}{\eta} = 1 + \left(\frac{\tau}{\tau_{1/2}}\right)^{\alpha-1}$ η_0 = zero shear rate viscosity $\tau_{1/2}$ = value of shear stress at $\eta = \eta_0/2$ α =dimensionless constant	• Ellis model is expressed in terms of the shear stress, τ, rather than shear rate, $\dot{\gamma}$. • α in this model is equivalent to 1/n in power law model. • Because of simple form many analytical results available for Ellis model
Carreau	$\frac{\eta - \eta_\infty}{\eta_0 - \eta_\infty} = [1 + (\lambda * \gamma)^2]^{(n-1)/2}$ η_0 = zero shear rate viscosity η_∞ = infinite shear rate viscosity λ = a time constant n = same as power law index	• Carreau model provides a very good whole range $\eta/\dot{\gamma}$ fit for many polymers systems • η_∞ is often taken as solvent viscosity (i.e., no dilatant region) • This is a four-parameter model comparted with the simpler two-parameter power law model
Bingham	$\eta = \infty \Rightarrow \tau < \tau_0$ $\eta = \mu_0 + \frac{\tau_0}{\dot{\gamma}} \Rightarrow \tau \geq \tau_0$ τ_0 = fluid yield stress below which no motion occurs μ_0 = constant with dimensions of viscosity	• Used mainly for pastes, slurries and drilling muds, which are collectively known as "Bingham plastics"
Herschel-Buckley	$\tau = \tau_o + C\dot{\gamma}^n \quad \tau > \tau_0$ $\tau_o = yield\ stressat\ starting\ flow$ y = shear rate	• When $\tau_0 = 0$, the model reduces to power law model and when $n = 1$ reduce to Bingham plastic model/

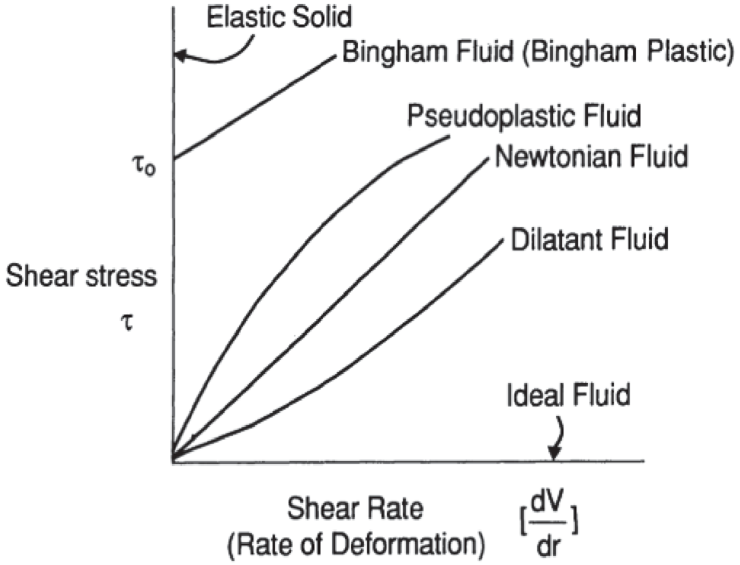

Figure 2-16 Different types of shear stress/shear rate behavior found in polymeric fluids (Sorbie, 1991)

HPAM exhibits Newtonian and non-Newtonian behavior at low and high shear rates, respectively, and can exhibit shear thinning and thickening regions. Its rheology primarily depends on its molecular weight, degree of hydrolysis, polymer concentration, and temperature, and its viscosity is significantly reduced in aqueous solutions with high salinity. In contrast, xanthan gum has better resistance to shear stress than HPAM due to its triple helix configuration, which makes its structure more rigid. Moreover, its rheology is not significantly affected by salinity and temperature, indicating good stability. Table 2-6, shows the background obtained from studies with xanthan gum (Kamal et al., 2015).

Table 2-6 Laboratory works on Xanthan Gum for EOR application

(Source)	Findings
Wei et al. (2014)	Polymer selection depends on reservoir conditions and the intended EOR application. Xanthan gum is stable under high salinity and mechanical shear, with lower retention than HMSPAM but higher than HPAM.
Jang et al. (2015)	The shear viscosity of Xanthan gum solutions is less sensitive to increasing temperatures and salinity compared to HPAM. Therefore, Xanthan gum injection can be more effective than HPAM, particularly under higher salinity reservoir conditions.
Ghoumrassi-Barr and Aliouche (2015)	Xanthan gum is affected by salt cations at low polymer concentrations, with divalent cations having a more significant impact. Strong alkalis affect its rheology more than weak alkalis. Xanthan gum's relative viscosity increases with temperature, but it is less sensitive to changes in mixing water.
Sveistrup et al. (2016)	Xanthan gum and Scleroglucan are powerful biopolymers with long chains and special structures that make them highly viscous. But they react differently to electrolytes and surfactants. Scleroglucan is less affected by electrolytes, while surfactants reduce the viscosity of Xanthan gum. This is because the interactions between the biopolymers and surfactants affect their structure.
Ghoumrassi-Barr and Aliouche (2016)	The viscosifying power and shear-thinning behavior of xanthan gum increases with increasing concentration. The addition of alkali slightly reduces the viscosity, but the shear thinning behavior is still maintained. Temperature has an impact on viscosity, but it remains stable at reservoir temperature. An order-disorder transition occurs between xanthan gum and brine, resulting in a solution that yields unique rheological properties.
(de Moura & Moreno, 2019)	Xanthan gum shows strong pseudoplastic behavior, especially in the semi-diluted region where it greatly increases viscosity. However, it has a limited ability to build viscosity in the diluted region. The effect of temperature on viscosity reduction is more significant than salinity, but higher salinities can help protect xanthan gum in the semi-diluted region from temperature-related viscosity reduction.
(Dakhil et al., 2019)	The study examines the flow behavior of aqueous salt-free xanthan solutions at high shear rates up to 10s−1, focusing on the infinite-shear viscosity plateau. Depending on the xanthan concentration, there are two regimes for the infinite-shear viscosity plateau with different scaling laws for viscosity. At high concentrations, the aqueous xanthan solutions behave like nematic liquid crystals. The normal stress differences increase with an exponent of about 1 in the infinite-shear viscosity plateau, suggesting that they arise from collisions between the polymers rather than viscoelastic deformation.
(Said et al., 2021)	This study modified xanthan gum with acrylic acid (AC) and found that the resulting modified gum had improved rheological properties and increased viscosity at high temperatures. Core flooding experiments showed that the modified gum had a higher rate of oil recovery compared to pure xanthan gum, attributed to its increased viscosity.
(Clinckspoor et al., 2021)	Scleroglucan, Schizophyllan, and Xanthan Gum show similar behavior. Schizophyllan has the highest viscosity and may be a potential EOR additive. Xanthan Gum and Scleroglucan pseudoplasticity allows for better injectivity control. Schizophyllan requires lower concentrations than Xanthan Gum for a target viscosity. Scleroglucan and Xanthan Gum have similar behavior, while Guar Gum is practically Newtonian.
(Freire Filho & Moreno, 2022)	The study compared xanthan and guar gum for improving oil recovery and delaying water production in carbonate rocks. Guar gum had lower retention, provided higher oil recovery, but required a higher polymer concentration and had higher polymer utilization. Xanthan had higher retention, delayed oil recovery improvement, and should be cautiously assessed due to its high retention. Guar gum may be a better option for polymer flooding in carbonate reservoirs at moderate temperatures and salinities.

2.4 Polymer Injectivity

The Injectivity term can be interpreted as a qualitative term (Al-Shakry, Shiran, et al., 2019) expressing how fast a fluid can be injected and spread into a reservoir formation. Mathematically, it is defined as the injection rate divided by the difference between the injection pressure and the average reservoir pressure, as shown in Equation (2.9)

$$I = \frac{Q}{P_w - \bar{P}} = \frac{k_w * h_i}{141.2 * \mu_w * B_w \left(ln \frac{r_e}{r_w} + S \right)} \tag{2.9}$$

where I is the injectivity index [Bbl/Day/psi]; Q is the injection rate [Bbl/Day]; P_w is the bottom hole pressure [psi]; $\bar{P}$ is the reservoir average pressure [psi]; k_w is the permeability [mD]; h_i is the injection height [ft]; μ_w is the water viscosity [cP]; B_w is the water formation volume factor [Bbl/STB]; $\frac{r_e}{r_w}$ is the ratio between wellbore and drainage radio; S is the skin factor.

Injectivity is a term to be very careful about, as it can be crucial for Polymer Flooding project profitability (Lu et al., 2018) since it directly influences the change in flow rate injection (Li & Delshad, 2014). In equation (2.9), there are two variables for which obtaining an exact value is a difficult task, especially in areas close to the wellbore; these are viscosity and downhole pressure (Thomas et al., 2019). The behavior of the polymer within the porous medium depends a lot on its shear rate due to its non-Newtonian fluid nature (Alzaabi et al., 2020).

2.4.1 Background

Reports such as (Manrique et al., 2017) show that the study of commercial and pilot polymer flooding projects had an average reduction of 56% Injectivity. In (Standnes & Skjevrak, 2014), the Injectivity was crucial mainly for six offshore projects of 72 that they studied, and 92% of the cases used synthetic polymer.

To begin any polymer flooding design at any application scale, whether laboratory, pilot test, or commercial (Field), the desired polymer viscosity must be the first term established (Thomas et al., 2019). Considering this, an adequate volume will be defined based on the characteristics of the objective reservoir or core flooding.

Different core-flooding tests that he carried out with polymers, surfactants, and alkaline show that chemical slug size would have a negligible effect on final oil recovery if the fingering and adsorption mechanisms are not dealt with carried out experiments with different injection PV with the same concentration, in which it was shown that slug size greater than 0.5 maintains a good final recovery of oil. However, values between 0.75 and 1 did not show any difference (Ding et al., 2020). It could give us the idea that an optimal size would be between 0.5 to 0.75PV (Juárez et al., 2020).

On the other hand (Seright, 2017) grouped the different polymer applications into three time periods, as shown in Table 2-7. In the first Polymer Flooding applications, there were two beliefs that were disproved over the years, and that can be attributed to one of the reasons why they used low slug volumes. The first one is that there would be a significant improvement in the mobility ratio when injecting polymer after Waterflooding since it would provide a reduction in permeability. In core tests, it can be seen that it would be challenging to have this behavior throughout all reservoirs. The second one, water injection after the Polymer Flooding, would allow the displacement of oil from the less permeable strata due to the fact that the polymers would move through the more permeable zones.

Table 2-7 Polymer Projects grouped by time (Seright, 2017)

Period	Projects	Concentration (ppm)	Polymer Type	PV injected
1960-1980	92	250-260	Mostly HPAM	0.17 Pilots 0.05 Field
1980-1990	171	460	Mostly HPAM	0.1-0.5
1990-Today	NM	1000	HPAM	0.5-1.2

It is necessary to take into account the differences and similarities that exist between waterflooding and Polymer Flooding. Some mechanisms affect them, and knowing them well will significantly help design Polymer Flooding (Glasbergen,2015). Firstly, Polymer Flooding has yet to reach the level of maturity that Waterflooding did (Sieberer et al., 2017). Polymers help to improve the mobility ratio by increasing the viscosity of the injected water (Al-Shakry, Shiran, et al., 2018; Mohsenatabar Firozjaii & Saghafi, 2020). To start a Polymer Flooding, the injection flow rate used in the Waterflooding can be used as a reference while monitoring the viscosity until reaching a suitable value (Thomas et al., 2019). Polymer flooding projects are more profitable than waterflooding when these cases are compared in different scenarios to obtain the best NVP (Raniolo et al., 2013).

2.4.2 Comparison with Waterflooding

In Waterflooding applications, besides injecting water to displace the oil, another objective is maintaining pressure, directly affecting the injection flow. An essential term for Waterflooding and Polymer Flooding is Voidage Replacement Ratio (VRR), which describes the ratio of injected fluid volume to produced fluid volume (Manrique et al., 2017). Mathematically, it is written as Equation (2.10)

$$VRR = \frac{Q_{wi}B_{wi}}{Q_oB_o + Q_{wp}B_{wp}} \tag{2.10}$$

where VRR is the Voidage Replacement Ratio [Dimensionless]; Q is the injection rate [Bbl/Day]; B is the Water volume factor [STB/Bbl]. The subscripts “wi”, “wp” denote initial water and water produced, respectively; The subscript “o” denotes oil.

Many companies aim to maintain a VRR equal to 1 for waterflooding applications, especially if it is a light oil reservoir; this means the pressure remains stable and does not decline. In the case of heavy oil reservoirs, the other way around, obtaining a value less than one turns out to be optimal for oil recovery, as shown in Figure 2-17, since it helps in the activation of mechanisms such as solution gas drive, foamy gas drive, three-phase relative permeability. Obtaining values greater than two shows a severe problem, such as fluid loss in the applied pattern. Just as for heavy oil, in Polymer Flooding applications, having a value less than one does not necessarily mean that the project will no longer be profitable; depending on the strategy with which it is managed, it may have a favorable response for oil recovery (Delamaide et al., 2013; Manrique et al., 2017; Thomas et al., 2019; Vittoratos & Kovscek, 2017).

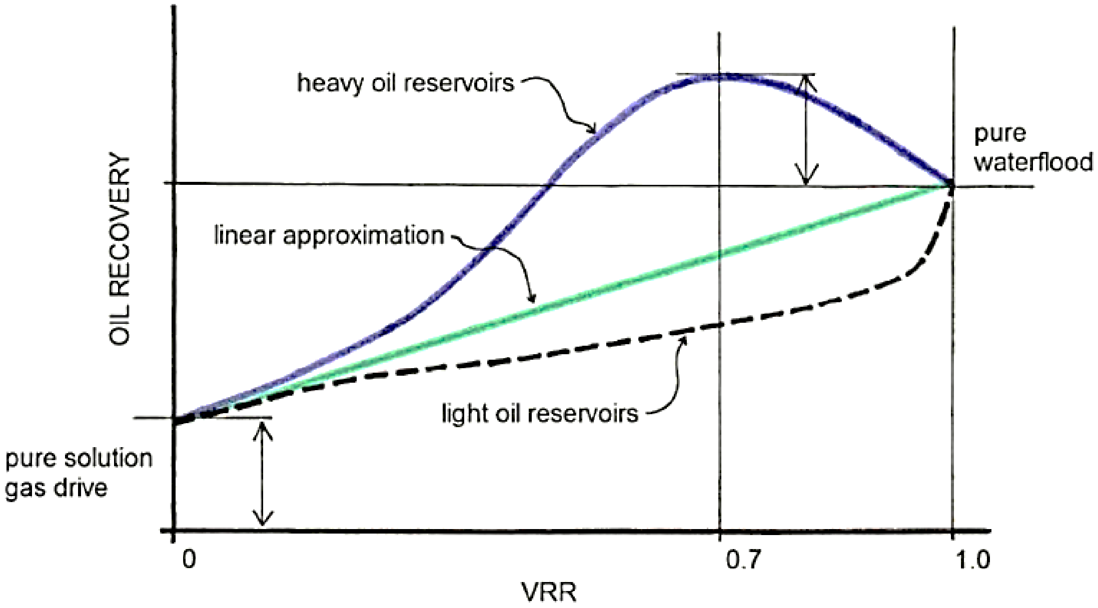

Figure 2-17: Recovery at optimal VRR (Vittoratos & Kovscek, 2017)

Polymer injectivity loss in relation to water is a phenomenon that will always occur (Seright et al., 2008). Figure 2-18 compares different viscosities of Newtonian and non-Newtonian fluids are compared with water viscosity (1cP). After performing injections of 0.1PV for concentrations of 100ppm of Xanthan and HPAM, a drop between 83 and 98% is expected.

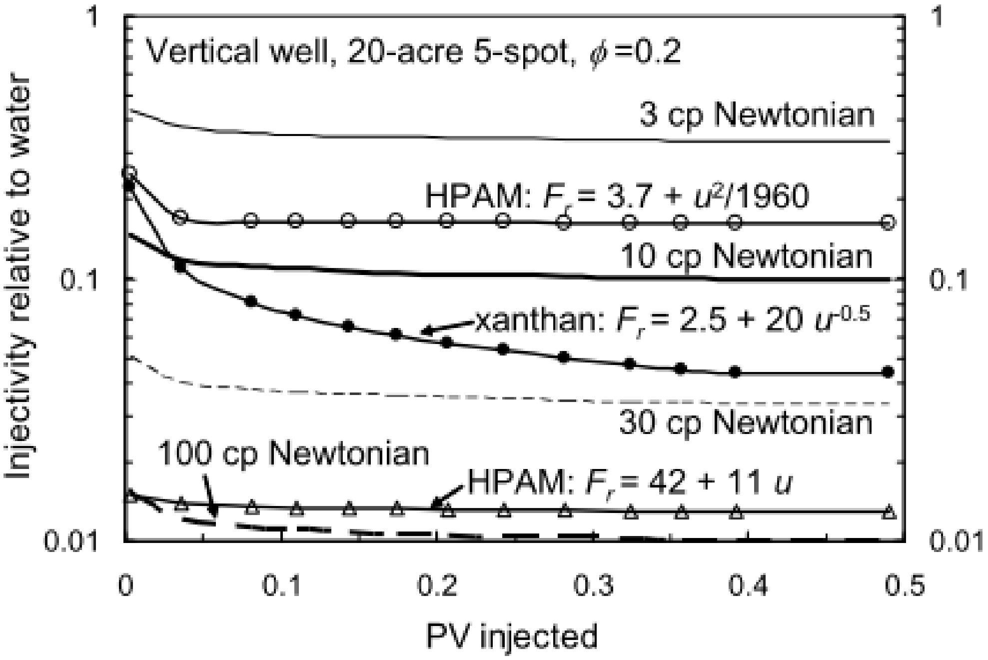

Figure 2-18: Injectivity losses expected for viscous injectants in a unfractured vertical well (Seright et al., 2009)

An example to understand the effect that injectivity has on polymer flooding would be the following: There is an injection of 100bbl/d in the waterflooding stage with a water cut of 95%, and there is a 1 VRR (the oil production would be 5bbl/d). A polymer flooding starts and maintains the same VRR, assuming that the water cut decreased to 75% and there is a 70% injectivity loss (the oil production of 7.5bbl/d would be obtained).

For this case, it is observed that even with a loss of 70%, the oil production in the Polymer Flooding is greater than the waterflooding. In any case, if a more robust analysis had been carried out to make the Injectivity Lossless, it would have been possible to have a better performance for the final oil recovery. This is a simple case to show that injectivity is a crucial parameter for profitability. The water cut reduction plays a favorable role in polymer flooding, while higher losses in injectivity could be detrimental to oil production (Thomas et al., 2019).

2.4.3 Injectivity Loss Mechanisms

Polymer injectivity is a crucial variable for the applicability assessment of polymer flooding projects due to the complexity of reservoir conditions (e.g., the polymers could start having a good performance from the rheometer and end up with poor injectivity in the porous media). It could be classified into three classes (i.e., generic reservoir flooding-related mechanisms, anticipated mechanisms for polymer flood, and undesired mechanisms for polymer flood) (Alfazazi et al., 2020; Glasbergen et al., 2015; Sun et al., 2019)

To evaluate the loss of injectivity, the polymer solution injectivity can be compared to the water injectivity in the same core. For this, it is necessary to know the volumetric injection ratio or superficial velocity and the differential pressure obtained after injecting the brine and the polymer solution. The loss of injectivity is given by Equation (2.11). Getting a value between 0.5 and 0.9 is acceptable. Although to obtain values higher than 0.9, it would be necessary to make an adjustment with the polymer concentration or with the polymer injection rate (Scott et al., 2020).

$$I_{rel} = \frac{I_p}{I_b} = \frac{\upsilon_p/\nabla P_p}{\upsilon_b/\nabla P_b} \tag{2.11}$$

where I is the injectivity index, ∇P is the pressure gradient, and u is the Darcy Velocity. The subscripts p and b denote polymer and brine phases, respectively. The subscript rel refers to relative.

The generic one is related to mechanisms that could be evaluated in waterflooding, e.g., poor connectivity and floodability, clay swelling, fines migration, scaling, and emulsions. If the polymer flooding was realized without applying waterflooding, these mechanisms could be the mean factor for Injectivity decline. The anticipated one is associated with the fluid/polymer design, which has is relevant for the lower performance due to the increased viscosity. The undesired ones are the less predictable of these mechanisms and focus significantly on the water/polymer quality; assays include the water quality, polymer preparation, impurities, incompatibilities between water and polymer, and infrastructure (Glasbergen et al., 2015).

2.4.3.1 Properties that affect Injectivity Loos

Injectivity Loss can affect the project's profitability through different mechanisms (Glasbergen et al., 2015). For example, Increasing polymer viscosity is the main reason (Yerramilli et al., 2013). The size of polymer molecules increases as the molecular weight rises, which can result in a larger inaccessible pore volume (IPV) (Mohsenatabar Firozjaii & Saghafi, 2020). Rocks with low permeability (Ezekwe, 2010). A common problem with Waterflooding is the presence of fine particles that affect the injectors (Sharma et al., 1997). Injectivity is also affected by the poor mixture of polymers (Shuler et al., 1987).

On the other hand, an injectivity improvement is achieved by using polymers with low salinity (Kakati et al., 2020). Injecting the above Formation Parting Pressure helps improve injectivity (Seright et al., 2008). Obtaining a high injectivity allows a greater reach of the polymer within the reservoir (Sieberer et al., 2017).

Simulations that are carried out to estimate the injectivity, in general, give a poor prediction, compared to the results obtained in the field. This is due to the fact that there is still a need to have a better understanding of factors that are not taken into consideration, for example, the near wellbore polymer behavior (Thomas et al., 2019).

In Equation (2.9), injectivity loss can be manifested with pressure drop increase (e.g., when face plugging occurs). The Daqing field had many problems with the rise in pressure due to plugging; this problem caused ten injection wells to be unable to continue injecting polymer, and 40% of injector wells were in the B1DX block. This block had a pressure increase of 841psi (5.8Mpa); although this rise is considerable, there was still a margin between Formation Parting

Pressure between 2030 and 2175 Psi. Table 2-8 shows increase in pressure of injections with several blocks in Daqing Field (Guo & Song, 2021).

Table 2-8 Pressure Increase due plugging in Daqing Field (Guo & Song, 2021)

Block	Water injection pressure (Psi)	Polymer Injection pressure (Psi)	Pressure Increase (Psi)
X4-6N	850	1617	767
X4-6S	831	1617	786
X4-5Z	1227	1852	625
X4W	1056	1700	644
X1-2E	1233	1710	477
B1DX	798	1639	841
Y	943	1611	814

In the Tambaredjo field in Suriname, were carried out some injectivity test; the Injectivity index was stable at around 3 BPD/psi as the injection rate increased until it reached 2304 BPD; at this point, the pressure dropped because of the opening of minor fractures that were appearing. The injection rate was increased until 3600 BPD, where the bottomhole pressure dropped to 800 psi, and the injectivity index rose until it reached 6 BPD/day, as shown in Figure 2-19. The creation of Fissures where the fluid can be channeled faster to the producing well causes a rapid breakthrough and could lead to a waste of energy by simply injecting fluids within formations when the injection pressure is near the Formation Parting Pressure (Moe Soe Let et al., 2012).

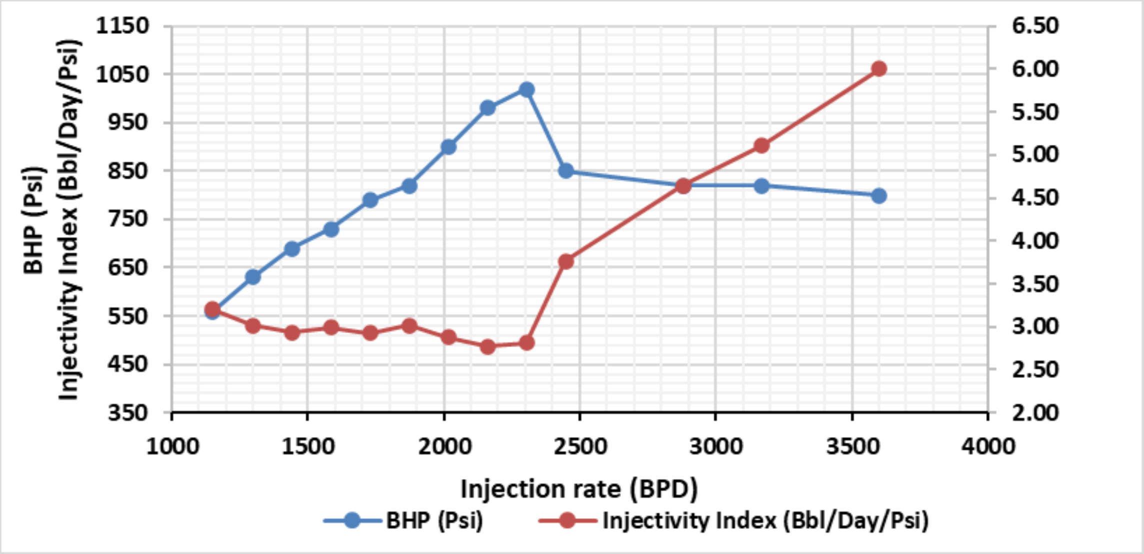

Figure 2-19: Injectivity test from Tambaredjo Field (Moe Soe Let et al., 2012)

Another Injectivity test in Tambaredjo Field showed that the opening of the fractures could have an almost reversible effect. The test consisted of performing some injections (100, 150, and 175 BPD) interspersed between 650 BPD; the Injectivity index was measured in each stage. The injectivity increase for each pair of injections (one lower and one at 650BPD) indicated partial closure of the generated fracture. One more test was carried out by injecting polymer with a viscosity of 45cp at 175BPD. The injectivity was 0.40 BPD/psi (a 72% reduction over water injection at the same flow rate). The question is whether the value obtained was good or bad. Applying the Darcy equation and considering no open fractures, the result obtained was 0.0144 BPD/psi. So, **did the presence of fractures help to have better injectivity?** That statement with presented data needs to be clarified (Moe Soe Let et al., 2012). Although everything seems to indicate that the relationship is evident, it must be considered that the viscosity varies as a function of the shear rate, especially in the near-wellbore zone. Also, mechanical degradation of the polymer induces a decrease in viscosity and salinity present in the water formation.

The Hall Plot method is a powerful tool for determining well injection performance (Buell et al., 1990). The diagnosis is made using a graph based on the integral of the pressure vs. the accumulated injected fluid. In the Hall plot, the injectivity index is the inverse Hall slope under conditions where matrix injection is maintained with ideal radial flow (De Simoni et al., 2018). An example is observed with Figure 2-20, the slope increased when the injection of the 1500 polymer began. The results indicate that the injectivity decreased twice compared to the injectivity obtained with waterflooding.

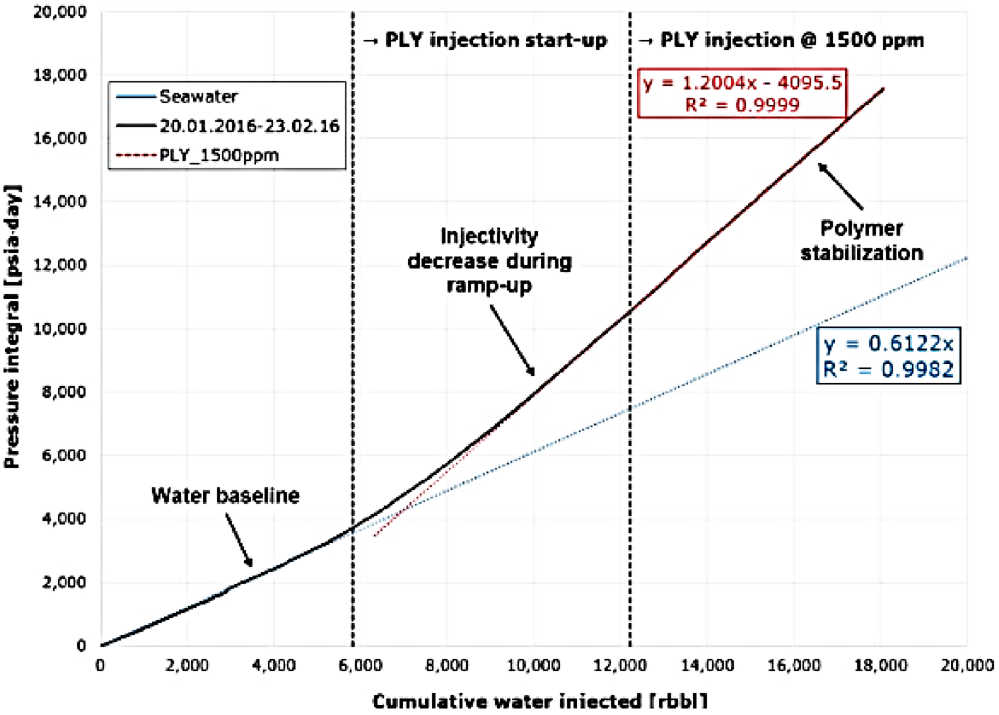

Figure 2-20: Hall Plot diagnostic from Dalia Field (De Simoni et al., 2018)

According to (Thomas et al., 2019) the situations that can occur are:

- If the Hall slope increases on the graph in relation to the water slope, it indicates that there is injectivity loos or plugging.
- If the Hall slope decreases on the graph in relation to the water slope, it indicates the existence of possible fractures due to being injected at a pressure close to the partition pressure.
- If the slope is maintained there would be no change in relation to waterflooding.

Table 2-9 Polymer Injectivity Summary Problems

Characteristic	Problem	
Poor Polymer Injectivity	Can result in a significant financial loss for oil and gas companies, as it can decrease the amount of oil that can be extracted from a reservoir and increase the amount of money required to inject the polymer solution	**(Glasbergen et al., 2015; Thomas, 2016)**
High Molecular Weight polymers	If the viscosity of the polymer solution is too high, it can result in blockages or resistance during injection, which can decrease the efficiency of the EOR operation	**(Moe Soe Let et al., 2012; Scott et al., 2020)**
Selection Injection Method and Well design	The wrong injection method or poor well design can significantly reduce the efficiency of an enhanced oil recovery (EOR) operation, particularly in polymer flooding. This can lead to decreased polymer injectivity, uneven fluid distribution, and ineffective sweep efficiency, resulting in suboptimal recovery of oil. It's essential to carefully evaluate the injection method and well design before implementing an EOR operation to ensure optimal efficiency and effectiveness.	**(Thomas, 2016)**
Surface Facility	Poorly maintained injection equipment can significantly impact the efficiency of the EOR operation and may require additional work to repair or replace equipment.	**(Glasbergen et al., 2015)**
Reservoir pressure	Low reservoir pressure can limit the effectiveness of polymer flooding and other EOR techniques, making it difficult to achieve the desired level of oil recovery.	**(Moe Soe Let et al., 2012)**
Formation damage	Can significantly decrease the efficiency of the EOR operation by reducing permeability and injectivity. It maybe requires additional work to repair the damage caused by injection	**(Moe Soe Let et al., 2012; Seright et al., 2009)**
Polymer Degradation over time	Polymer degradation can significantly decrease the effectiveness of the EOR operation and may require additional work to maintain or improve injectivity.	**(Al-Shakry, Skauge, et al., 2019)**
Polymer adsorption	If a significant amount of the polymer is adsorbed onto the rock, it can decrease the efficiency of the EOR operation and reduce the amount of oil that can be recovered.	**(Al-Shakry, Skauge, et al., 2019)**
Heterogeneity	Low permeability and high heterogeneity of reservoirs can pose challenges to achieving the desired level of oil recovery in polymer flooding EOR operations. Formation heterogeneity can significantly affect the efficiency of the operation, which may require additional efforts to optimize the injection process.	**(Guo & Song, 2021; Moe Soe Let et al., 2012)**
Water Quality	Poor water quality can significantly impact the efficiency of the EOR operation and may require additional work to optimize the water treatment and preparation process	**(Glasbergen et al., 2015)**

3 Material and Methods

This chapter presents the methodology and procedures utilized for applying single-phase injections into carbonate rocks to accomplish the investigation's objectives. The workflow encompasses the materials, methods, equipment, and core-flooding protocols employed for single-phase core flooding.

Designing a core flooding experiment to measure the injectivity of fluids requires careful consideration of various experimental parameters to ensure accurate measurement and comparison of the injectivity values. Some key factors to consider in the experimental design include:

- Core sample selection: The core sample should accurately represent the reservoir and possess well-defined permeability and porosity properties. Before conducting experiments, cleaning the sample thoroughly to eliminate any residual fluids is essential.
- Fluid selection: The fluids used in the experiment should be compatible with the core sample and represent the fluids used in the field application. For example, if the goal is to compare polymer and water injectivity for EOR applications, the polymer and water used in the experiment should represent the polymer and water used in the field.
- Flow rate and pressure: The flow rate and pressure used in the experiment should be controlled and consistent for both fluids to compare the injectivity values accurately.
- Experimental setup: The experimental setup should be designed to minimize potential sources of error or bias, such as ensuring that the fluids are injected into the core sample evenly and that the sample is held in place securely.
- Data acquisition: The experiment should be designed to collect accurate and precise data, such as measuring the flow rates and pressures of the fluids, the volume of the fluids injected, and any additional data that may be relevant to the specific application.

Figure 3-1 shows the experimental workflow aims to determine the dynamic properties of polymers in porous media under varying conditions of polymer concentration and flow rate injection during single-phase core flooding. The properties to be evaluated include Resistance Factor, Residual Resistance Factor, *In-situ* Viscosity, and Relative Injectivity.

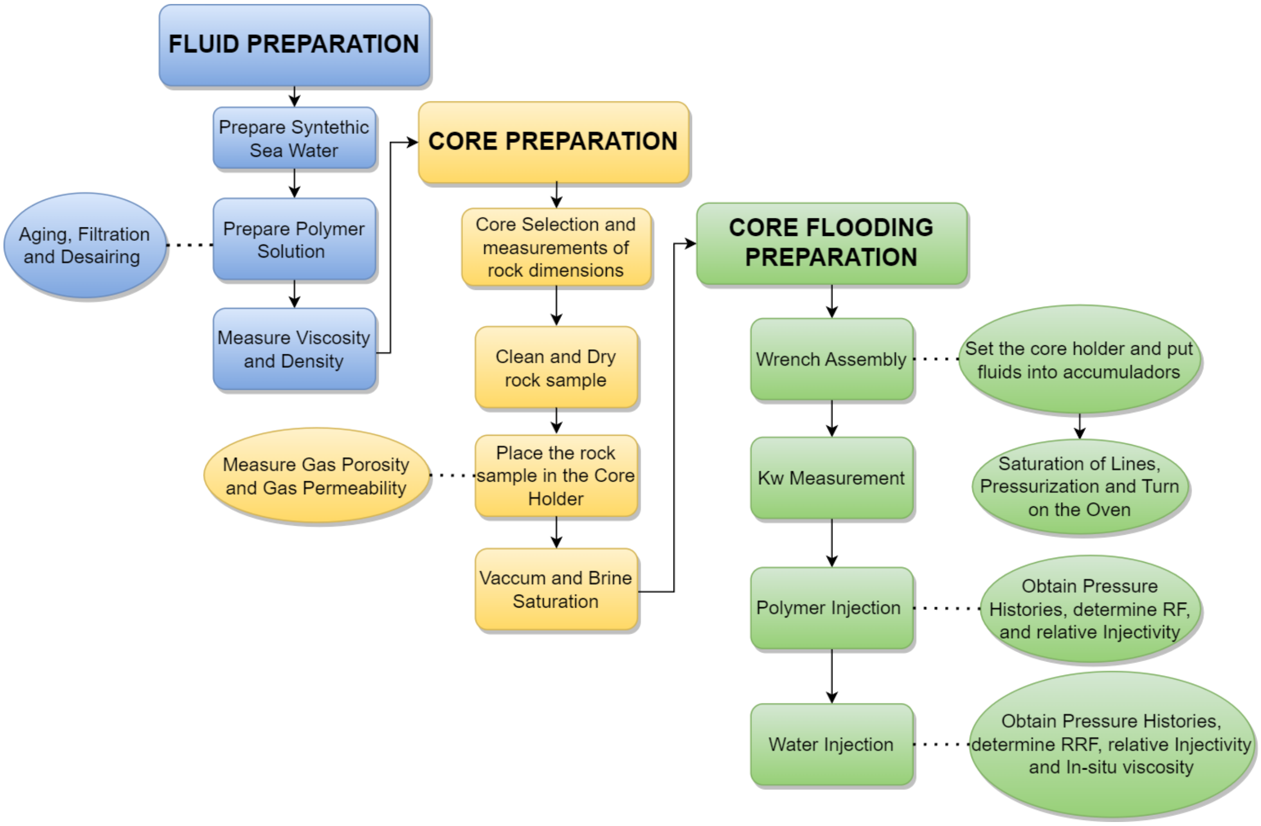

Figure 3-1. Experiment Workflow

3.1 Materials

3.1.1 Core Samples

The core samples were a series of Indiana Limestone Cores for single-phase displacement provided by (Kocurek Industries, Inc., Caldwell, Texas, USA) with a range of 180-220md and 16-19% permeability and porosity, respectively. Its average composition is calcite 97.1%, magnesite 1.2%, silica 0.8%, alumina 0.7%, iron oxide 0.1% and undetermined material 0.1% (INDIANA LIMESTONE INSTITUTE, 2007). Table 3-1 displays the properties of the rock samples that were measured after the cleaning process.

Table 3-1 Indiana Limestone Rock Properties

Rock Code	Type	Porosity	Permeability to Gas (mD)	Length (cm)	Diameter (cm)	Mass (g)
IL-45	Limestone	17.59	173.32	19.9	3.78	499.89
IL-37	Limestone	17.95	171.27	19.9	3.78	500.16
IL-33	Limestone	17.59	142.60	19.9	3.78	502.91
IL-46	Limestone	16.50	160.10	19.9	3.78	501.85
IL-34	Limestone	18.38	639.77	20.0	3.78	501.50

3.1.2 Fluids

The Synthetic Sea Water (SSW) used to prepare polymers comprises nine types of salts and has a TDS of 30905 ppm, a composition to simulate water formation during injection processes, as shown in Table 3-2. Three commercial polymers were chosen to perform singe-phase core flooding: Xanthan Gum and Guar Gum, provided by Sigma Aldrich, and Scleroglucan by Biosynth Carbosynth.

Table 3-2 Synthetic Sea Water (SSW)

Composition	Chemical Formula	Concentration 100% (ppm)
Potassium chloride	KCl	749.3
Calcium Chloride Dihrydrate	CaCl2 2H2O	484.2
Magnesium chloride Hydrate	MgCl2 H2O	1271.3
Strontium Chloride Hexahydrate	SrCl2 6H2O	5.2
Barium Chloride Hexahydrate	BaCl2 2H2O	2.0
Lithium Chloride	LiCl	1.2
Sodium Bromide	NaBr	82.4
Sodium Sulfate	Na2SO4	57.7
Sodium Chloride	NaCl	28252.2
Total TDS		30905.5

3.2 Methods

3.2.1 Fluid Preparation

Annex A provides a detailed workflow outlining the steps to prepare biopolymer solutions. The biopolymer solutions were prepared using the procedure proposed in (Rueda et al., 2020), which is a modification of the Recommended Practices for Evaluation of Polymers Used in Enhanced Oil Recovery Operations (American Petroleum Institute, 1990).

To prepare a stock solution of 4000 ppm, the mass of the polymer was measured and slowly added to a beaker containing deionized water positioned at the periphery of the vortex created by a magnetic stirrer. Considering the susceptibility of biopolymers to biological degradation, Glutaraldehyde (50% water) was added to the solution at a concentration of 4000 ppm of the bulk solution. The solution was left with high agitation for around 24 hours at ambient temperature (25°C) to ensure complete dissolution and achieve the desired polymer viscosity; for Scleroglucan, seven days with high agitation was required. Subsequently, rheology measurements were conducted using the Thermo rheometer, as depicted in Figure 3-2. Viscosity measurements were performed at a shear rate of 10 s-1, a standard value commonly employed by the LABORE group.

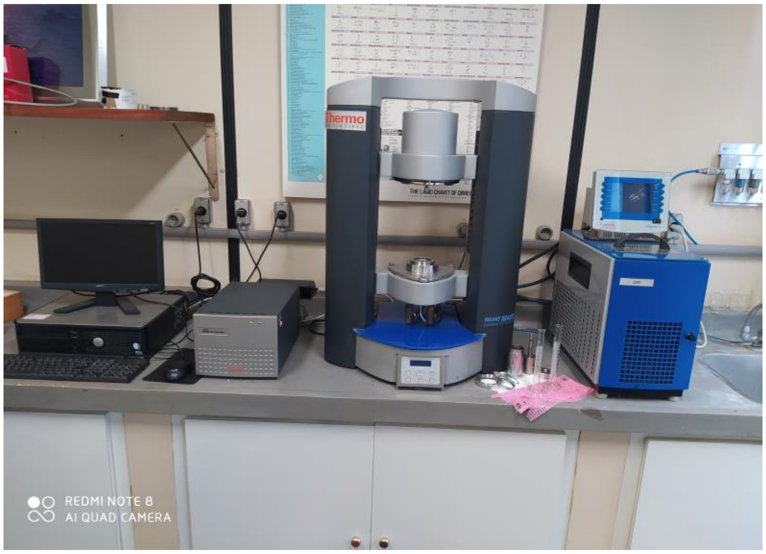

Figure 3-2 Thermo Rheometer

The polymer was then dissolved to reach 100% of SSW (123.618 ppm) and the concentration was reduced for further filtration procedure. Table 3-3 shows the pre-established concentrations before the filtration tests. Different concentrations were established to filter the polymers because Guar Gum required higher polymer concentrations to achieve the same viscosity as xanthan gum and Scleroglucan solutions. For the last two tests, the concentration was 2000 ppm because the test concentrations selected for those experiments were greater than 1000 ppm.

Table 3-3 Polymer concentration before filtration

CODE	Polymer	Concentration before filtration (ppm)
IL-45	Xanthan Gum	1000
IL-37	Guar Gum	3000
IL-33	Scleroglucan	1000
IL-46	Xanthan Gum	2000
IL-34	Xanthan Gum	2000

The filtration test for biopolymers before core-flooding injections is an imperative step to enhance the quality of dissolution and avoid rock plugging. Also, the filtration process improves the injectivity.(Fournier et al., 2018; Glasbergen et al., 2015; Sorbie, 1991; D. Wever et al., 2017). The filtration was performed using the (V. H. S. Ferreira & Moreno, 2020) procedures, which recommend aging at least 24hrs for Xanthan Gum and Scleroglucan and 3hrs for Guar Gum due to its poor thermal stability (Pu et al., 2018). The aging was realized to obtain better solubility (Freire Filho & Moreno, 2022). After aging, the polymer solution was initially filtered using an 8µm membrane filter and passed through a 1.2µm membrane filter, which served as a reference for the filtration rate measurements provided by Equation (3.1). To mitigate membrane filter clogging during the injection of Guar Gum, a pre-filtration process was implemented using ceramic filters. This pre-filtration step greatly enhanced the overall filtration process by reducing process time. The filters were used in the following sequence: 55µm, 20µm and 12µm. Figure 3-3 shows the filtration equipment for the experiments. The apparatus on the left is for ceramic filters, and the one on the right is for membrane filters. The entire filtering process was conducted under a constant pressure of 30 psi, with nitrogen (N2) injected to displace the polymer solution.

Figure 3-3 Filtration Equipment

For the Analysis of the filtration data Equation (3.1) it is recommended for measurements of the filtration rate (American Petroleum Institute, 1990). Some literature suggests acceptable F_r values between 1 and 1.2 from 1.2 µm meshes for polymer solutions (Glasbergen et al., 2015; Sheng, 2013; D. Wever et al., 2017)

$$F_r = \frac{t_{V500} - t_{V400}}{t_{V200} - t_{V100}} \tag{3.1}$$

where t_{V500}, t_{V400}, t_{V200}, and t_{V100} are the time required to filter volumes of 500, 400, 200 and 100ml.

After the filtration test, the viscosity was measured to compare the viscosity loos occur between the viscosity of aging and the viscosity after 1.2 µm mesh, according to Equation (3.2). Before placing the fluids inside the accumulators, the solution is prepared at the concentration of the experiment. Each experiment has three solutions at different concentrations, and then vacuum deaeration is performed to extract the more significant amount of air in solution from the polymer solution, and fluid density was measured by a hydrometer-type density meter

$$VL = \frac{\mu_{aging} - \mu_{1.2\mu mesh}}{\mu_{aging}} \tag{3.2}$$

where VL is the Viscosity loss due to the filtration, μ_{aging} is the Viscosity after the period of aging and $\mu_{1.2\mu mesh}$ is the viscosity reached after the filtration process.

These measurements were conducted using the Thermo viscometer, made available by the Petroleum Department within the Faculty of Mechanical Engineering at UNICAMP. Table 3-4 summarizes the processes used for each experiment.

Table 3-4 Summary of each preparation processes

Code	IL-45	IL-37	IL-33	IL-46	IL-34
Polymer	Xanthan Gum	Guar Gum	Scleroglucan	Xanthan Gum	Xanthan Gum
Overlap Concentration C*	285 (ppm)	950 (ppm)	175 (ppm)	285 (ppm)	285 (ppm)
Biocide	Yes	Yes	Yes	Yes	Yes
Agitation	1 day	1 day	7 days	1 day	1 day
Dissolution before Aging	1000 ppm	3000 ppm	1000 ppm	2000 ppm	2000 ppm
Aging Time	1 day	3hours	1 day	1 day	1 day
Filtration	8µm + 1.2µm	55µm+20µm+12µm + 8µm +1.2µm	8µm + 1.2µm	8µm + 1.2µm	8µm + 1.2µm
Concentration test	50-100-700 (ppm)	100-300-1200 (ppm)	100-500-800 (ppm)	100-1100-1500 (ppm)	100-700-1100 (ppm)

3.2.2 Core Sample Preparation

Measuring rock porosity and permeability is essential for any core flooding experiment. A series of procedures were carried out to obtain it. The recommended procedure for core flooding (American Petroleum Institute, 1998) begins removing all original fluids from the sample.

Figure 3-4 shows the Soxhlet with the core sample. The solvent was heated to a boiling temperature of 64.4°C. The solvent vapor passed through a distillation path, flooding the core sample chamber. The condenser ensures that any solvent vapor cools and drips back into the chamber that contains the core. The chamber containing the core was slowly filled with the solvent so that part of the compound dissolved. When the Soxhlet chamber is almost complete, the chamber is emptied with the siphon. The solvent is returned to the distillation flash. Following two cleaning cycles using methanol, as per the standard practice in the LABORE group for the dimensions and type of rock used, the core sample is placed in an oven at a temperature of 80°C for an entire day to ensure complete drying The use of methanol is recommended for removing formation salts and oil, as it effectively helps in their dissolution and removal (American Petroleum Institute, 1998).

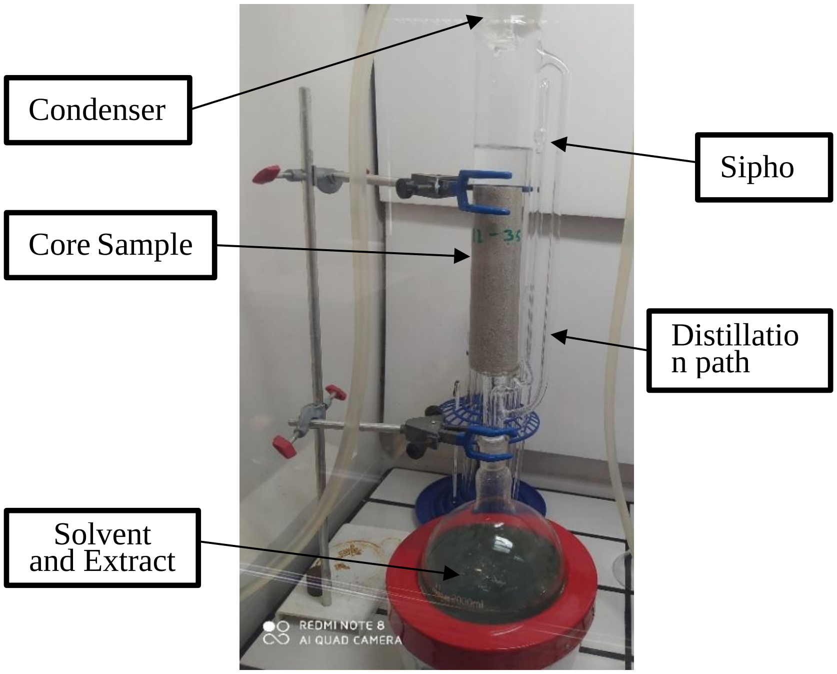

Figure 3-4 Cleaning process with Soxhlet Chamber

Once dry, the core sample is placed inside the Core Holder to perform porosity and permeability measurements. The porosity was calculated using a gas porosimeter, as Figure 3-5 shows. The equipment is governed by the Boyle-Mariotte law, one of the gas laws that relates volume and pressure at a constant temperature. Its operation consists of reaching a pressure of 100 psi in a chamber inside the porosimeter so that a valve opens to flow inside the core holder. The volume is measured, but you must correct the dead volume of the lines and valves. The corrected value represents the pore volume of the core.

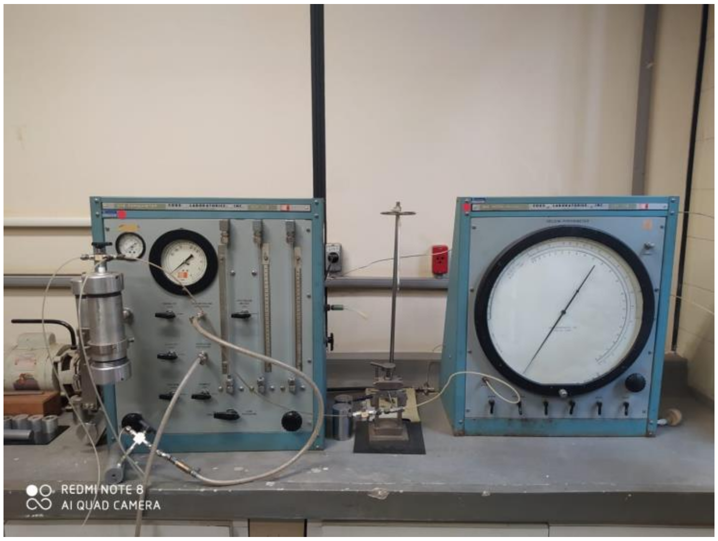

Figure 3-5 Permeability-meter and Porosimeter

The permeability measurement was performed using a Nitrogen (N_2) in the permeability meter, as shown on the left in the Figure 3-6, provided by the manufacturer. However, as gas measurements tend to overestimate the absolute permeability of the core due to the sliding effect of the gas, which affects the free path of the gas within the porous medium, parameters such as temperature, pressure, and gas type can influence this overestimation. Therefore, the Klinkenberg correction was applied as described in Equation (3.4) (Rosa,2011, API RP 40)

$$k = \frac{C \cdot Q_g \cdot h_w \cdot L}{200 \cdot A} \tag{3.3}$$

$$k_g = 0.68 \cdot (k)^{1.06} \tag{3.4}$$

where k refers to the gas permeability obtained by the permeability meter, C is the height of the mercury column, Q_g is the flow, h_w is the height of the water column, L is the length of the core, A is the cross-sectional area of the core and k_g is the gas with the klinkerberg correction applied.

In the final stage, the core holder is connected to a vacuum pump, with valves at the inlet and outlet connections. The vacuum pump is left connected to the outlet connection for 24 hours until a pressure of 0.8 mbar is reached. Then, A Mariotte bottle filled with Deaerated 100% synthetic seawater (SSW) is connected to the inlet connection. Then, the valve is opened, allowing the SSW to enter the core due to the pressure differential. The process ends when the SSW flow is observed at the output connection, indicating that the core has been completely saturated, displacing any residual air that may have remained after the vacuum. This step helps ensure that the fluid used for saturation effectively fills the pore spaces of the core sample, providing accurate results for subsequent analysis. Finally, the core is left in contact with the brine to stabilize ionically.

3.2.3 Core-Flooding procedures

After all the equipment has been installed inside the stove, the saturation of the lines begins to eliminate any air present in the connection lines, valves, and pressure taps, as shown in Figure 3-6. Once this process is complete, the stove is sealed and heated to 60°C, allowing the entire system to achieve thermal stabilization overnight.

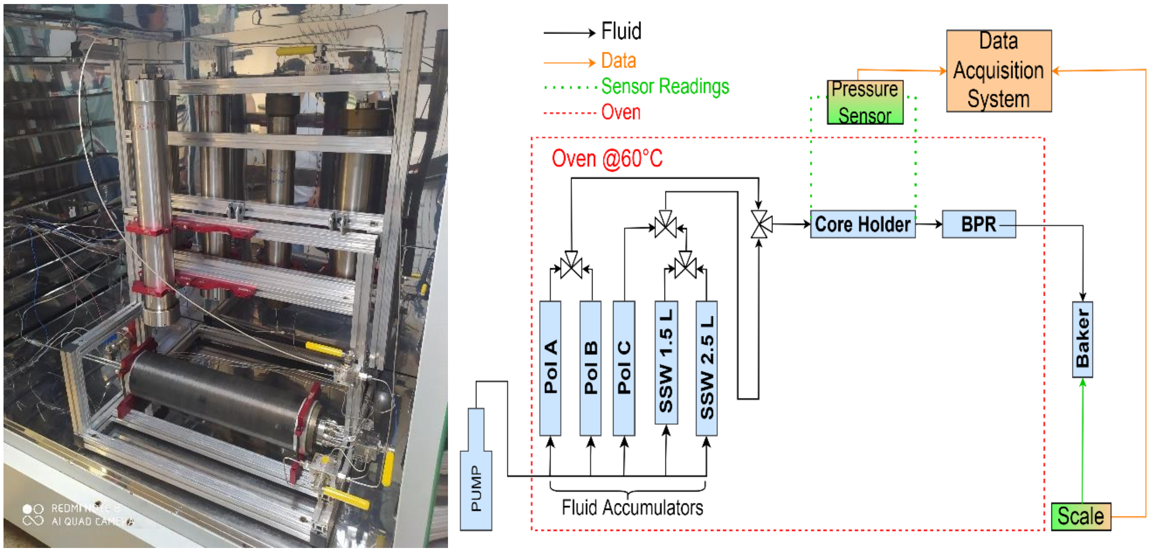

Figure 3-6 Core Flooding Setup and Scheme

Figure 3-7 shows the diagram of how each pressure transducer was placed along each rock, allowing us to obtain pressure drops for each section and the total rock. Pressure taps are crucial in core flooding experiments as they directly measure pressure differentials across the core sample during fluid flow. They provide valuable information for understanding flow behavior, evaluating fluid displacement efficiency, and validating numerical models. The rubber cover already establishes the spacing.

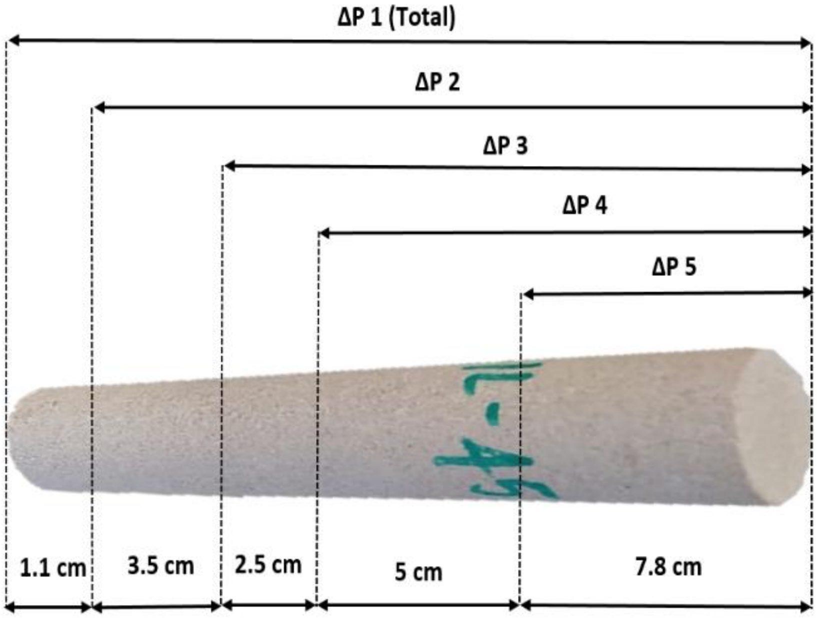

Figure 3-7 Pressure Taps Position

Pressure profiles obtained from the taps help characterize fluid velocities, pressure drops, and flow patterns within the porous media. These measurements aid in assessing the effectiveness of fluid displacement, optimizing processes like oil recovery or groundwater remediation, and improving the accuracy of numerical simulations. Pressure taps play a vital role in core flooding experiments by providing essential data for analyzing fluid flow in porous media and optimizing various applications. The pressure taps used for the experiment are illustrated in Figure 3-8. On the left side, pressure sensors, capable of measuring up to 9 and 36 psi, are used for the first and second rounds of equipment. On the right side, the sensors are designed to measure pressures up to 15,000 psi.

Figure 3-8 Pressure Sensor

After the thermal stabilization period, the first injection of SSW is performed to determine the absolute water permeabilities for each experiment. The same flow rates used in the experiments are employed during this injection, and the pressure drop data is recorded to calculate the other variables necessary for experimenting. The time required to reach the set volumes is also registered as shown in Table 3-5. A final flow rate of 0.5 and 1 cm^3/min is maintained to avoid additional disturbances due to flow rate changes.

Table 3-5 Flow rates for K absolute

Flow Rate (ml/min) IL-45, IL37, IL33, IL-46	Volume (ml)	Flow Rate (ml/min) IL-34	Volume (ml)
0.2	2-2.50-3	0.2	2-2.5-3
0.7	5-8-9	0.5	3-5-7
1	5-8-10	2	7-11-15
2	7-11-15	4	15-25-30
4	15-20-30	8	30-50-70
6	15-30-45	12	50-80-110
0.5	3-5-7	14	70-100-130
		1	5-8-10

Figure 3-9 shows the injection scheme; it starts from polymer A (lower concentration polymer) and reaches polymer C (higher concentration polymer). It was established that the pore injection volume is 5PV for each injection flow rate, but later, it was established that the volume should be reduced to 3PV since the pressures were rapidly stabilized within the first experiment. After each injection of the polymer solution, an injection of SSW follows; this process is performed two more times.

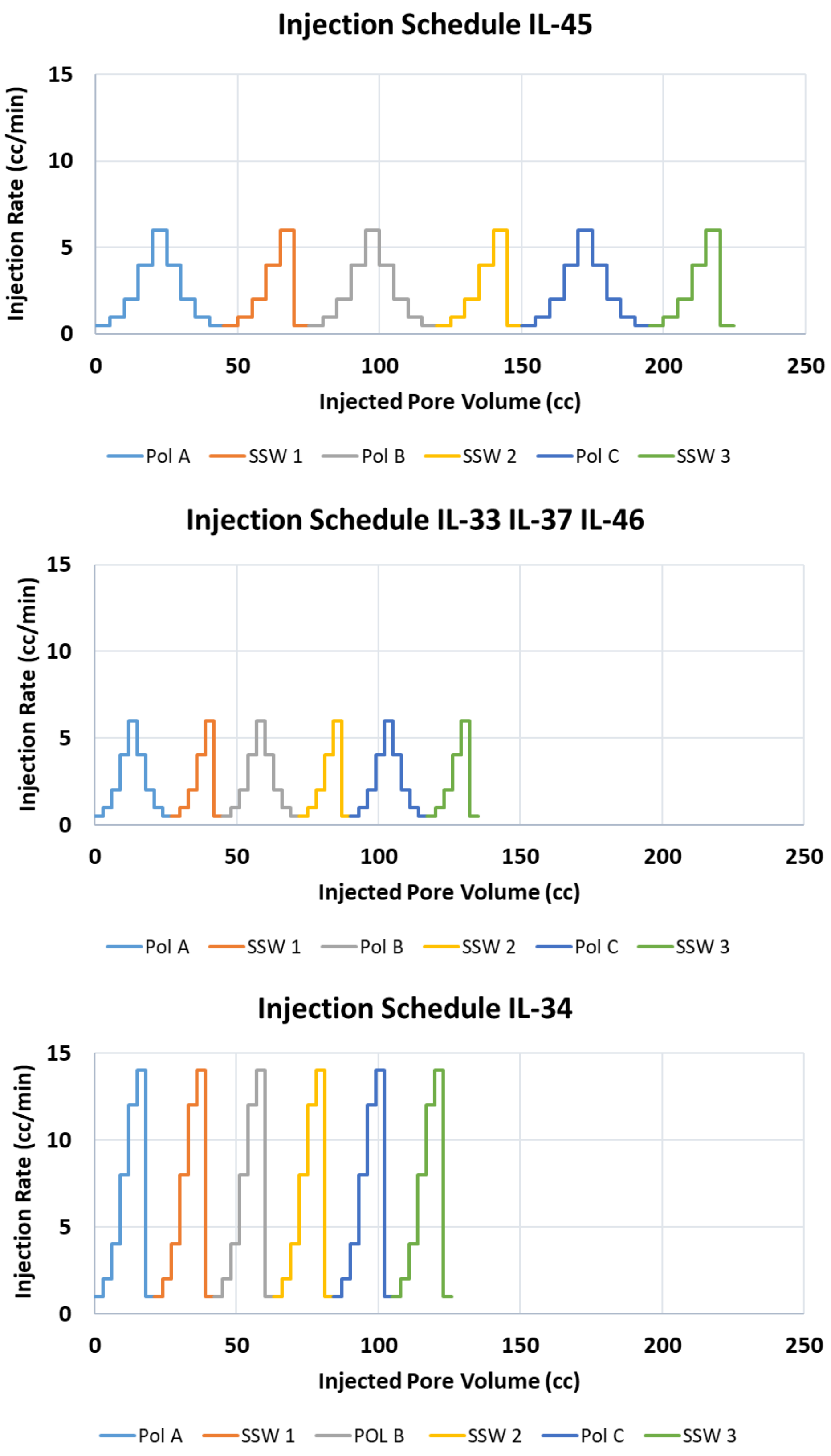

Figure 3-9 Injection Scheme

4 Results and Discussion

This chapter presents the results obtained from the experiments conducted in the previous chapter. The results for each experiment with the three biopolymers used are presented and compared in terms of rock and fluid properties, and filterability results. The core flooding tests enabled the determination of the Resistance Factor and Residual Resistance Factor data, which respectively indicate the change in mobility of the polymer compared to the first Synthetic Sea Water (SSW) injection and the loss of permeability within the core due to polymer absorption and retention. The *in-situ* viscosity results provide insights into the behavior of the polymers within the rock, and the calculation of relative injectivity allows for a better understanding of the effectiveness of each polymer under different conditions.

4.1 Filtration test

A filtration test is an essential step to carry out any core flooding since it allows us to improve the quality of the solution to avoid core plugging (de Sousa Ferreira, 2019; Freire Filho & Moreno, 2022). The rheology of the solutions was measured with a rheometer to quantify the viscosity loss that occurred during the filtration process. Figure 4-1 shows the rheological curves of the experiments IL_45, IL_46, and IL_34 with Xanthan Gum. On the left, IL_45 shows the filtration of a solution at 1000ppm while on the right show's filtrations with a solution with Xanthan Gum at 2000ppm because the concentrations for core flooding were higher than IL_45. A noticeable difference in viscosity is observed, and the solution maintains its shear-thinning behavior. For both, filtration was performed with an 8 µm mesh filter followed by a 1.2 µm one. For the filtration of the Xanthan Gum of the IL_45, there was a viscosity loss of 31.2% measured at the shear rate of ($10s^{-1}$) and, for experiments IL_46 and IL_34, the loss of viscosity obtained was relatively higher than 37.3% and 37.5% respectively. Due to the high concentration with which they worked; viscosity loss was higher.

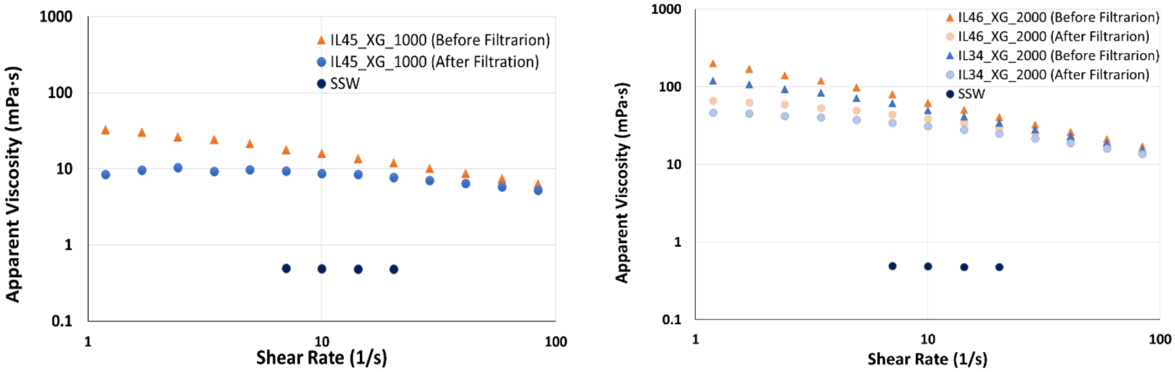

Figure 4-1 Viscosity Loss from Xanthan Gum due the Filtration Process

Figure 4-2 shows the curves for Guar Gum and Scleroglucan, which were also filtered prior to the core flooding experiments, except for Guar Gum which required pre-filtration to improve its performance with ceramic filters of 55 µm, 20 µm and 12 µm due to the presence of too many impurities. It can be observed that Guar Gum had the highest viscosity loss of 75.1% at a shear rate of (10s^{-1}). This may be due to the presence of impurities such as proteins and fibers that were suspended in the solution (Freire Filho & Moreno, 2022). On the other hand, Scleroglucan went through the same process as the Xanthan Gum experiments and showed a lower viscosity loss of 26.63% for 1.2 µm mesh filter.

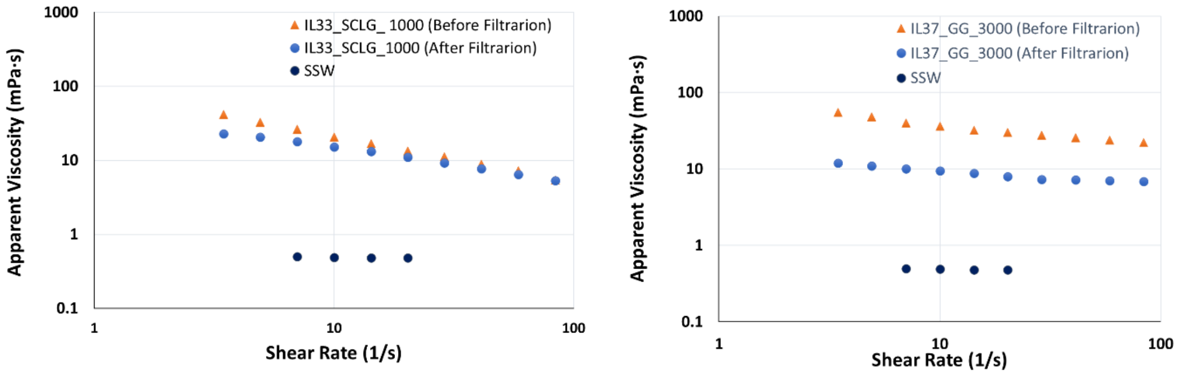

Figure 4-2 Viscosity Loss from Guar Gum and Scleroglucan due the Filtration Process

The filtration ration of the solution was calculated with Equation, all solutions obtained were in the acceptable range (Glasbergen et al., 2015; Sheng, 2013; D. Wever et al., 2017) where an optimal filtration range is between 1 and 1.2 for a 1.2µm mesh filter. The importance of carrying out filtration is to avoid clogging of the porous medium of the rock, as the results obtained by other filters showed very high values, using various filters to obtain better results. The clearest example was from experiments carried out with Guar Gum, where in its first attempt, the solution could not pass through the first 8µm mesh filter, so a modification was made to the model proposed by Vitor (V. H. S. Ferreira & Moreno, 2020), which was to include pre-filtration with ceramic filters of higher capacity to have a solution with fewer large molecules. The results are shown in In IL-46 and IL-34 experiments with Xanthan Gum, a higher viscosity loss was observed compared to IL-45. This is due to the fact that the concentration used for filtration was twice as high, resulting in a greater retention of particles.

Table 4-1. In IL-46 and IL-34 experiments with Xanthan Gum, a higher viscosity loss was observed compared to IL-45. This is due to the fact that the concentration used for filtration was twice as high, resulting in a greater retention of particles.

Table 4-1 Viscosity Loss and Filtration Rate results

Parameter	**Rock Samples**				
	IL-45	**IL-46**	**IL-34**	**IL-37**	**IL-33**
Polymer	Xanthan Gum	Xanthan Gum	Xanthan Gum	Guar Gum	Scleroglucan
Polymer Concentration	1000	2000	2000	3000	1000
Aging	24hr	24hr	24hr	3hr	24hr
Viscosity @($10s^{-1}$)	0.56 0.67 4.40	0.66 10.71 20.51	0.67 3.73 8.51	0.49 0.62 2.30	0.73 4.46 9.81
Polymer Concentration Test	50 100 700	100 1100 1500	100 700 1100	100 300 1200	100 500 800
Fr @ 1.2 mesh filter	1.03	1.03	1.04	1.05	1.02
Viscosity loss @ ($10s^{-1}$)	31.2%	37.3%	37.5%	75.10%	26.63%

4.2 Petrophysics

The rocks used for these experiments were all Indiana Limestone, with similar characteristics as described in Table 4-2, and were provided (KOCUREK Industries, Inc., Caldwell, Texas, USA). The petrophysical characterization of these rocks was carried out after cleaning and drying as explained in Chapter 3. The absolute gas permeability of the rock was measured using a permeameter, and according to Equation (3.4) to obtain a more appropriate value, taking into account various parameters that influence gas behavior, such as pressure. The Klinkenberg correction is important in porosity measurements because it adjusts for the non-Darcy flow behavior observed at low gas pressures, ensuring accurate determination of permeability and porosity. It enables reliable characterization of porous materials and is particularly valuable in low-pressure gas permeability tests, providing more precise results.(Rosa et al., 2006).

Table 4-2 Rock Characteristics

Parameters	Units	Rock Samples				
		IL_45	IL_37	IL_33	IL_46	IL_34
Mass	(g)	499.89	500.16	502.91	500.16	501.65
Length	(cm)	19.90	20.00	19.90	19.90	20.00
Diameter	(cm)	3.78	3.78	3.78	3.78	3.78
Area	(cm2)	11.22	11.22	11.22	11.22	11.22
Total Volume	(cm^3)	223.32	224.44	223.32	223.32	224.44
Gas Permeability (kg)	(mD)	173.32	171.27	142.60	160.10	639.77
Pore Volume	(cm^3)	39.30	40.30	39.30	34.50	41.25
Porosity	-	17.60	17.96	17.60	15.45	18.38

After completing the fluid and rock preparation procedures and assembling the equipment as described in Chapter 3, each experiment was left to inject at a low flow rate of 0.2cc/min overnight to achieve thermal stabilization throughout the system and ensure that everything was ready to start the corresponding experiment. The first step was to obtain the absolute permeabilities to water.

4.3 Core Flooding

In this section of the chapter will be divide it into 2 parts. The first part will focus on obtaining the results of the first injection of 100% SSW for each experiment in order to determine the absolute water permeability. This will also provide reference values for the residual resistance factor (RRF) and injectivity prior to polymer injection. The second part will focus on obtaining the results for each injection of the biopolymers used in the different cores, taking into consideration the concentration and injection rates.

4.3.1 First Water Injection

The first injection was conducted to obtain data on absolute permeabilities and establish a reference value for calculating the residual resistance factors (RRF). For the first four experiments, injection rates were set according to the values specified in Chapter 3, including intermediate values of 0.2, 0.5, 0.7, 1.0, 2.0, 4.0, and 6.0 cm^3/min. For experiment IL-34, higher injection rates were used to better understand the behavior of Xanthan Gum in the porous medium under high shear rates, with values of 1.0, 2.0, 4.0, 8.0, 12.0, and 14.0 cm^3/min.

In all cases, a steady-state behavior was achieved, and the Darcy law was applied to obtain the permeability values, taking into account considerations such as constant temperature and linear flow. The permeability value was obtained from the slope of the points obtained for each experiment, which should exhibit a linear behavior as shown in Figure 4-3. The Kw values for each experiment were obtained based on the total pressure drop or from pressure transducer 1. It is clear that the IL_35, IL_37, IL_33, and IL_46 rocks have similar permeability values ranging from 127.7mD to 156.5mD. The first injection was performed to obtain the absolute permeability data and establish a reference value for calculating the residual resistance factors (RRF). For the first four experiments, injection rates were based on the values established in Chapter 3, including intermediate values of 0.2, 0.5, 0.7, 1.0, 2.0, 4.0, and 6.0 cm^3/min.

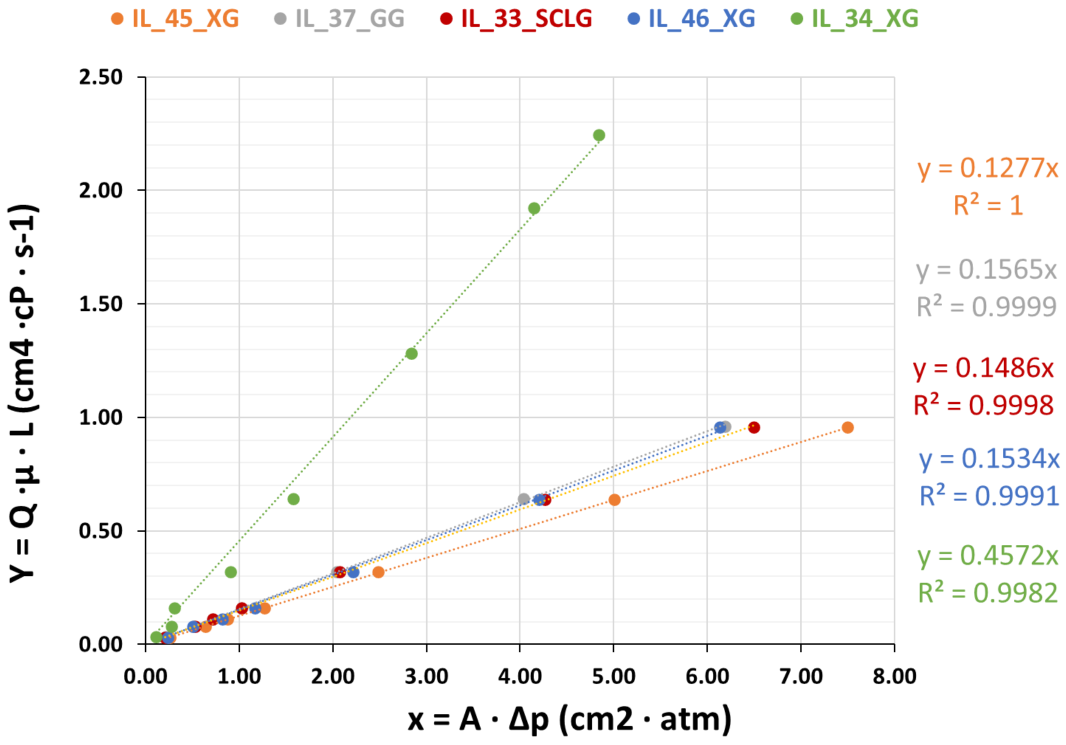

Figure 4-3 Absolute Water Permeability

To verify the obtained values, the same method was used to calculate the permeability of each section of each rock, and a weighted average was performed based on the length and permeability of each section to verify the obtained permeability. As shown in Table 4-3 section A has a very low permeability. The reasons for this may be that the fluid encounters more resistance to flow through that section, or it could be due to the configuration of the rock, which has a smaller size for the fluid to pass through. It is also possible that the first section acts as an additional filter, and larger particles are retained in the section closest to the inlet.

Table 4-3 Permeability along Core

Experiment	parameters	Total	Section A	Section B	Section C	Section D	Section E	Avg K
	L (cm)	19.9	1.1	3.5	2.5	5.0	7.8	
IL_45	K (mD)	127.8	20.8	277.3	114.7	191.3	182.8	127.6
IL_33	K (mD)	147.1	45.6	184.8	140.2	136.9	205.4	147.0
IL_46	K (mD)	156.7	32.9	249.6	200.2	169.2	204.9	156.0
	L (cm)	20.0	1.2	3.5	2.5	5.0	7.8	
IL_37	K (mD)	156.4	29.1	228.5	199.8	190.0	239.8	156.3
IL_34	K (mD)	476.3	66.4	718.9	806.5	817.3	770.9	473.1

4.3.2 Polymer Flooding and Post Waterflooding

After the first water injection, the predetermined injection schedules were followed for each experiment as described in the Figure 3-9. Three concentrations of polymer solutions were used for each rock with different injection rates, and after each polymer injection, a post-waterflooding was carried out. As shown in Figure 4-4 an average representation of the pressure differential for each experiment is shown, and with these pressure drops, we can calculate the variables mentioned in Chapter 2 to understand the behavior of the different polymers within the rocks.

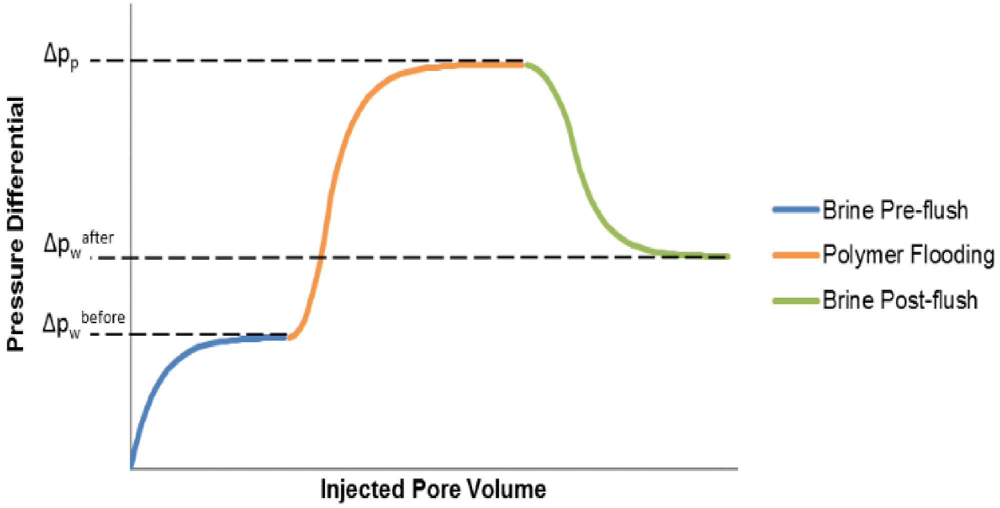

Figure 4-4 Typical core pressure drops for polymer flooding (de Sousa Ferreira, 2019)

Once the data treatment of the experimental results was carried out, a comparative study was performed by analyzing the pressure drop values of each injected fluid to obtain the RF and RRF values, as shown in Figure 4-4. The RF is the ratio between the polymer flooding and brine pre flush, while the RRF is the ratio between the brine pre flush and the brine post flush.

In experiments with Xanthan Gum, a stable Resistance Factor (RF) behavior was observed, which is due to its more Newtonian behavior at concentrations below the C* value. For XG, this value was 285 ppm at a shear rate of ($10s^{-1}$) and with 30905 TDS, which is similar to the value reported in (Clinckspoor et al., 2021). Figure 4-5 shows that at high concentrations, the RF values are higher because the polymer solution has a greater interaction with the surface of the pores, leading to greater adsorption and decreased fluid mobility, hindering its flow through the pores. However, as the injection rate increases, the RF value decreases due to mechanical degradation that generates high shear rates. Comparing the injection rates of 0.5 to 6 cm^3/min, a significant reduction is observed. For example, the reduction for a concentration of 1500 ppm was 63.07%, while for 1100 ppm and 700 ppm it was 56.44% and 44%, respectively. It should be highlighted that as the flow rate increases, the reduction in RF decreases. Also, the reduction between higher values becomes progressively smaller, with values below 10% except for the 1500 concentration, which reached 12.69%. Annex B provides comprehensive tables displaying the detailed results corresponding to the graphs presented in this section.

In Figure 4-6, the behavior of Guar Gum and Scleroglucan under the same injection conditions is shown, but with different concentrations relative to the viscosity of water, which has a reference value of 0.48 cP at a shear rate of ($10s^{-1}$) and 30905 TDS. For experiment IL-37, low values were obtained, so concentrations below its overlap concentration C* were used, 100 and 300 ppm, and one slightly above of 1200 ppm. For Scleroglucan, a concentration below C* was used, as well as two concentrations above it, similar to IL-46.

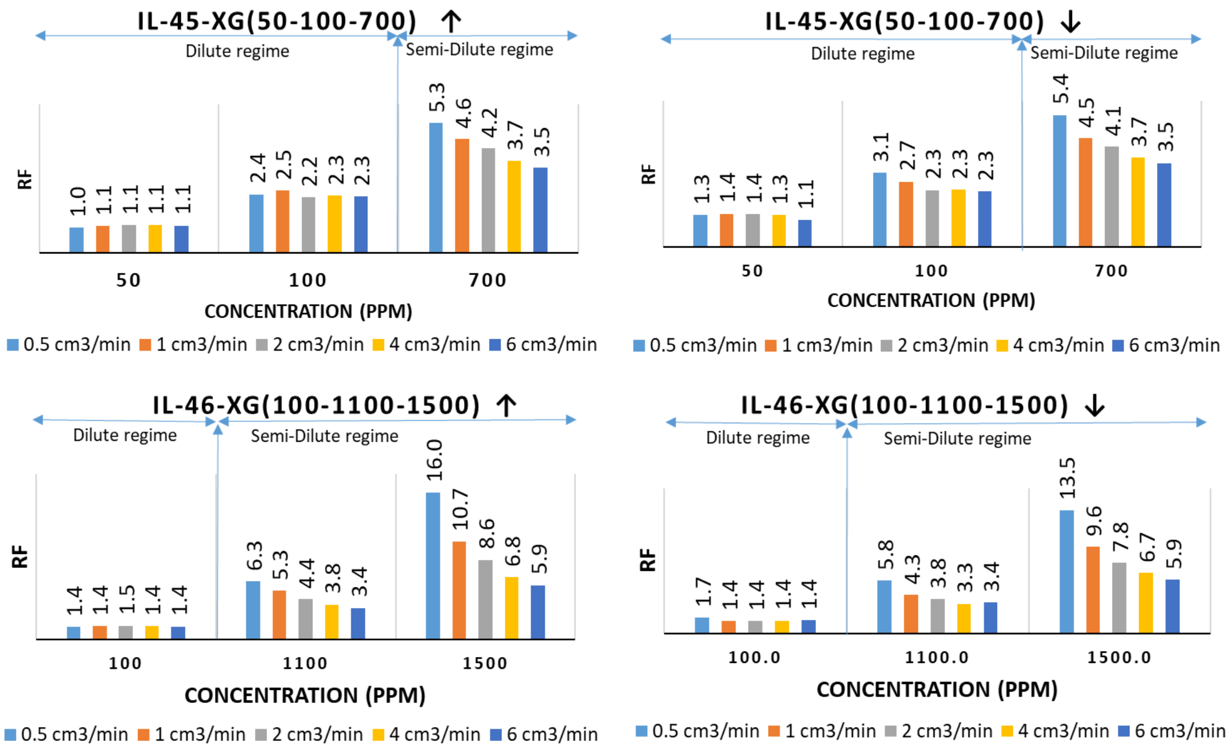

Figure 4-5 Resistance Factors IL-45 & IL-46

The results for Guar Gum show reduced values because at these concentrations it behaves similarly to a Newtonian fluid. Even though the concentration of 1200 ppm almost doubled the values obtained from concentrations of 100 and 300 ppm, they are still lower compared to other biopolymers. This is due to the fact that it requires a higher concentration to reach high viscosities (Clinckspoor et al., 2021; Freire Filho & Moreno, 2022). In the case of Scleroglucan, high values were obtained for a concentration of 800 ppm, reaching a value of 13.7 at a flow rate of 0.5 cm^3/min. Furthermore, as the injection flow rate increased, there was a reduction in RF of 35% and 48% for concentrations of 500 and 800 ppm, respectively. The reduction in RF becomes increasingly smaller as the flow rate increases, reaching a reduction of approximately 10% from 4 to 6 cm^3/min as shown in Figure 4-6.

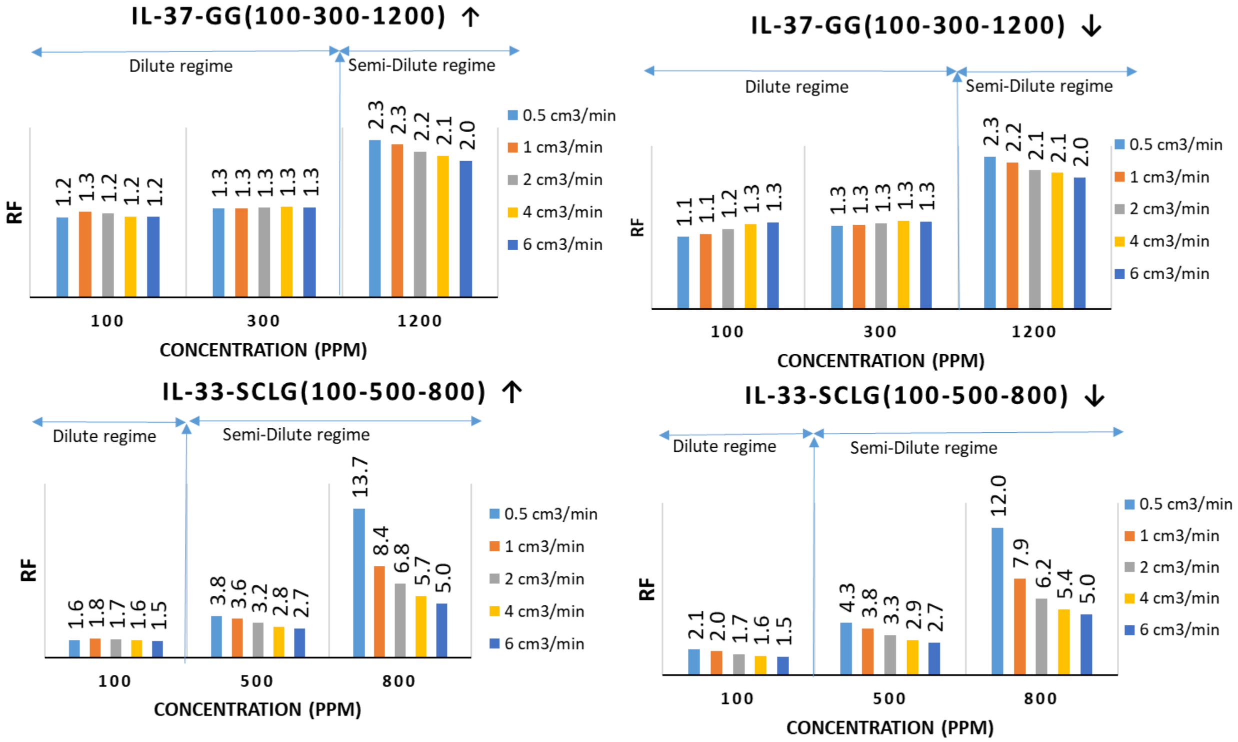

Figure 4-6 Resistance Factors IL-37 & IL-33

The hysteresis effect in core flooding experiments was analyzed using a stepped approach, as illustrated in Figure 3-9. The injection flow rate was incrementally increased and then decreased. The results indicated that as the flow rate increased, the difference in Resistance Factors (RF) between upward and downward injections became less pronounced for Xanthan Gum polymer solutions. However, at lower flow rates, particularly at higher concentrations, a significant difference in RF was observed between the two directions. That highlights the importance of considering the injection flow rate and polymer concentration regime when analyzing the behavior of polymer solutions in core flooding experiments. Figure 4-7 displays the RF values obtained from experiments IL-46 and IL-45. The injection flow rate of 6 cm^3/min was not considered in the analysis, as the same value was used for both cases to determine RF and Residual Resistance Factor (RF)

. In the case of IL-46, the RF value was 15.6 when the injection began at a flow rate of 0.5 cm^3/min with a concentration of 1500 ppm. However, upon re-injection at the same flow rate, the RF value decreased to 13.5. This difference in RF values can be attributed to the initial injection not reaching the maximum absorption capacity of the pore surface at a concentration of 1500 ppm, resulting in higher flow resistance compared to the subsequent injection at the same concentration and flow rate.

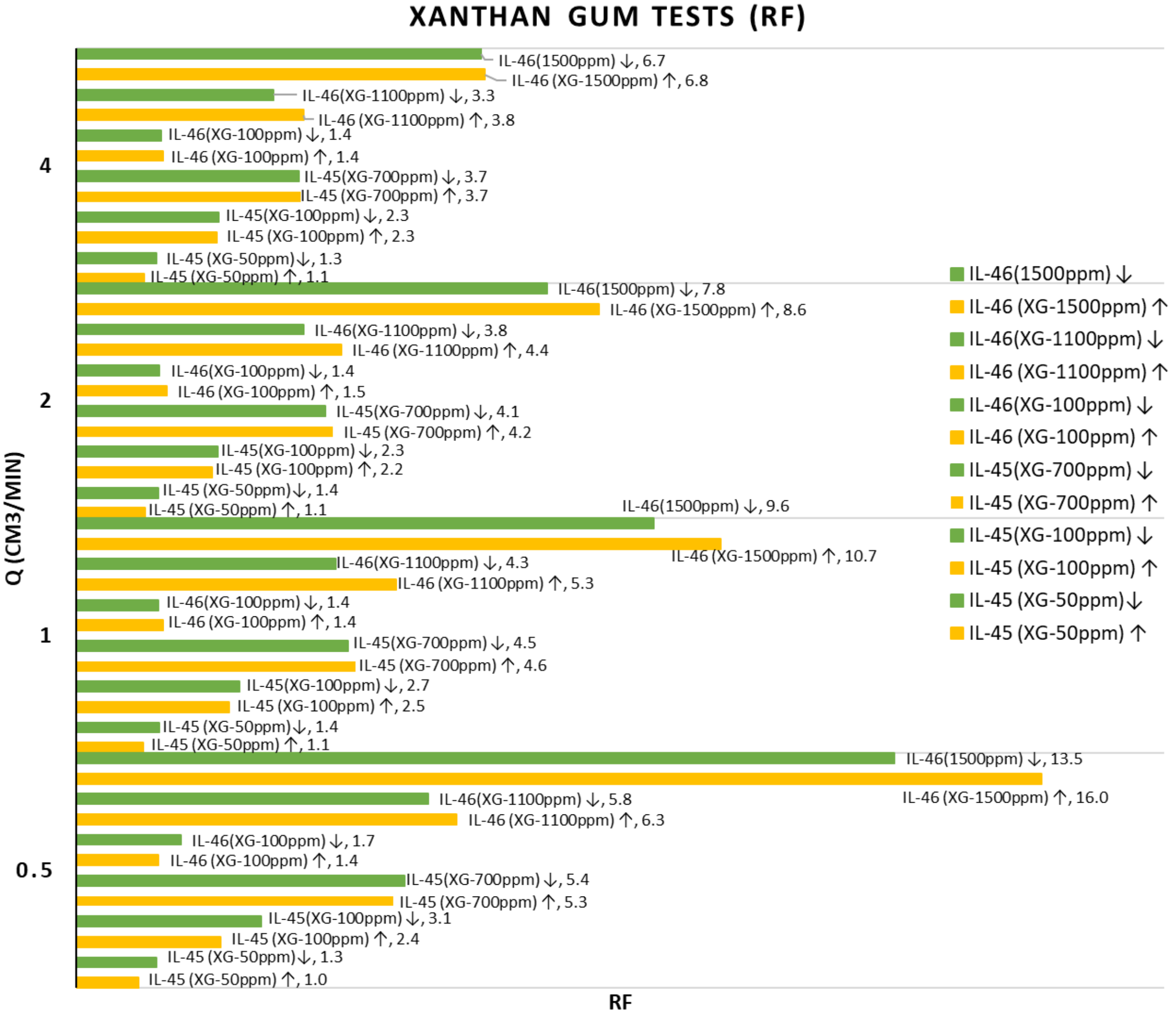

Figure 4-7 Hysteresis effect in Xanthan Gum RF results

Figure 4-8 presents the Resistance Factor (RF) results of IL-37 and IL-33 from a different perspective. It can be observed that the use of Guar Gum in IL-37 resulted in no significant difference in RF values across different injection flow rates. On the other hand, Scleroglucan exhibited a small difference at low flow rates, which gradually reduced as the flow rate increased. This suggests that at high flow rates, there may not be a noticeable difference if an experiment is conducted with the same sequence and design, as the polymer solution may undergo mechanical degradation due high shear rates that the biopolymer experience.

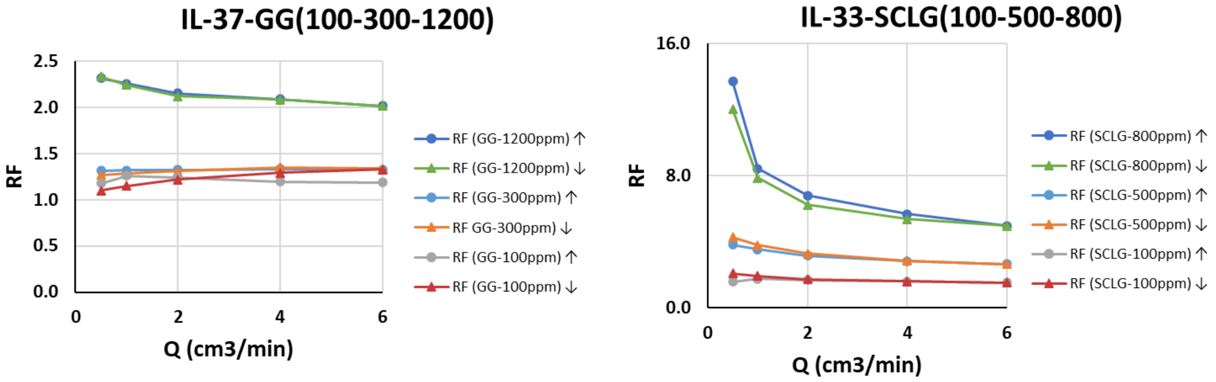

Figure 4-8 Comparison between Increasing and Decreasing the injection flow rate in IL-37 & IL-33

The results of the Residual Resistance Factor (RRF) showed a similar behavior to the RF, considering that both are related to the same properties, with the difference being that the RRF is based on the relationship between post- and pre-waterflooding. Figure 4-9 shows the permeability reduction of the different cores resulting from the injection of the biopolymers used.

The results showed that Scleroglucan had the highest RRF values, reaching 5,9 at an injection rate of 0.5 cm^3/min and 3,2 at 6 cm^3/min, at a concentration of 800ppm, compared to the other biopolymers tested. This suggests that Scleroglucan is more effective at reducing the flow through the rock, leading to a better oil recovery. To further understand the interaction of biopolymers with oil, experiments with the presence of oil would be necessary. Xanthan Gum and Scleroglucan have similar viscosities at concentrations of 700 and 500ppm, respectively, but the results indicate that Xanthan Gum is better at reducing the permeability of the rock at those concentrations. Additionally, increasing the concentration of Scleroglucan showed a significant increase in RRF, surpassing the results obtained with Xanthan Gum, which had a higher viscosity as in the IL-46 experiment.

.

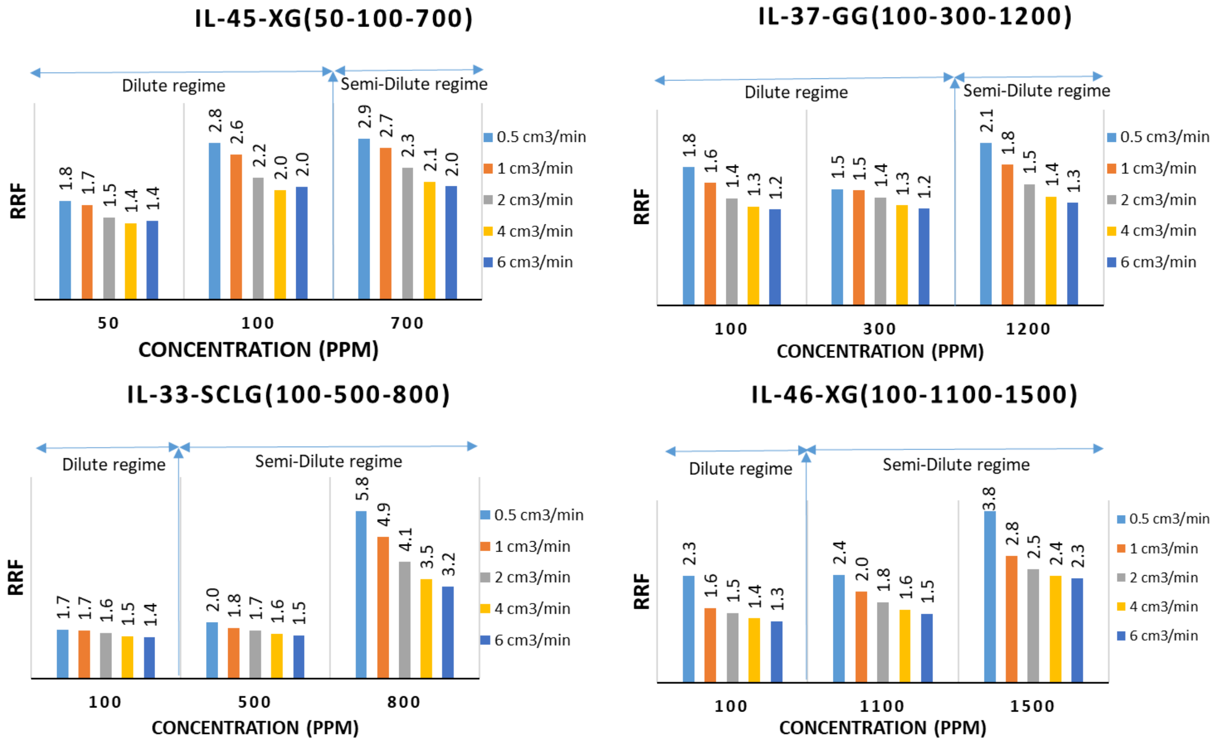

Figure 4-9 Residual Resistance Factor IL-45, IL-37, IL-33 & IL-46

In core flooding experiments, having a uniform flow throughout the core is an important factor as it ensures that the injection fluid is evenly distributed, leading to consistent and accurate results (S. R. Liu et al., 2016). Non-uniform flow can cause variations in pressure and flow in the core, resulting in some areas receiving more injection fluid than others. To ensure uniformity, an analysis was conducted for each core based on the sections separated by pressure taps. Figure 4-10 displays the RRF values for each section of the cores used in experiments, indicating that a uniform flow was maintained throughout the core except for section A, where all sections displayed disproportionately high values compared to the others. This cause an abrupt drop in pressure on the rock face (Freire Filho & Moreno, 2022), may be due to as particles are mainly retained in that section close to the entrance face of the core (Sorbie, 1991).

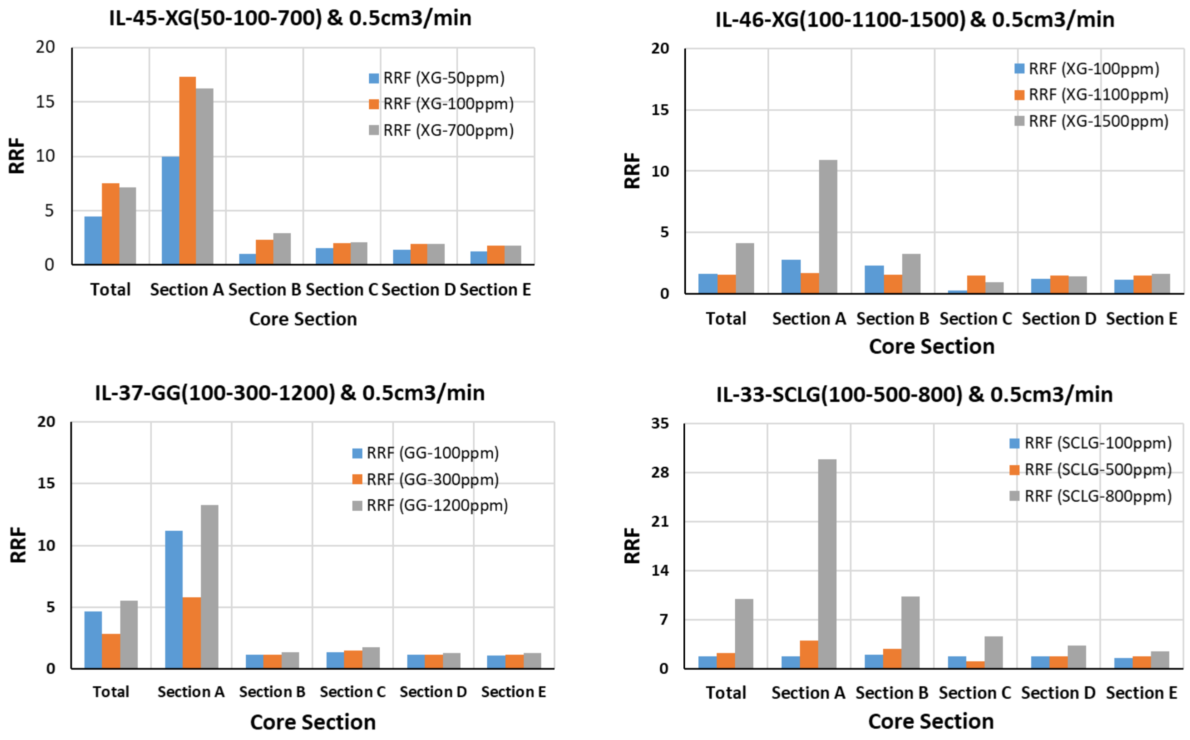

Figure 4-10 Residual Resistance Factor by Core Sections

Figure 4-11 shows the results of the Resistance Factor (RF) and Residual Resistance Factor (RRF) from the latest experiment IL-34. This experiment used a Xanthan Gum solution with concentrations similar to those in experiments IL-45 and IL-46 but with higher injection rates of up to 14 cm^3/min. It is important to note that the rock with the highest permeability among the available options was selected for this experiment. Using cores with higher permeability for polymer flooding with high injection rates would be the best way to perform core flooding with biopolymers (Sorbie, 1991).

Different studies showed diverse behaviors in terms of permeability reduction with respect to flow rate. Some studies observed increasing, decreasing, or constant RRF values with increasing flow rate, while others reported a hysteresis effect in the RRF with respect to the flow rate. One study found that the FRR is independent of the flow rate, but the experimental design may have affected the results (de Sousa Ferreira, 2019).

The results show an increase in the mobility of the polymer solution as the injection rates increase. It is also worth noting that increasing the concentration increases the RF results. In IL-34, comparing the RF results of 1 and 14 cm^3/min, there is a drastic reduction of approximately 60% of the value obtained with 1 cm^3/min. However, as the injection rate increases, the reduction becomes less significant compared to the previous rate. That is due to the shorter time that the solution has to be in contact with the surface of the pores, as the study by Mishra, Bera, and Mandal (2014 mentions that adsorption is also a function of the time the polymer interacts within the rock. On the other hand (AlSofi et al., 2017) mention that the low decrease in the Residual Resistance Factor (RRF) with increasing injection rate is due to mechanical trapping.

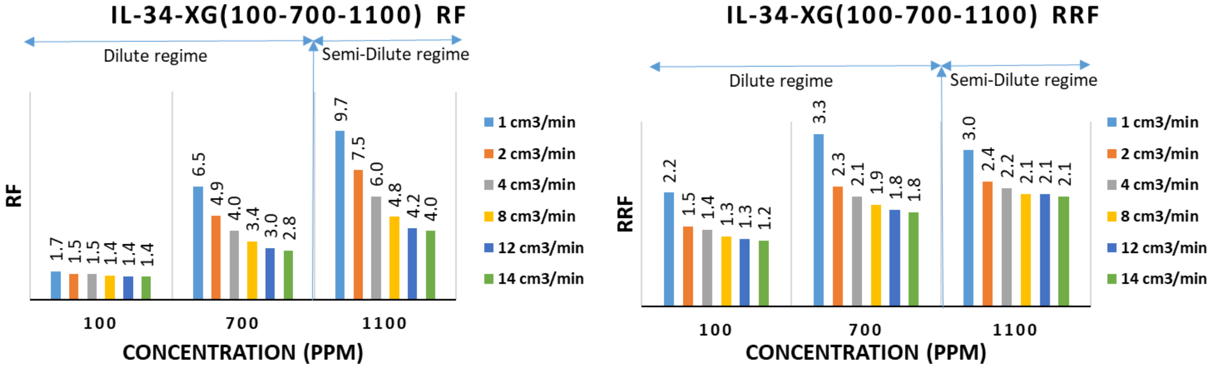

Figure 4-11 Resitance Factor and Residual Resistance Factor from IL-34

Figure 4-12 displays the *in-situ* viscosity results obtained from experiments IL-45, IL-37, IL-33, and IL-46. The behavior of the polymer solutions varied based on their concentrations relative to the overlap concentration C*. Concentrations below C* exhibited Newtonian behavior. This behavior was observed for 50 and 100 ppm concentrations in IL-45 and 100 and 300 ppm in IL-37. Concentrations above C* showed shear-thinning behavior, except for Guar Gum at 1200 ppm, which also behaved as Newtonian fluid indicated by the behavior index n close to unity.

For concentrations above the overlap concentration C*, they showed a shear thinning behavior except for Guar Gum of 1200, which has not been enough to obtain a pseudoplastic behavior, as can be seen in Table 4-4 that its behavior index 'n' is more significant than unity indicating dilatant behavior. Regarding Scleroglucan, it was observed that the viscosities remain similar across different concentrations. However, Xanthan Gum showed a more pronounced shear-thinning behavior at higher concentrations, with a more significant reduction in viscosity as the shear rate increased. Additionally, the results indicate that the decrease in viscosity between flow rates of 4 and 6 cm3/min was less significant than the reduction observed between flow rates of 0.5 and 1 cm3/min. As a result, it was decided to conduct the IL-34 experiment at higher injection rates.

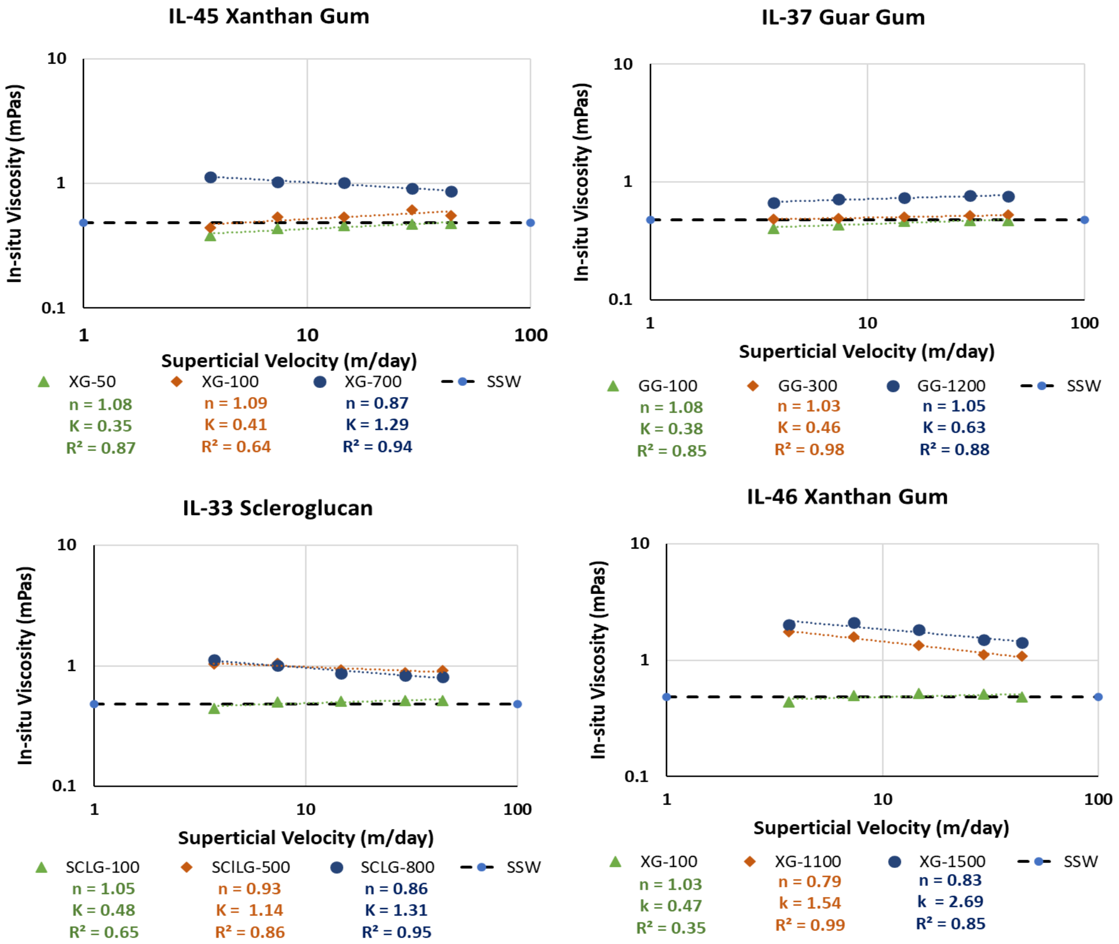

Figure 4-12 ***In-situ*** **Viscosity from IL-45, IL-37, IL-33 & IL-46**

Figure 4-13 displays the viscosity results from the IL-34 experiment, which utilized Xanthan Gum but with different injection flow rates, as discussed in the previous chapter. Notably, even at the 100ppm concentration, increasing the permeability caused a thinning behavior compared to the IL-45 and IL-46 experiments with the same concentration. The difference in the viscosity behavior observed in the core flooding experiment with Xanthan Gum solution can be attributed to the cores' permeability variation. When the solution with higher permeability was injected into the core, the effects of the shear rate decreased, and the flow was better. As a result, the solution showed a higher viscosity in the semi-diluted region compared to the other cores with lower permeability. On the other hand, the cores with lower permeability experienced higher shear rates due to the restricted flow and higher deformation, resulting in reduced viscosity and a more Newtonian behavior with a slight shear thinning behavior. This indicates that the viscosity of the Xanthan Gum solution is dependent on the flow conditions and can vary based on the permeability of the core.

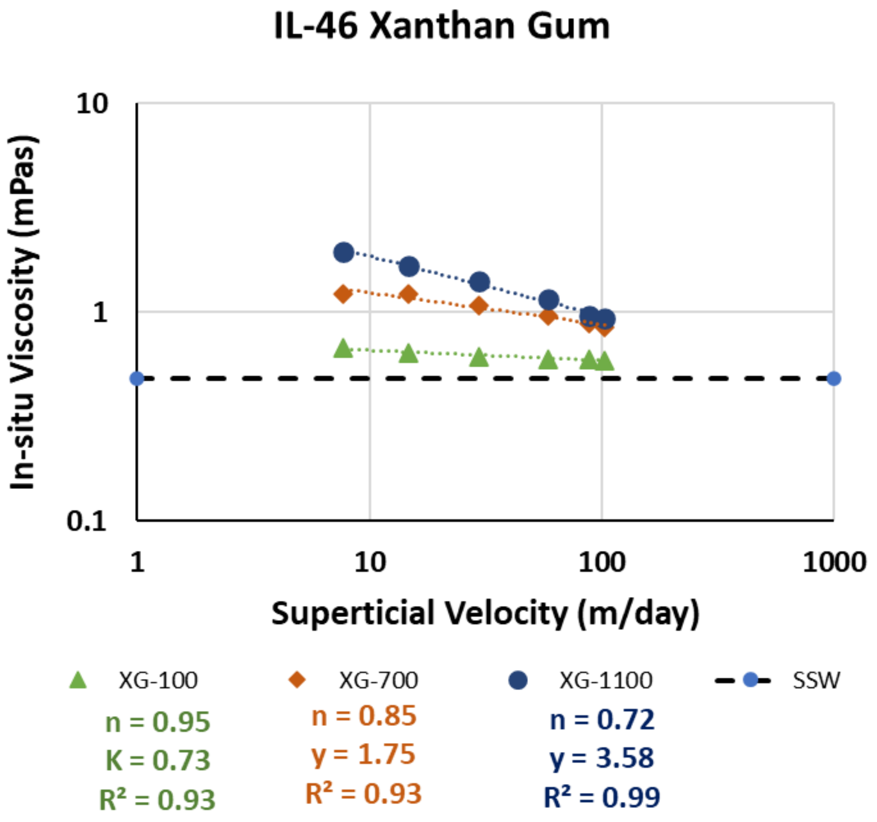

Figure 4-13 ***In-situ*** **Viscosity from IL-34**

Table 4-4 displays the values of the behavior index and the consistency coefficient for the viscosity curves shown in Figure 4-12 and Figure 4-13. The behavior index, also known as the flow behavior index, measures the degree of shear thinning behavior of a fluid, with values less than 1 indicating shear thinning and values greater than one indicating shear thickening. The consistency coefficient, also called the apparent viscosity or the zero-shear viscosity, is a measure of a fluid's resistance to flow, with higher values indicating a more viscous fluid. These values are important for understanding the rheological properties of the different solutions and can be used to determine their suitability for specific applications.

Table 4-4 Pow Law Coefficients

Experiment	Concentration(ppm)	k	n	R^2
IL-45	XG-50	0.35	1.08	0.87
IL-45	XG-100	0.41	1.09	0.64
IL-45	XG-700	1.29	0.87	0.94
IL-37	GG-100	0.38	1.08	0.85
IL-37	GG-300	0.46	1.03	0.98
IL-37	GG-1200	0.63	1.05	0.88
IL-33	SCLG-100	0.48	1.05	0.65
IL-33	SClLG-500	1.14	0.93	0.86
IL-33	SCLG-800	1.31	0.86	0.95
IL-46	XG-100	0.47	1.03	0.35
IL-46	XG-1100	1.54	0.79	0.99
IL-46	XG-1500	2.69	0.83	0.85
IL-34	XG-100	0.73	0.95	0.93
IL-34	XG-700	1.75	0.85	0.93
IL-34	XG-1100	3.58	0.72	0.99

The relative injectivity is determined using equation 2.11, which correlates the pressure drops of polymeric solutions with that of the first brine injection. Figure 4-14 demonstrates that increased injection flow rates lead to higher relative injectivity across all experiments under a semi-diluted regime.

For IL-45, which involved xanthan gum solutions at concentrations of 50, 100, and 700 ppm, the slight difference in injectivity between the 100 ppm and 700 ppm solutions may be attributed to plugging occurring at the initial surface of the core, displaying irregular behavior compared to the rest of the core sections.

The interaction between the polymer and the porous medium could explain the behavior observed in Figure 4-14 for guar gum solutions. At lower injection rates, the polymer has more time to interact with the porous medium, leading to higher adsorption and plugging effects, which results in lower injectivity. However, as the injection flow rate increases, the polymer has less time to interact with the rock surface, reducing adsorption and higher relative injectivity. In the case of the 300ppm experiment, the higher polymer concentration may have caused more initial adsorption and plugging effects, but since the polymer is still in the dilute region, its viscosity is not high enough to significantly impede flow. As a result, injectivity remains relatively stable as the injection flow rate increases.

Regarding IL-33, the behavior of the Scleroglucan solution can be understood by considering the viscosity of the polymer solution at different concentrations. As the Scleroglucan concentration increases, the viscosity of the solution also increases, resulting in higher pressure drops and lower relative injectivity. This behavior is expected, as higher polymer concentrations generally increase flow resistance. However, in-situ viscosity measurements show similar viscosities for the 500 ppm and 800 ppm polymer solutions, which may seem contradictory. It's important to note that in-situ viscosity measurements can be influenced by factors such as shear rate and the configuration of the pore space, which can vary in different core sections.

The behavior observed in IL-46 aligns with the rheological properties of xanthan gum solutions. As the xanthan gum concentration increases, the bulk viscosity of the solution also increases, resulting in higher pressure drop and lower injectivity due to increased flow resistance through the porous media. The higher xanthan gum concentration may also lead to more severe fluid-rock interactions, causing more significant damage and reduction in the relative injectivity. Therefore, the obtained results in this case are consistent with the expected behavior of high-concentration xanthan gum solutions.

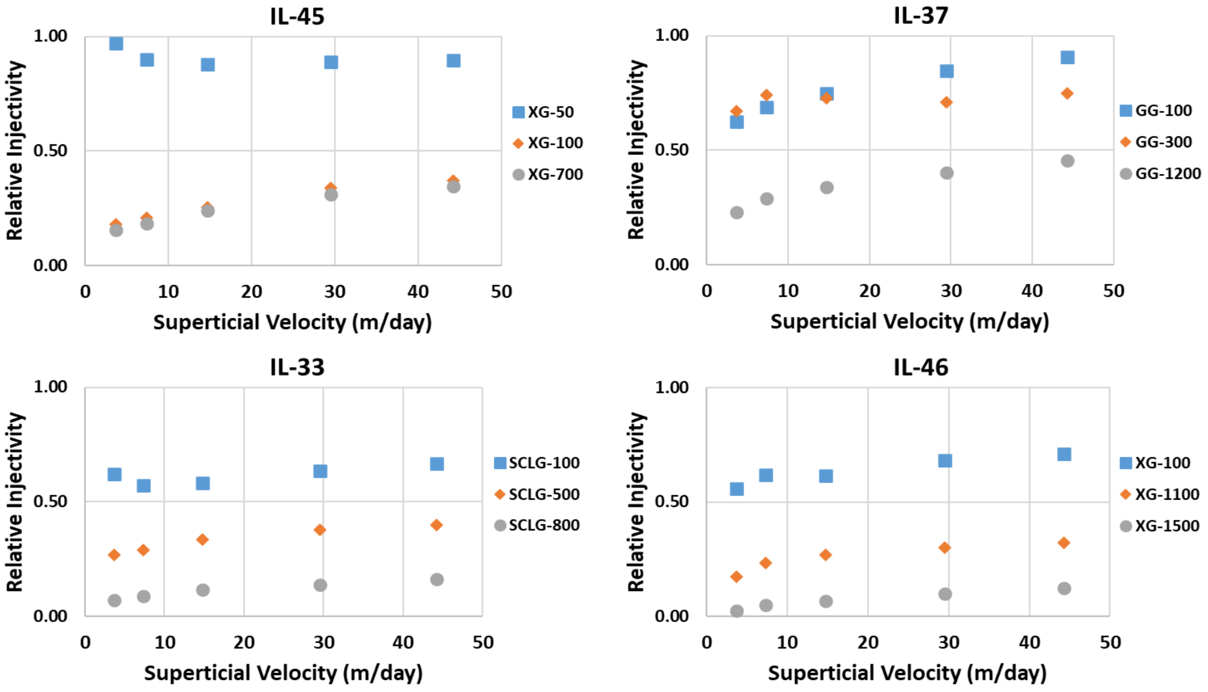

Figure 4-14 Relative Injectivity from IL-45, IL-37, IL-33 & IL-46

Figure 4-15 shows the injectivity of the core with the highest permeability. Xanthan Gum solutions of 700ppm and 1100ppm resulted in similar injectivity values despite having different concentrations. This observation may indicate an optimal concentration range for Xanthan Gum where higher concentrations do not provide any additional benefits in relative injectivity. Another possibility is that the 1100 ppm solution may have a higher tendency to adsorb onto the rock surface, causing a reduction in injectivity. It is also important to note that permeability and rock properties can play a significant role in the injectivity behavior of the solutions.

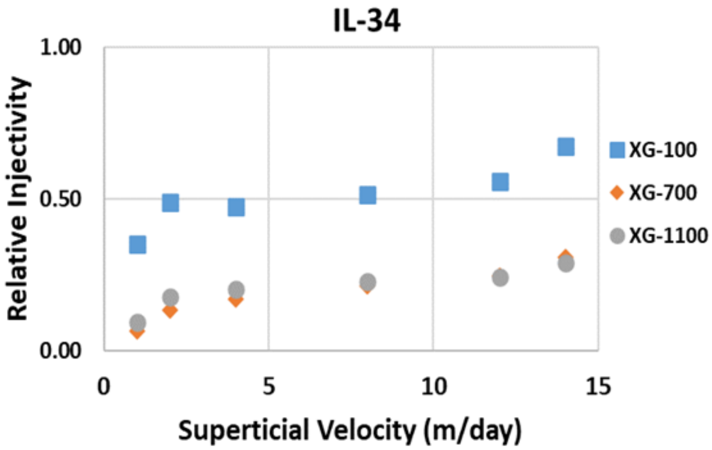

Figure 4-15 Relative Injectivity from IL-34

Based on the results presented in Figure 4-17Figure 4-16 and Figure 4-16, it is evident that the pressure drops of the experiments vary as a function of the distance from the pressure taps, which have been divided into five sections. Section A, located at the inlet surface of the core, shows an abnormal drop in pressure compared to the other sections. This difference in pressure drop can become even more abrupt as the injection rate increases, as observed in the case of IL-45. It is likely that section A has the lowest permeability compared to the other sections of the core. This hypothesis can be further verified by calculating the effective permeability to water during the initial water injections before the polymer injection. However, it is essential to note that neither of these methods can provide absolute certainty, and further studies, such as topographic imaging, are needed to confirm these conditions.

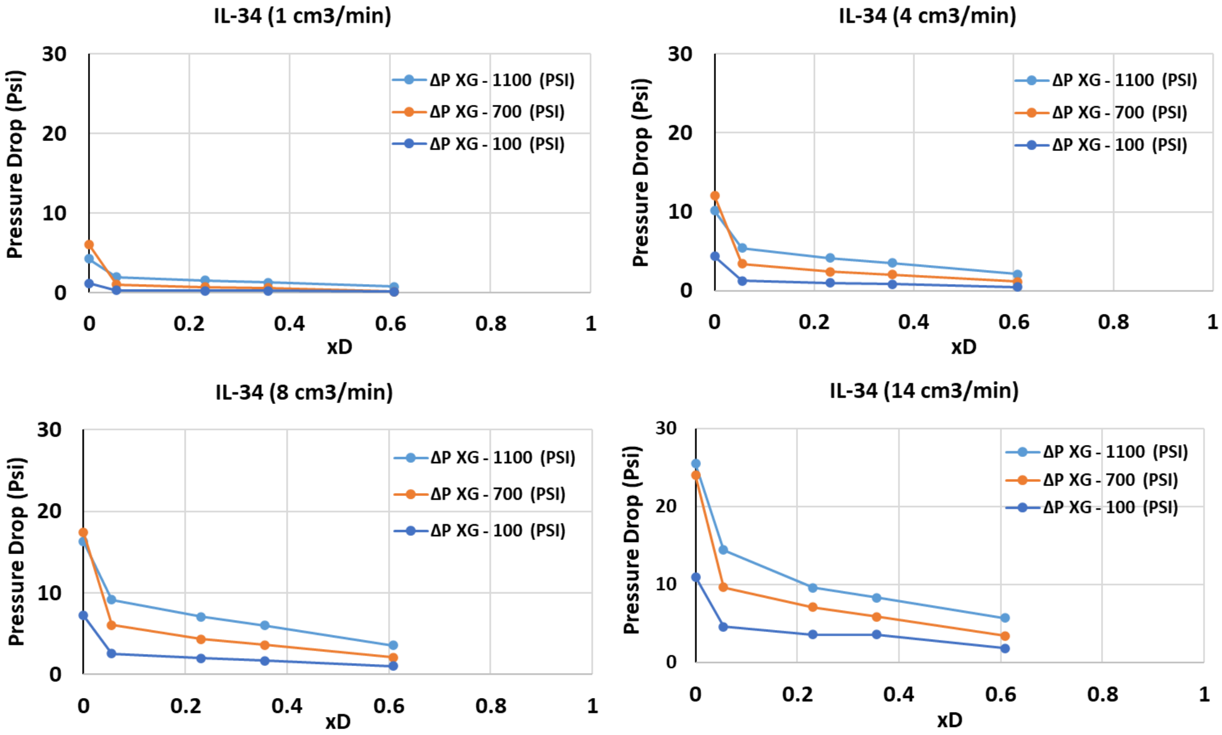

Figure 4-16 Pressure Drop from IL-34

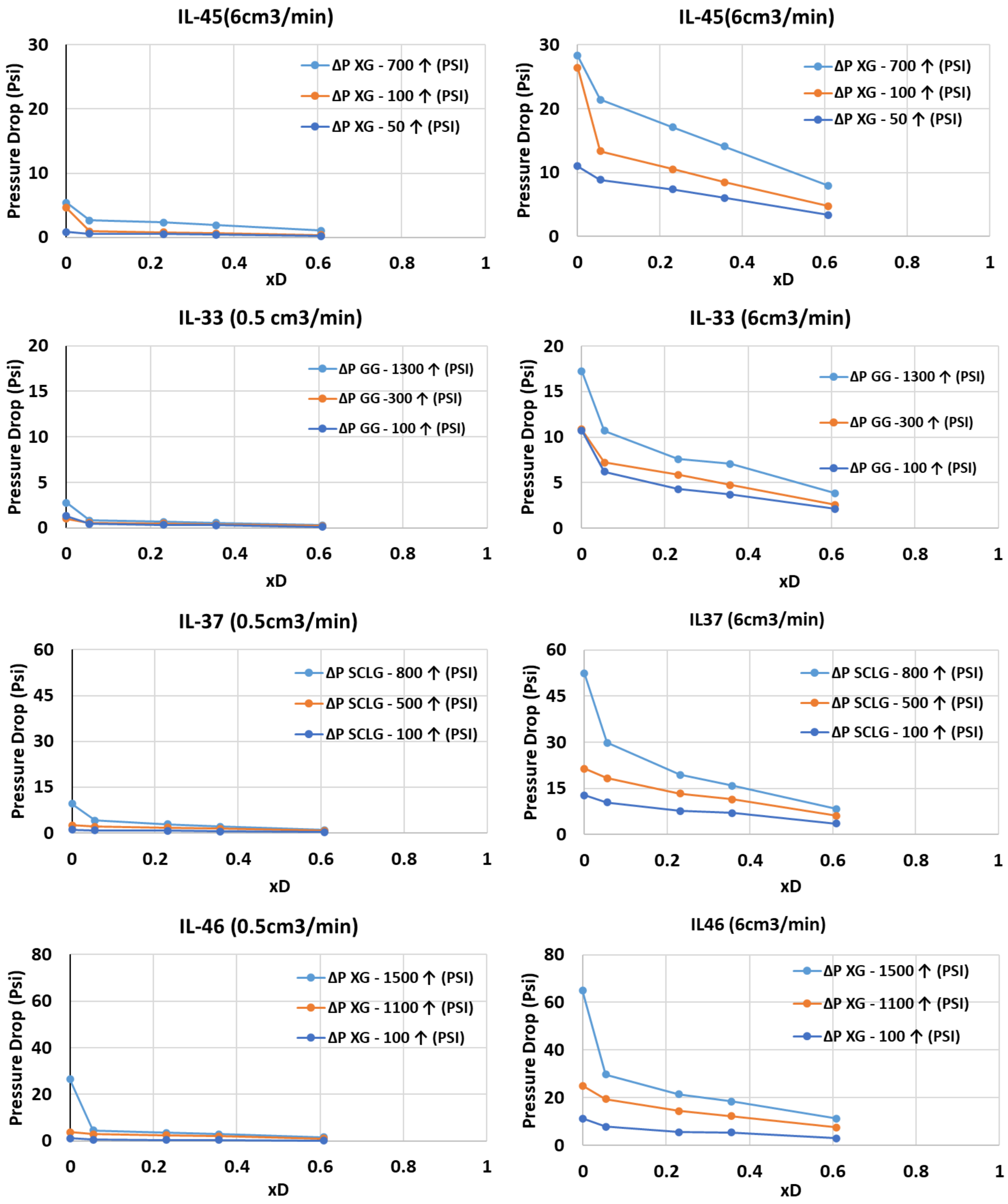

Figure 4-17 Pressure Drop of IL-45, IL-33, IL-37 & IL-46

5 CONCLUSIONS AND RECOMMENDATIONS

This chapter presents the conclusions of an experimental laboratory study conducted to explore the application of biopolymer injection for EOR. The main findings and recommendations for future work are summarized below.

5.1 Conclusions

- A significant decrease in the solution's apparent viscosity was observed during filtration (around 30 - 40% for Xanthan Gum,30% for Scleroglucan, and 75% for Guar Gum). Although the viscosity loss levels, XG and SCLG shear-thinning behavior persisted for solutions with polymer content higher than critical concentration. Higher Xanthan Gum concentration in the solution leads to higher viscosity loss during filtration.
- Guar Gum required additional pre-filtration and experienced the highest viscosity loss, attributed to impurities such as proteins and fibers suspended in the solution. Conversely, Scleroglucan underwent a filtration process similar to that of Xanthan Gum and presented the lowest viscosity loss among the three tested polymers.
- Under diluted regimes, the Resistance Factor remained constant. However, at concentrations higher than the critical one (semi-diluted concentration regime), the resistance factor increased with an increase in polymer concentration and decreased with an increase in the flow rate.
- The results for the Residual Resistance Factor showed a consistent and similar trend with the Resistance Factor, indicating a relationship between these two parameters. Among the biopolymers, Scleroglucan exhibited the highest RRF values, suggesting that it is particularly effective in reducing the chasing water flow through the rock and enhancing oil recovery.
- The hysteresis evaluation showed a significant difference in resistance between upward and downward flow injections at low flow rates, particularly at higher concentrations. However, that difference became less pronounced as the flow rate increased.

- The in-situ viscosity of the polymer solutions varied based on their concentrations and the polymer type. Xanthan Gum and Scleroglucan exhibited a shear-thinning behavior for concentrations above the critical concentration, while Guar Gum behaved as a Newtonian fluid for the tested concentration range, presenting a behavior index close to unity.
- The flooding of Xanthan Gum through cores with different levels of permeability, flow rates, and polymer concentrations indicated the in-situ viscosity dependence on those parameters. In the same way, the Guar Gum core flooding tests evidenced the correlation between the flow rate, contact time between the polymer solution and the surface of the pores, and the injectivity. As the injection flow rate increases, the polymer has less time to interact with the rock surface, reducing adsorption and higher relative injectivity.

5.2 Recommendations

Glutaraldehyde is crucial when working with biopolymers due to their susceptibility to microbial degradation. Additionally, it is essential to ensure that the biopolymer is constantly exposed to light to prevent the growth of fungi. However, it is vital to exercise caution and employ appropriate safety equipment when handling glutaraldehyde, as it can pose risks to human health.

Further studies are recommended to gain a more comprehensive understanding of the impact of biopolymer concentration and injection rate on injectivity under varying reservoir conditions. Specifically, it would be beneficial to test a broader range of injection rates and measure the resulting injectivities, which could help establish optimal injection rates for different polymer solutions and rock types. Additionally, two-phase core flooding experiments could be performed to assess the performance in the presence of oil and analyze the capillary pressure, which could provide valuable insights into the system's behavior. By conducting such studies, it may be possible to gain a deeper understanding of the factors that influence injectivity and develop more effective strategies for enhancing oil recovery using biopolymer flooding techniques.

REFERENCES

Aadnøy, B. S., & Looyeh, R. (2019). Shale Oil, Shale Gas, and Hydraulic Fracturing. In *Petroleum Rock Mechanics* (pp. 357–389). Elsevier. https://doi.org/10.1016/B978-0-12-815903-3.00016-9

Abbasi, J., Raji, B., Riazi, M., & Kalantariasl, A. (2017). A simulation investigation of performance of polymer injection in hydraulically fractured heterogeneous reservoirs. *Journal of Petroleum Exploration and Production Technology*, *7*(3), 813–820. https://doi.org/10.1007/s13202-016-0295-x

Ahmed, T. (2010). Reservoir Engineering Handbook 4th Edition. In *Reservoir Engineering Handbook*. Elsevier. https://linkinghub.elsevier.com/retrieve/pii/B9781856178037500018

Akbari, S., Mohammad, S., Hadian, N., & Al-hajri, S. (2019). A critical review of concept and methods related to accessible pore volume during polymer-enhanced oil recovery. *Journal of Petroleum Science and Engineering*, *182*(July), 106263. https://doi.org/10.1016/j.petrol.2019.106263

Al-Mjeni, R., Arora, S., Cherukupalli, P., Van Wunnik, J., Edwards, J., Felber, B. J., Gurpinar, O., Hirasaki, G. J., Miller, C. A., Jackson, C., Kristensen, M. R., Lim, F., & Ramamoorthy, R. (2010). Has the time come for EOR? *Oilfield Review*, *22*(4), 16–35.

Al-Shakry, B. (2021). *Polymer Injectivity : Experimental Studies of Flow in Porous Media for EOR Polymers*. https://bora.uib.no/bora-xmlui/handle/11250/2727318

Al-Shakry, B., Shiran, B. S., Skauge, T., & Skauge, A. (2018). Enhanced oil recovery by polymer flooding: Optimizing polymer injectivity. *Society of Petroleum Engineers - SPE Kingdom of Saudi Arabia Annual Technical Symposium and Exhibition 2018, SATS 2018*. https://doi.org/10.2118/192437-ms

Al-Shakry, B., Shiran, B. S., Skauge, T., & Skauge, A. (2019). Polymer injectivity: Influence of permeability in the flow of EOR polymers in porous media. *Society of Petroleum Engineers - SPE Europec Featured at 81st EAGE Conference and Exhibition 2019*. https://doi.org/10.2118/195495-ms

Al-Shakry, B., Skauge, T., Shiran, B. S., & Skauge, A. (2018). Impact of mechanical degradation on polymer injectivity in porous media. *Polymers*, *10*(7), 1–23. https://doi.org/10.3390/polym10070742

Al-Shakry, B., Skauge, T., Shiran, B. S., & Skauge, A. (2019). Polymer injectivity: Investigation of mechanical degradation of enhanced oil recovery polymers using in-situ rheology. *Energies*, *12*(1). https://doi.org/10.3390/en12010049

Aldhaheri, M. N., Wei, M., & Bai, B. (2016). Comprehensive guidelines for the application of in-situ polymer gels for injection well conformance improvement based on field projects. *SPE - DOE Improved Oil Recovery Symposium Proceedings*, *2016-Janua*. https://doi.org/10.2118/179575-ms

Alfazazi, U., Thomas, N. C., Alameri, W., & Al-Shalabi, E. W. (2020). Experimental investigation of polymer injectivity and retention under harsh carbonate reservoir conditions. *Journal of Petroleum Science and Engineering*, *192*(January), 107262. https://doi.org/10.1016/j.petrol.2020.107262

AlSofi, A. M., Wang, J., Leng, Z., Abbad, M., & Kaidar, Z. F. (2017). Assessment of polymer interactions with carbonate rocks and implications for EOR applications. *Society of Petroleum Engineers - SPE Kingdom* *of Saudi Arabia Annual Technical Symposium and Exhibition 2017*, 881–902. https://doi.org/10.2118/188086-ms

Alvarado, V., & Manrique, E. (2010). ENHANCED OIL RECOVERY Field Planning and Development Strategies. In *Enhanced Oil Recovery* (p. iv). Elsevier. https://doi.org/10.1016/B978-1-85617-855-6.00002-4

Alzaabi, M. A., Jacobsen, J. G., Masalmeh, S., Al Sumaiti, A., Pettersen, Ø., & Skauge, A. (2020). Polymer injectivity test design using numerical simulation. *Polymers*, *12*(4), 1–23. https://doi.org/10.3390/POLYM12040801

American Petroleum Institute. (1990). *Recommended Practices for Evaluation of Polymers Used in Enhanced Oil Recovery Operations*.

American Petroleum Institute. (1998). *Recommended Practices for Core Analysis*. *February*.

ANP. (2022). Relatório de Gestão da ANP 2022. *ANP*.

Batonyi, A., Thorburn, L., Molnar, S., & Corporation, E. (2016). *A Reservoir Management Case Study of a Polymer Flood Pilot in Medicine Hat Glauconitic C Pool Field Description and Development History*.

Bchini, Q., Crenes, M., & Prunel, B. (2022). Enerdata – Global Energy & Climate Trends - 2022 Edition - The post-pandemic rebound. Faster, Stronger, Harder. *Enerdata*.

Beteta, A., Nurmi, L., Oyj, K., Rosati, L., & Hanski, S. (2020). *Polymer Chemical Structure and its Impact on EOR Performance Introduction*. https://doi.org/https://doi.org/10.2118/200441-MS

BP. (2022). BP Statistical Review of World Energy 2022,(71st edition). *Bp*, 1–60.

Buell, R. S., Kazemi, H., & Poettmann, F. H. (1990). Analyzing injectivity of polymer solutions with the Hall plot. *SPE Reservoir Engineering (Society of Petroleum Engineers)*, *5*(1). https://doi.org/10.2118/16963-pa

Carolina, Y., Itriago, A. De, North, S. G. S., Fresky, M. A., & Houston, I. C. (2019). *Polymers for EOR in Offshore Reservoirs : Recommended Practices for Laboratory Screening*.

Chandran, N., Sarathchandran, C., & Thomas, S. (2019). Introduction to rheology. In *Rheology of Polymer Blends and Nanocomposites: Theory, Modelling and Applications*. Elsevier Inc. https://doi.org/10.1016/B978-0-12-816957-5.00001-X

Civan, F. (2000). *Reservoir Formation Damage* (Vol. 1999, Issue December). Gulf Professional Publishing.

Clinckspoor, K. J., De Sousa Ferreira, V. H., & Barros Zanoni Lopes Moreno, R. (2021). Bulk rheology characterization of biopolymer solutions and discussions of their potential for enhanced oil recovery applications. *CTyF - Ciencia, Tecnologia y Futuro*, *11*(1), 123–135. https://doi.org/10.29047/01225383.367

Corlay, P., Lemouzy, P., Eschard, R., & Zhang, L. R. (1992). *Fully integrated reservoir study and numerical forecast simulations of two-polymer pilots in Daqing field*. 331–340. https://doi.org/10.2523/22364-ms

Dakhil, H., Auhl, D., & Wierschem, A. (2019). Infinite-shear viscosity plateau of salt-free aqueous xanthan solutions. *Journal of Rheology*, *63*(1), 63–69. https://doi.org/10.1122/1.5044732

De Melo, M. A., De Holleben, C. R. C., Da Silva, I. P. G., De Barros Correia, A., Da Silva, G. A., Rosa, A. J., Lins, A. G., & De Lima, J. C. (2005). Evaluation of polymer injection projects in Brazil. *SPE Latin American and Caribbean Petroleum Engineering Conference Proceedings*, *2005-June*. https://doi.org/10.2118/0106-0050-jpt

de Moura, M. R. V., & Moreno, R. B. Z. L. (2019). Concentration, brine salinity and temperature effects on xanthan gum solutions rheology. In *Applied Rheology* (Vol. 29, Issue 1, pp. 69–79). https://doi.org/10.1515/ARH-2019-0007

De Simoni, M., Boccuni, F., Sambiase, M., Spagnuolo, M., Albertini, M., Tiani, A., & Masserano, F. (2018). Polymer injectivity analysis and subsurface polymer behavior evaluation. *Society of Petroleum Engineers - SPE EOR Conference at Oil and Gas West Asia 2018*, *2018-March*(March), 26–28. https://doi.org/10.2118/190383-ms

de Sousa Ferreira, V. H. (2019). *Key parameters on the flow of polymer solutions through porous medium experimental and modeling studies* [Universidade Estadual de Campinas]. https://hdl.handle.net/20.500.12733/1639101

Delamaide, E. (2014). Polymer flooding of heavy oil - From screening to full-field extension. *Society of Petroleum Engineers - SPE Heavy and Extra Heavy Oil Conference - Latin America 2014, LAHO 2014*, 707–736. https://doi.org/10.2118/171105-ms

Delamaide, E., Zaitoun, A., Renard, G., Tabary, R., & IFP. (2013). Pelican Lake Field: First Successful Application of Polymer Flooding in a Heavy Oil Reservoir and René Tabary, IFP Energies nouvelles *Now with Poweltec. *SPE Internacional*, *18*(Cenovus 2011), 22. https://www.onepetro.org/download/conference-paper/SPE-165234-MS?id=conference-paper%2FSPE-165234-MS

Ding, L., Wu, Q., Zhang, L., & Guérillot, D. (2020). Application of fractional flow theory for analytical modeling of surfactant flooding, polymer flooding, and surfactant/polymer flooding for chemical enhanced oil recovery. *Water (Switzerland)*, *12*(8). https://doi.org/10.3390/w12082195

Dong, H. Z., Fang, S. F., Wang, D. M., Wang, J. Y., Liu, Z., & Hong, W. H. (2008). Review of practical experience & management by polymer flooding at Daqing. In *Proceedings - SPE Symposium on Improved Oil Recovery* (Vol. 3). https://doi.org/10.2118/114342-ms

Ezekwe, N. (2010). *Petroleum Reservoir Engineering Practice*. Pearson Education.

Ferreira, V. H. de S., & Moreno, R. B. Z. L. (2018). Workflow for Oil Recovery Design by Polymer Flooding. *Volume 8: Polar and Arctic Sciences and Technology; Petroleum Technology*, *8*. https://doi.org/10.1115/OMAE2018-78359

Ferreira, V. H. S., & Moreno, R. B. Z. L. (2020). Experimental evaluation of low concentration scleroglucan biopolymer solution for enhanced oil recovery in carbonate. *Oil and Gas Science and Technology*, *75*(September). https://doi.org/10.2516/ogst/2020056

Fournier, R., Tiehi, J. E., & Zaitoun, A. (2018). Laboratory Study of a New EOR-Grade Scleroglucan. *Society of Petroleum Engineers - SPE EOR Conference at Oil and Gas West Asia 2018*, *2018-March*(March), 26–28. https://doi.org/10.2118/190451-ms

Freire Filho, M. E. N., & Moreno, R. B. Z. L. (2022). Injection of Xanthan Gum and Guar Gum Through

Carbonate Rocks Evaluated by Two-Phase Core Flooding. *Journal of Energy Resources Technology, Transactions of the ASME*, *144*(11), 1–12. https://doi.org/10.1115/1.4054135

Gbadamosi, A. O., Junin, R., Manan, M. A., Agi, A., & Yusuff, A. S. (2019). An overview of chemical enhanced oil recovery: recent advances and prospects. In *International Nano Letters* (Vol. 9, Issue 3). Springer Berlin Heidelberg. https://doi.org/10.1007/s40089-019-0272-8

Ghahremani, H., Mobaraki, S., Khalilinezhad, S. S., & Jarrahian, K. (2018). An experimental study of the performance of low-molecular weight polymer for enhanced heavy oil recovery in a heterogeneous media. *Geosystem Engineering*, *21*(2), 95–102. https://doi.org/10.1080/12269328.2017.1385424

Glasbergen, G., Wever, D., Keijzer, E., & Farajzadeh, R. (2015, October 11). Injectivity Loss in Polymer Floods: Causes, Preventions and Mitigations. *All Days*. https://doi.org/10.2118/175383-MS

Green, D. W., & Willhite, G. P. (2018). Enhanced Oil Recovery. In *Geothermics* (Vol. 19, Issue 2). Society of Petroleum Engineers (SPE). https://doi.org/10.2118/9781613994948

Guo, H., & Song, K. (2021). Polymer injectivity learned from 20 years polymer flooding field practices. *IOR 2021 - 21st European Symposium on Improved Oil Recovery*, *April 2021*. https://doi.org/10.3997/2214-4609.202133062

Han, M., Fuseni, A., Zahrani, B., & Wang, J. (2014, March 31). Laboratory Study on Polymers for Chemical Flooding in Carbonate Reservoirs. *All Days*. https://doi.org/10.2118/169724-MS

Hasan, A. M. A., & Abdel-Raouf, M. E. (2018). Applications of guar gum and its derivatives in petroleum industry: A review. *Egyptian Journal of Petroleum*, *27*(4), 1043–1050. https://doi.org/10.1016/j.ejpe.2018.03.005

INDIANA LIMESTONE INSTITUTE. (2007). *Indiana Limestone Handbook* (22nd ed.). Indiana Limestone Institute of America, Inc. http://www.iliai.com

Jang, H. Y., Zhang, K., Chon, B. H., & Choi, H. J. (2015). Enhanced oil recovery performance and viscosity characteristics of polysaccharide xanthan gum solution. *Journal of Industrial and Engineering Chemistry*, *21*, 741–745. https://doi.org/10.1016/j.jiec.2014.04.005

Jensen, T., Kadhum, M., Kozlowicz, B., Sumner, E. S., Malsam, J., Muhammed, F., & Ravikiran, R. (2018). Chemical EOR under Harsh conditions: Scleroglucan as a viable commercial solution. *Proceedings - SPE Symposium on Improved Oil Recovery*, *2018-April*, 1–16. https://doi.org/10.2118/190216-ms

Jones, M. A. (1966). Waterflood Mobility Control: A Case History. *Journal of Petroleum Technology*, *18*(09), 1151–1156. https://doi.org/10.2118/1427-pa

Juárez, J. L., Bertin, H., Omari, A., Romero, C., Jouenne, S., Morel, D., & Neillo, V. (2020). Polymer Injection for EOR: Influence of Mobility Ratio and Slug Size on FinalOil Recovery. *Society of Petroleum Engineers - SPE Europec Featured at 82nd EAGE Conference and Exhibition*. https://doi.org/10.2118/200611-ms

Kakati, A., Kumar, G., & Sangwai, J. S. (2020). Low Salinity Polymer Flooding: Effect on Polymer Rheology, Injectivity, Retention, and Oil Recovery Efficiency. *Energy and Fuels*, *34*(5), 5715–5732. https://doi.org/10.1021/acs.energyfuels.0c00393

Kamal, M. S., Sultan, A. S., Al-Mubaiyedh, U. A., & Hussein, I. A. (2015). Review on polymer flooding:

Rheology, adsorption, stability, and field applications of various polymer systems. *Polymer Reviews*, *55*(3), 491–530. https://doi.org/10.1080/15583724.2014.982821

Kaminsky, R. D., Wattenbarger, R. C., Szafranski, R. C., & Coutee, A. S. (2007). Guidelines for polymer flooding evaluation and development. *International Petroleum Technology Conference 2007, IPTC 2007*, *1*, 243–250. https://doi.org/10.2523/iptc-11200-ms

Kozlowicz, B., Muhammed, F., Kadhum, M., Khambete, M., Jensen, T., Sumner, E., Ravikiran, R., & Ray, C. (2019). Qualification and Field Injection of Scleroglucan. *IOR 2019 – 20th European Symposium on Improved Oil Recovery*, *April 2019*, 1–14. https://doi.org/10.3997/2214-4609.201900161

Li, Z., & Delshad, M. (2014). Development of an analytical injectivity model for non-Newtonian polymer solutions. *SPE Journal*, *19*(3), 381–389. https://doi.org/10.2118/163672-PA

Li, Z., Sun, Z., Nicolas Espinoza, D., & Balhoff, M. T. (2020). Grain-scale modeling of polymer-driven fracture initiation and wellbore injectivity. *Proceedings - SPE Symposium on Improved Oil Recovery*, *2020-Augus*. https://doi.org/10.2118/200412-ms

Littmann, W., Kleinitz, W., Christensen, B. E., & Stokke, B. T. (1992). Late results of a polymer pilot test. Performance, simulation adsorption, and xanthan stability in the reservoir. *Eighth Symposium on Enhanced Oil Recovery*, 177–188. https://doi.org/10.2523/24120-ms

Liu, S. R., Kang, W. L., Zhu, L. Bin, Han, B., Yang, X. H., Zhang, X. Q., Zhang, H. L., & Lei, P. (2016). Experimental study on uniform mobility displacement method for heterogeneous reservoir. *Journal of Applied Science and Engineering*, *19*(3), 321–328. https://doi.org/10.6180/jase.2016.19.3.10

Liu, Z., Liang, Y., Wang, Q., Guo, Y., Gao, M., Wang, Z., & Liu, W. (2020). Status and progress of worldwide EOR field applications. *Journal of Petroleum Science and Engineering*, *193*(December 2019), 107449. https://doi.org/10.1016/j.petrol.2020.107449

Lu, X., Liu, F., Liu, G., Pei, Y., Jiang, H., & Chen, J. (2018). A Polymer Injectivity Model Establishment and Application for Early Polymer Injection. *Arabian Journal for Science and Engineering*, *43*(5), 2625–2632. https://doi.org/10.1007/s13369-017-2950-z

Machale, J., Majumder, S. K., Ghosh, P., & Sen, T. K. (2020). Role of chemical additives and their rheological properties in enhanced oil recovery. *Reviews in Chemical Engineering*, *36*(7), 789–830. https://doi.org/10.1515/revce-2018-0033

Manrique, E., Ahmadi, M., & Samani, S. (2017). Historical and recent observations in polymer floods: An update review. *CTyF - Ciencia, Tecnologia y Futuro*, *6–6*(5–5), 17–48. https://doi.org/10.29047/01225383.72

Martino, L. A., Righi, E. F., Gandi, S., Thompson, A., Giaquinta, A. D., & Ypf, S. A. (2017). *Surveillance and Initial Results of an Existing Polymer Flood : A Case History From The Rayoso Formation*.

Moe Soe Let, K. P., Manichand, R. N., & Seright, R. S. (2012). Polymer flooding a ∼500-cp oil. *SPE - DOE Improved Oil Recovery Symposium Proceedings*, *2*, 1670–1682. https://doi.org/10.2118/154567-ms

Mohsenatabar Firozjaii, A., & Saghafi, H. R. (2020). Review on chemical enhanced oil recovery using polymer flooding: Fundamentals, experimental and numerical simulation. *Petroleum*, *6*(2), 115–122. https://doi.org/10.1016/j.petlm.2019.09.003

Muhammed, N. S., Haq, B., & Al-shehri, D. (2020). *Comparative Study of Green and Synthetic Polymers for Enhanced Oil Recovery*. 1–32.

Ostermann, R. (2016). Enhanced Oil Recovery — Do You Have the Right EOR Strategy ? *Elsevier*, 1–12. https://www.elsevier.com/__data/assets/pdf_file/0017/230831/RDS_OG_EP_WP_-EOR-Right-Strategy_DIGITAL.pdf

Pérez, R., Castro Garcia, R. H., Jimenez, R., Maya, G. A., Leon Hinestrosa, J. M., Reyes, J. D., Mendez, A., Castillo Mejia, A. F., Romero, M. P., Fernandez Bedoya, F., Quintero Roa, L. M., & Quintero, H. (2017). Mature field revitalization using polymer flooding: Palogrande - Cebú field case. *SPE Latin American and Caribbean Petroleum Engineering Conference Proceedings*, 1–14. https://doi.org/10.2118/185552-ms

Pu, W., Shen, C., Wei, B., Yang, Y., & Li, Y. (2018). A comprehensive review of polysaccharide biopolymers for enhanced oil recovery (EOR) from flask to field. *Journal of Industrial and Engineering Chemistry*, *61*, 1–11. https://doi.org/10.1016/j.jiec.2017.12.034

Puskas, S., Vágó, Töro, M., Ördög, T., Kálmán, G. Y., Tabajd, R., Dékány, I., Dudás, J., Nagy, R., Bartha, L., Lakatos, I., Thomas, A., & Garcia, R. (2017). First surfactant-polymer EOR injectivity test in the Algyo Field, Hungary. *IOR NORWAY 2017 - 19th European Symposium on Improved Oil Recovery: Sustainable IOR in a Low Oil Price World*, *April 2017*. https://doi.org/10.3997/2214-4609.201700244

Putz, A. G., Production, E. A., Bazin, B., Pedron, B. M., & Production, E. A. (1994). *Commercial Polymer Injection in the Courtenay Field, 1994 Update*. 7. https://doi.org/https://doi.org/10.2118/28601-MS

Pye, D. J. (1964). Improved Secondary Recovery by Control of Water Mobility. *Journal of Petroleum Technology*, *16*(08), 911–916. https://doi.org/10.2118/845-pa

Raniolo, S., Dovera, L., Cominelli, A., Callegaro, C., & Masserano, F. (2013). History match and polymer injection optimization in a nature field using the Ensemble Kalman Filter. *Saint Petersburg Russia - From Fundamental Science to Deployment: 17th European Symposium on Improved Oil Recovery, IOR*, *April*. https://doi.org/10.3997/2214-4609.20142642

Rellegadla, S., Prajapat, G., & Agrawal, A. (2017). Polymers for enhanced oil recovery: fundamentals and selection criteria. *Applied Microbiology and Biotechnology*, *101*(11), 4387–4402. https://doi.org/10.1007/s00253-017-8307-4

Romero-Zeron, L. (2012). Advances in Enhanced Oil Recovery Processes. In *Introduction to Enhanced Oil Recovery (EOR) Processes and Bioremediation of Oil-Contaminated Sites*. InTech. https://doi.org/10.5772/45947

Rosa, A. J., Carvalho, R. de S., & Xavier, J. A. D. (2006). *Engenharia de Reservatórios de Petróleo* (1st ed.). Interciência.

Rueda, E., Akarri, S., Torsæter, O., & Moreno, R. B. Z. L. (2020). Experimental Investigation of the Effect of Adding Nanoparticles to Polymer Flooding in Water-Wet Micromodels. *Nanomaterials*, *10*(8), 1489. https://doi.org/10.3390/nano10081489

Said, M., Haq, B., Shehri, D. Al, Rahman, M. M., Muhammed, N. S., & Mahmoud, M. (2021). Modification of xanthan gum for a high-temperature and high-salinity reservoir. *Polymers*, *13*(23), 1–13. https://doi.org/10.3390/polym13234212

Sandiford, B. B. (1964). Laboratory and Field Studies of Water Floods Using Polymer Solutions to Increase Oil Recoveries. *Journal of Petroleum Technology*, *16*(08), 917–922. https://doi.org/10.2118/844-pa

Scott, A. J., Romero-Zerón, L., & Penlidis, A. (2020). Evaluation of polymeric materials for chemical enhanced oil recovery. *Processes*, *8*(3). https://doi.org/10.3390/PR8030361

Seright, R. S. (2017). How Much Polymer Should Be Injected During a Polymer Flood? Review of Previous and Current Practices. *SPE Journal*, *22*(01), 1–18. https://doi.org/10.2118/179543-PA

Seright, R. S., Seheult, M., & Talashek, T. (2008). Injectivity characteristics of EOR polymers. *Proceedings - SPE Annual Technical Conference and Exhibition*, *2*, 767–780. https://doi.org/10.2118/115142-ms

Seright, R. S., Seheult, M., & Talashek, T. (2009). Injectivity characteristics of EOR polymers. *SPE Reservoir Evaluation and Engineering*, *12*(5), 783–792. https://doi.org/10.2118/115142-PA

Shahin, G. T., & Thigpen, D. R. (1996). Injecting Polyacrylamide into Gulf Coast Sands: The White Castle Q Sand Polymer-Injectivity Test. *SPE Reservoir Engineering (Society of Petroleum Engineers)*, *11*(3), 174–179. https://doi.org/10.2118/24119-pa

Sharma, M. M., Pang, S., Wennberg, K. E., & Morgenthaler, L. (1997). Injectivity decline in water injection wells: An offshore Gulf of Mexico case study. *SPE - European Formation Damage Control Conference, Proceedings*, *May 1997*, 341–351. https://doi.org/10.2118/38180-ms

Sheng, J. J. (2013). Polymer Flooding-Fundamentals and Field Cases. In *Enhanced Oil Recovery Field Case Studies* (First Edit). Elsevier Inc. https://doi.org/10.1016/B978-0-12-386545-8.00003-8

Sheng, J. J., Leonhardt, B., & Azri, N. (2015). *Status of Polymer-Flooding Technology*. *March*.

Shuler, P. J., Kuehne, D. L., Uhl, J. T., & Walkup, G. W. (1987). Improving Polymer Injectivity At West Coyote Field, California. *SPE Reservoir Engineering (Society of Petroleum Engineers)*, *2*(3), 271–280. https://doi.org/10.2118/13603-PA

Sieberer, M., Jamek, K., & Clemens, T. (2017). Polymer-flooding economics, from pilot to field implementation. *SPE Economics and Management*, *9*(3), 51–60. https://doi.org/10.2118/179603-pa

Skauge, A., Zamani, N., Gausdal Jacobsen, J., Shaker Shiran, B., Al-Shakry, B., & Skauge, T. (2018). Polymer Flow in Porous Media: Relevance to Enhanced Oil Recovery. *Colloids and Interfaces*, *2*(3), 27. https://doi.org/10.3390/colloids2030027

Sofia, G. B., & Djamel, A. (2016). A Rheological Study of Xanthan Polymer for Enhanced Oil Recovery. *Journal of Macromolecular Science, Part B: Physics*, *55*(8), 793–809. https://doi.org/10.1080/00222348.2016.1207544

Sorbie, K. S. (1991). *Polymer-Improved Oil Recovery*. Springer Netherlands. https://doi.org/10.1007/978-94-011-3044-8

Standnes, D. C., & Skjevrak, I. (2014). Literature review of implemented polymer field projects. *Journal of Petroleum Science and Engineering*, *122*, 761–775. https://doi.org/10.1016/j.petrol.2014.08.024

Sun, L., Li, B., Jiang, H., Li, Y., & Jiao, Y. (2019). An injectivity evaluation model of polymer flooding in offshore multilayer reservoir. *Energies*, *12*(8). https://doi.org/10.3390/en12081444

Tackie-Otoo, B. N., Ayoub Mohammed, M. A., Yekeen, N., & Negash, B. M. (2020). Alternative chemical agents for alkalis, surfactants and polymers for enhanced oil recovery: Research trend and prospects. *Journal of Petroleum Science and Engineering*, *187*(September 2019), 106828. https://doi.org/10.1016/j.petrol.2019.106828

Thomas, A. (2016). Polymer Flooding. In *Chemical Enhanced Oil Recovery (cEOR) - a Practical Overview* (Vol. 11, Issue tourism, p. 13). InTech. https://doi.org/10.5772/64623

Thomas, A., Giddins, M. A., & Wilton, R. (2019). Why is it so Difficult to Predict Polymer Injectivity in Chemical Oil Recovery Processes? *IOR 2019 – 20th European Symposium on Improved Oil Recovery*, *April 2019*, 1–25. https://doi.org/10.3997/2214-4609.201900114

Tiab, D., & Donaldson, E. C. (2016). Naturally Fractured Reservoirs. In *Petrophysics* (pp. 415–481). Elsevier. https://doi.org/10.1016/B978-0-12-803188-9.00008-5

Tiwari, D., Marathe, R. V., Patel, N. K., Ramachandran, K. P., Maurya, C. R., & Tewari, P. K. (2008). Performance of polymer flood in Sanand Field, India-A case study. *SPE Asia Pacific Oil and Gas Conference and Exhibition 2008 - "Gas Now: Delivering on Expectations," 1*(Fig 2), 372–380. https://doi.org/10.2118/114878-ms

Ustick, R. E. (1967). Comparison of Polymer Flooding and Waterflooding at Huntington Beach, California. *Journal of Petroleum Technology*, *19*(09), 1103–1111. https://doi.org/10.2118/1734-pa

Veerabhadrappa, S. K., Doda, A., Trivedi, J. J., & Kuru, E. (2013). On the effect of polymer elasticity on secondary and tertiary oil recovery. *Industrial and Engineering Chemistry Research*, *52*(51), 18421–18428. https://doi.org/10.1021/ie4026456

Vittoratos, E., & Kovscek, A. (2017). Doctrines and realities in reservoir engineering. *SPE Western Regional Meeting Proceedings*, *2017-April*(April), 402–409. https://doi.org/10.2118/185633-ms

Wang, D. (2013). Polymer Flooding Practice in Daqing. In *Enhanced Oil Recovery Field Case Studies* (First Edit, pp. 83–116). Elsevier. https://doi.org/10.1016/B978-0-12-386545-8.00004-X

Wever, D. A. Z., Picchioni, F., & Broekhuis, A. A. (2011). Polymers for enhanced oil recovery: A paradigm for structure-property relationship in aqueous solution. *Progress in Polymer Science (Oxford)*, *36*(11), 1558–1628. https://doi.org/10.1016/j.progpolymsci.2011.05.006

Wever, D., Karpan, V., Glasbergen, G., Koltsov, I., Shuster, M., Volokitin, Y., Gaillard, N., & Daguerre, F. (2017). Polymer Injectivity De-risking for West Salym ASP Pilot. *IOR NORWAY 2017 - 19th European Symposium on Improved Oil Recovery: Sustainable IOR in a Low Oil Price World*, 24–27. https://doi.org/10.3997/2214-4609.201700241

Wu, X., Zhang, S., Xiong, C., Cnpc, D., & Liu, S. (2016). *Successful Field Test of a New Polymer Flooding Technology for Improving Heavy Oil Reservoir Recovery -- Case Study of Strongly Heterogeneous and Multi-Layer Conglomerate Heavy Oil Reservoir XJ6*. 1–14.

Yerramilli, S. S., Zitha, P. L. J., & Yerramilli, R. C. (2013). Novel Insight into Polymer Injectivity for Polymer Flooding Modeling of Polymer Flow in Porous Media. *SPE European Formation Damage Conference*, *SPE 165195*(2009), 1–23.

Yin, D., Song, S., Xu, Q., & Liu, K. (2020). Experimental research on the optimization and evaluation of the polymer/chromium-ion deep profile control system for the fractured low-permeability reservoirs. *Processes*, *8*(9). https://doi.org/10.3390/pr8091021

Zhou, X., & Kamal, M. S. (2019). Experimental Study on the Relationship between Carbonate Reservoir Quality Index and Dynamic Parameters of Chemical Solutions for Oil Recovery Practice. *Energy and Fuels*, *33*(10), 9747–9758. https://doi.org/10.1021/acs.energyfuels.9b02491

Zhu, D., Bai, B., & Hou, J. (2017). Polymer Gel Systems for Water Management in High-Temperature Petroleum Reservoirs: A Chemical Review. *Energy and Fuels*, *31*(12), 13063–13087. https://doi.org/10.1021/acs.energyfuels.7b02897

APPENDIX A: BIOPOLYMER SOLUTIONS PREPARATION MANUAL

This section unveils the meticulous methodology developed by the Labore/Cepetro/FEM research group at Universidade Estadual de Campinas for the preparation of polymeric solutions.

Figure A-1. Sequence Preparation

A.1. Stock solution preparation

1. Measure the polymer powder and deionized (DI) water masses required to achieve 4000 ppm of polymer;
    a. Use a clean aluminum foil for the polymer powder;
    b. Use a clean beaker or glass bottle for the DI water;
2. Put the DI water on a magnetic stirrer and adjust the rotation for the vortex to reach 75% of the fluid's height;
3. Pour the polymer powder on the shoulder of the vortex slowly;
    a. For example, for pouring 4g of polymer powder, this procedure should take around 10 minutes;
4. Keep the solution under high agitation for 24 hours, in the case of Scleroglucan, it is typically subjected to continuous and intensive agitation for a period of 7 days;
    a. When the vortex disappears, increase the rotation speed of the magnetic stirrer;
    b. Periodically (e.g., every 2 hours), pick up the beaker/bottle containing the solution and stir it by moving your hand in a circular motion;
5. Collect a solution sample and measure its flow curve (rheology);
6. Compare the measured flow curve with a reference curve under the same conditions.

A.2. Dilution before filtration

1. Put a clean glass bottle on the scale and tare it;
2. Pour the desired stock polymer solution mass in the bottle;
3. Pour 400% SSW and DI water in the same bottle until reach the desired concentration with 100% SSW;

   a. For example: pour 400% SSW until double the polymer solution. This will result in a 2000 ppm polymer in 200% SSW solution. Then pour DI water in the same bottle until the mass is doubled again. This will result in a 1000 ppm polymer in 100% SSW solution
   b. The mass by the end of this step should be four times the stock mass initially poured in the bottle;
4. Mix the resulting solution for about 10 minutes;
5. Collect a solution sample and measure its flow curve (rheology);
6. Compare the measured flow curve with a reference curve under the same conditions.

A.3. Aging

1. Put the 1000 ppm solution in a fluid container (i.e., the ones used for the core flooding procedures) inside the oven;
2. Bubble nitrogen gas in the solution for about 10 minutes;
3. Seal the fluid accumulator;
4. Close the oven, turn it on, and set its temperature to 90°C;
5. Let the solution age for 16~24 hours;
   a. The xanthan gum solution may experience a slight degradation by the end of the 24-hour period;
6. Collect a solution sample and measure its flow curve (rheology);
7. Compare the measured flow curve with a reference curve under the same conditions.

A.4. Filtration Process

A.4.1. Pre-Filtration

If the polymer is prone to causing clogging issues, a pre-filtering step using ceramic filters is implemented to ease the filtration process and prevent blockages. Figure A-2 shows the pre-filtration apparatus. Note that the fluid accumulator containing the polymer is inside the oven.

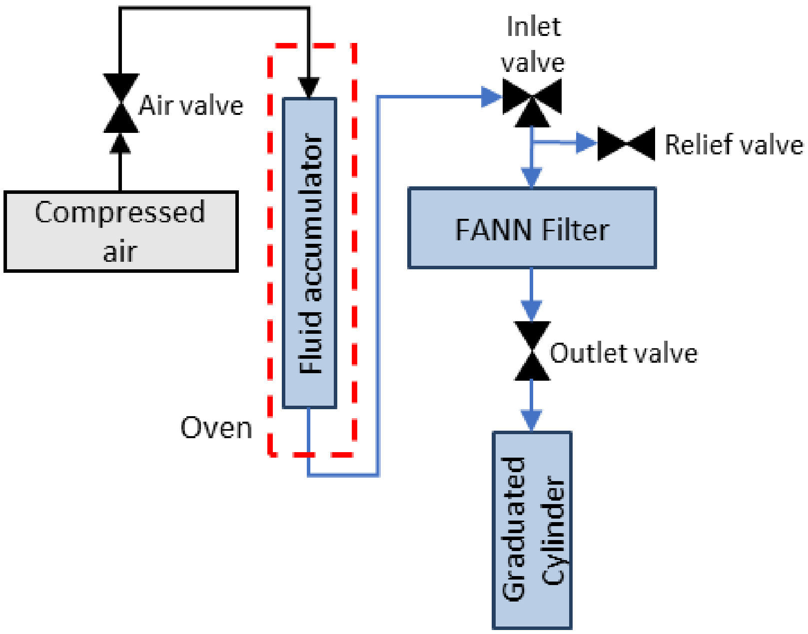

Figure A-2. Pre-filtration apparatus.

1. Set the compressed air pressure to 30 psi;
    a. Make sure the inlet, outlet, and relief valves are closed and the air valve is open;
2. Disassemble the FANN filter holder;
3. Put the 55 µm FANN filter in the filter holder;
4. Fill the filter holder chamber with the polymer in the accumulator;
5. Reassemble the FANN filter holder;
6. Position a graduated cylinder below the outlet valve and open the inlet valve;
7. Open the outlet valve;
8. Let the desired discard volume be produced;
    a. Usually, the discarded volume is 30 mL;
9. Change the graduated cylinder for another one at the same at that a timer is started;
    a. The graduated cylinder change should be done without closing the outlet or inlet valves;
10. Record the volume and elapsed time for several instants until all the polymer in the fluid accumulator is filtered;
    a. When the graduated cylinder is filled, change it to another one (without closing any valves) and continue to record data points;
11. Close the air and outlet valves;
12. Put a beaker after the relief valve and open it;
    a. CAUTION: the left oven fluid and gas can be very hot;
13. Let the system depressurize completely;
14. Collect a solution sample and measure its flow curve (rheology);
15. Compare the measured flow curve with a reference curve under the same conditions;
16. Disassemble the filter holder and throw the used filter in the thrash;
17. Put the 20 µm Millipore filter in the filter holder;
18. Repeat steps 4 through 16;

19. Put the 12 μm Millipore filter in the filter holder;
20. Repeat steps 4 through 16;
21. Clean the filter holder.

A.5. Filtration

Figure A-3 shows the filtration apparatus. Note that the fluid accumulator containing the polymer is inside the oven.

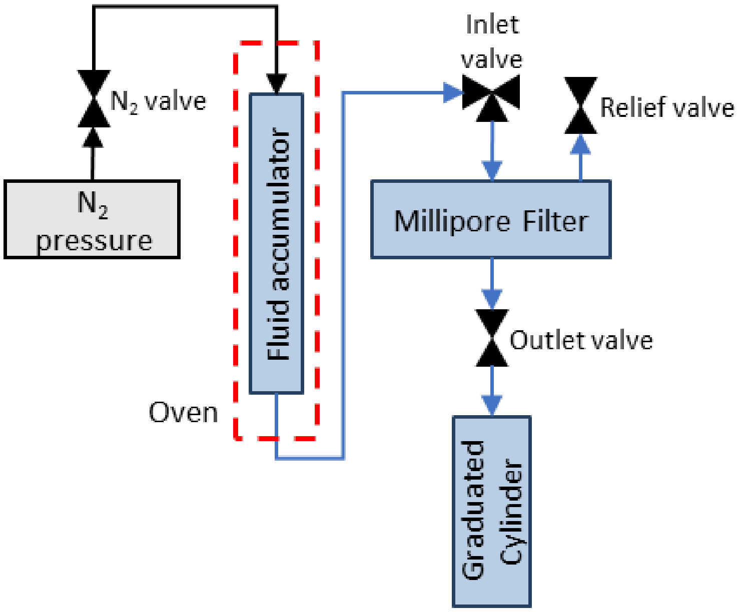

Figure A-3. Filtration apparatus.

1. Set the nitrogen gas (N2) pressure to 30 psi;
    a. Make sure that the inlet, outlet, and relief valves are closed and the N_2 valve is open;
2. Disassemble the Millipore filter holder;
3. Put the 8 μm Millipore filter in the filter holder;
    a. Follow the instructions on the filter box for the best practices;
4. Hydrate the filter with the polymer solution in the accumulator;
5. Reassemble the Millipore filter holder;
    a. Apply 6 Nm of torque in the filter holder's nuts;
6. Fill the top of the filter holder with the polymer in the accumulator;
    a. Tilt the filter holder from side to side to ensure that any air bubbles leave the system;
    b. This step and the ones that follow it should be done swiftly so that the polymer does not lose too much temperature;
7. Connect the inlet valve assembly to the filter holder;
8. Position a graduated cylinder below the outlet valve and open the inlet valve;
9. Open the outlet valve;

10. Let the desired discard volume be produced;
    a. Usually, the discarded volume is 30 mL;
11. Change the graduated cylinder for another one at the same at that a timer is started;
    a. The graduated cylinder change should be done without closing the outlet or inlet valves;
12. Record the volume and elapsed time for several instants until all the polymer in the fluid accumulator is filtered;
    a. When the graduated cylinder is filled, change it to another one (without closing any valves) and continue to record data points;
    b. The filter may clog after the filtration of a considerable amount of solution. In this case, follow the procedure:
        i. Close the inlet and outlet valves;
        ii. Put a beaker after the relief valve and open it;
        iii. Let the system depressurize completely, then close the relief valve;
        iv. Disassemble the filter holder;
        v. Remove the clogged filter and throw it in the thrash;
        vi. Put in a new filter in the filter holder;
        vii. Return to step 4;
13. Close the N_2 and outlet valves;
14. Put a beaker after the relief valve and open it;
    a. CAUTION: the left oven fluid and gas can be very hot;
15. Let the system depressurize completely;
16. Collect a solution sample and measure its flow curve (rheology);
17. Compare the measured flow curve with a reference curve under the same conditions;
18. Open the oven, then the fluid container and pour the filtered polymer back inside it;
19. Seal the fluid container and close the oven;
20. Close the inlet and relief valves;
21. Set the N_2 pressure to 30 psi and open the N_2 valve;
22. Disassemble the filter holder and throw the used filter in the thrash;
23. Put the 1.2 µm Millipore filter in the filter holder;
    a. Follow the instructions on the filter box for the best practices;
24. Repeat steps 4 through 17;
25. Disassemble the filter holder and throw the used filter in the thrash;
26. Clean the filter holder;
    a. All the wetted parts of the filter holder have to be cleaned with tap water, then deionized water, and then alcohol;
    b. All the parts of the filter holder have to be dried thoroughly after the cleanup procedure;
    c. The filter holder has to be assembled back in order to be stored.
27. Clean the fluid accumulator and fluid tubing.

A.6. Dilution to test concentration

1. Put a clean glass bottle on the scale and tare it;
2. Pour the desired filtered polymer solution mass in the bottle;
3. Pour 100% SSW in the same bottle until the desired polymer concentration is reached;
4. Mix the resulting solution for about 10 minutes;
5. Collect a solution sample and measure its flow curve (rheology);
6. Compare the measured flow curve with a reference curve under the same conditions, if available.

APPENDIX B: SUMMARY OF RESULTS

This section provides an overview of the results obtained through the procedures conducted in Chapter 3, further enhancing the visual representations and explanations presented in Chapter 4.

Table B-1 Summary of Rock and Fluid Properties

	Parameters	Units	Rock Samples				
			IL_45	IL_37	IL_33	IL_46	IL_34
Core	**Mass**	**(gr)**	499.89	500.10	502.91	500.16	501.65
	Length	**(cm)**	19.9	20.0	19.900	19.9	20.0
	Diameter	**(cm)**	3.78	3.78	3.78	3.78	3.78
	Area	**(cm2)**	11.22	11.22	11.22	11.22	11.22
	Total Volume	**(cm^3)**	223.3	224.4	223.3	223.3	224.4
	Kg	**(mD)**	173.33	171.27	142.61	160.11	639.77
	Kw	**(mD)**	127.67	156.39	147.03	156.07	473.16
	Pore Volume	**(cm^3)**	39.5	40.3	39.3	34.5	41.2
	Porosity	**-**	17.5	17.9	17.5	15.4	18.3
Fluid	**Overlap Concentration C***	**(ppm)**	285	950	175	285	285
	Filtration Filters	**µm**	8 + 12	55+20+12 + 8 +1.2	8 + 1.2	8 + 1.2	8+ 1.2
	Concentration test	**(ppm)**	50 100 700	100 300 1200	100 500 800	100 1100 1500	100 700 1100
	Viscosity (10s-1)	**(ppm)**	0.56 0.67 4.40	0.49 0.62 2.3	0.73 4.46 9.81	0.661 0.71 20.51	0.66 3.73 8.51
	Fr @ 1.2 mesh filter		1.03	1.05	1.02	1.03	1.04
	Viscosity loss		31.20%	75.10%	26.63%	37.30%	37.50%

Table B-2 Summary of Experimental results IL-45 Xanthan Gum

Variables	Unit	(ppm)	0.5	1	2	4	6	4	2	1	0.5
RF	-	50	1.03	1.11	1.13	1.12	1.11	1.31	1.35	1.37	1.33
RF	-	100	2.38	2.53	2.24	2.33	2.29	2.34	2.34	2.69	3.06
RF	-	700	5.25	4.61	4.24	3.71	3.45	2.98	3.43	4.00	4.73
RRF	-	50	1.76	1.68	1.46	1.36	1.40				
RRF	-	100	2.79	2.58	2.16	1.91	2.01				
RRF	-	700	2.86	2.70	2.34	2.11	2.01				
µ *in-situ*	cp	50	0.38	0.43	0.45	0.41	0.47	0.48	0.49	0.48	0.48
µ *in-situ*	cp	100	0.44	0.53	0.53	0.61	0.55	0.62	0.59	0.59	0.60
µ *in-situ*	cp	700	1.13	1.08	1.01	0.91	0.86	0.91	1.01	1.04	1.22
∇P	Psi/mt	50	4.33	9.23	18.58	37.07	55.13	0.87	0.82	0.83	0.81
∇P	Psi/mt	100	23.23	39.53	64.01	96.87	132.8	0.36	0.29	0.21	0.16
∇P	Psi/mt	700	27.25	45.34	67.8	105.9	142.2	0.33	0.29	0.25	0.21
Ir	-	50	0.97	0.90	0.87	0.88	0.89	0.87	0.82	0.83	0.81
Ir	-	100	0.18	0.21	0.25	0.34	0.37	0.36	0.29	0.21	0.16
Ir	-	700	0.15	0.18	0.24	0.31	0.34	0.33	0.29	0.25	0.21

Table B-3 Summary of Experimental results IL-33 Guar Gum

Variables	Unit	(ppm)	0.5	1	2	4	6	4	2	1	0.5
RF	-	100	1.18	1.20	1.22	1.19	1.19	1.141	1.123	1.13	1.19
RF	-	300	1.31	1.32	1.32	1.33	1.32	1.336	1.336	1.35	1.33
RF	-	1300	2.31	2.25	2.15	2.09	2.01	2.085	2.122	2.24	2.33
RRF	-	100	1.76	1.56	1.37	1.26	1.22				
RRF	-	300	1.48	1.46	1.37	1.28	1.23				
RRF	-	1300	2.07	1.79	1.55	1.39	1.31				
μ *in-situ*	cp	100	0.38	0.42	0.45	0.46	0.47	0.45	0.44	0.43	0.46
μ *in-situ*	cp	300	0.48	0.49	0.50	0.51	0.52	0.52	0.51	0.51	0.50
μ *in-situ*	cp	1300	0.66	0.71	0.74	0.76	0.75	0.77	0.75	0.75	0.75
∇P	Psi/mt	100	6.70	12.84	23.26	39.20	53.97	38.95	21.69	12.07	6.70
∇P	Psi/mt	300	5.03	9.43	19.07	38.46	55.86	36.74	18.08	8.90	4.37
∇P	Psi/mt	1300	14.68	23.39	39.70	65.73	89.23	61.43	33.02	17.75	9.68
Ir	-	100	0.62	0.64	0.70	0.84	0.91	0.84	0.75	0.69	0.62
Ir	-	300	0.83	0.88	0.85	0.85	0.88	0.89	0.90	0.93	0.96
Ir	-	1300	0.28	0.35	0.41	0.50	0.55	0.53	0.49	0.46	0.43

Table B-4 Summary of Experimental results IL-33 Scleroglucan

Variables	Unit	(ppm)	0.5	1	2	4	6	4	2	1	0.5
RF	-	100	1.59	1.77	1.68	1.59	1.53	1.60	1.73	1.95	2.09
RF	-	500	3.82	3.55	3.15	2.84	2.65	2.86	3.28	3.80	4.28
RF	-	800	13.68	8.42	6.80	5.68	4.95	5.36	6.23	7.85	12.02
RRF	-	100	1.71	1.68	1.59	1.48	1.44				
RRF	-	500	1.95	1.75	1.67	1.54	1.49				
RRF	-	800	5.83	4.93	4.07	3.47	3.19				
μ *in-situ*	cp	100	0.44	0.50	0.51	0.51	0.51	0.52	0.52	0.55	0.58
μ *in-situ*	cp	500	0.44	0.50	0.51	0.51	0.51	0.89	0.97	1.15	1.16
μ *in-situ*	cp	800	0.88	0.98	0.89	0.86	0.80	0.83	0.87	1.00	1.12
∇P	Psi/mt	100	5.61	11.84	23.38	44.05	64.08	44.1	23.73	12.9	7.23
∇P	Psi/mt	500	12.85	23.38	40.59	74.53	107.46	75.08	42.26	24.29	13.71
∇P	Psi/mt	800	47.76	75.36	115.0	203.5	262.8	274.3	138.3	89.9	61.3
Ir	-	100	0.73	0.69	0.69	0.75	0.78	0.74	0.68	0.64	0.58
Ir	-	500	0.31	0.35	0.40	0.44	0.47	0.43	0.38	0.34	0.30
Ir	-	800	0.08	0.10	0.14	0.16	0.19	0.17	0.16	0.13	0.10

Table B-5 Summary of Experimental results IL-46 Xanthan Gum

Variables	Unit	(ppm)	0.5	1	2	4	6	4	2	1	0.5
RF	-	100	1.36	1.43	1.49	1.43	1.39	1.40	1.37	1.36	1.73
RF	-	700	6.29	5.29	4.37	3.76	3.39	3.26	3.76	4.28	5.81
RF	-	1100	15.9	10.66	8.64	6.75	5.90	6.70	7.79	9.56	13.5
RRF	-	100	2.33	1.63	1.52	1.41	1.34				
RRF	-	700	2.3	2.01	1.76	1.60	1.50				
RRF	-	1100	3.7	2.79	2.49	2.35	2.29				
μ *in-situ*	cp	100	0.43	0.49	0.51	0.50	0.48	0.46	0.47	0.51	0.60
μ *in-situ*	cp	700	1.76	1.57	1.33	1.11	1.08	1.12	1.36	1.65	2.13
μ *in-situ*	cp	1100	2.02	2.10	1.81	1.50	1.40	1.49	1.77	2.08	2.34
∇P	Psi/mt	100	5.92	12.48	23.62	40.62	56.90	38.8	20.03	10.43	5.71
∇P	Psi/mt	700	19.0	32.66	53.69	91.68	125.7	90.33	54.75	33.00	19.2
∇P	Psi/mt	1100	133.1	152.4	207.5	274.3	326.1	274.3	138.2	89.98	61.3
Ir	-	100	0.69	0.65	0.69	0.82	0.88	0.84	0.81	0.79	0.73
Ir	-	700	0.21	0.25	0.30	0.36	0.40	0.36	0.29	0.25	0.21
Ir	-	1100	0.03	0.05	0.07	0.12	0.15	0.12	0.11	0.09	0.06

Table B-6 Summary of Experimental results IL-34 Xanthan Gum

Variables	Unit	(ppm)	1	2	4	8	12	14	1
RF	-	100	1.65	1.51	1.48	1.42	1.36	1.35	1.67
RF	-	700	6.54	4.86	4.01	3.39	2.99	2.84	6.12
RF	-	1100	9.74	7.48	5.96	4.79	4.16	3.98	9.78
RRF	-	100	2.15	1.51	1.44	1.32	1.27	1.24	1.43
RRF	-	700	3.27	2.27	2.08	1.92	1.83	1.78	2.50
RRF	-	1100	2.96	2.36	2.23	2.12	2.13	2.08	2.54
μ *in-situ*	cp	100	0.67	0.63	0.61	0.59	0.59	0.59	0.70
μ *in-situ*	cp	700	1.22	1.22	1.08	0.95	0.88	0.85	1.54
μ *in-situ*	cp	1100	1.95	1.66	1.40	1.16	0.96	0.94	2.15
∇P	Psi/mt	100	5.77	12.12	21.92	36.26	48.81	55.20	4.38
∇P	Psi/mt	700	30.36	44.69	60.38	87.45	110.5	120.4	14.81
∇P	Psi/mt	1100	21.30	33.31	50.97	81.78	112.1	127.9	18.46
Ir	-	100	0.35	0.49	0.47	0.51	0.55	0.67	0.46
Ir	-	700	0.06	0.13	0.17	0.21	0.24	0.30	0.13
Ir	-	1100	0.09	0.17	0.20	0.22	0.24	0.29	0.11